Stony Brook University

COUPLING LIGAND BINDING TO ION CHANNEL GATING IN NMDA RECEPTORS

A Dissertation Presented

by

Iehab Talukder

to

The Graduate School

in Partial Fulfillment of the

Requirements

for the Degree of

Doctor of Philosophy

in

Neuroscience

Stony Brook University

May 2011

Stony Brook University

The Graduate School

Iehab Talukder

We, the dissertation committee for the above candidate for the

Doctor of Philosophy degree, hereby recommend

acceptance of this dissertation.

Lonnie P. Wollmuth – Dissertation Advisor

Professor, Department of Neurobiology and Behavior

David McKinnon – Chairperson of Defense

Professor, Department of Neurobiology and Behavior

Hiro Furukawa

Assistant Professor, Neuroscience, Cold Spring Harbor Laboratory

Mark L. Mayer

Senior Investigator, Neuroscience, National Institutes of Health

This dissertation is accepted by the Graduate School

Lawrence Martin

Dean of the Graduate School

Abstract of the Dissertation

COUPLING LIGAND BINDING TO ION CHANNEL GATING

IN NMDA RECEPTORS

by

Iehab Talukder

Doctor of Philosophy

in

Neuroscience

Stony Brook University

2011

The NMDA receptor is a ligand-gated ion channel that mediates a fundamental component of excitatory synaptic transmission in the mammalian central nervous system. Aberrant NMDA receptor function causes and/or exacerbates multiple neurological and psychiatric disorders, thus creating the need for pharmacological modulation of its activity. The defining feature of ligand-gated ion channels is gating—the energetic coupling of ligand binding into opening of the associated ion channel pore. In an NMDA receptor subunit, gating is initiated in the extracellular ligand-binding domain (LBD) and is propagated via three linkers—S1-M1, M3-S2, and S2-M4—to the transmembrane domain (TMD) forming the ion channel. The M3-S2 linkers directly couples ligand binding to gating movements of the pore-lining M3 transmembrane segment, but how it does so, as well as the structural and functional contributions of the S1-M1 and S2-M4 linkers to the gating process, are unknown. My research focused on these LBD-TMD linkers to dissect out the mechanisms of gating in NMDA receptors. In an initial project, I identified key residues/positions within these linkers that are important to gating. These extracellularly accessible positions can modulate gating through a hypothesized disruption of transient contact interfaces dependent on the receptor gating state, thus qualifying for potential sites and mechanisms of drug action. I further studied the functional consequences of stabilizing such contacts amongst the linkers by engineered disulfide crosslinks. When M3-S2 was crosslinked to S2-M4 within an individual NMDA receptor subunit, I found symmetrical effects on the late gating steps comprising pore opening. Thus the NMDA receptor undergoes a pore opening mechanism through equivalent contributions of tightly-coupled subunits. When S1-M1 was crosslinked to S2-M4 either within or across subunits, I found strong impairments in pore opening. Therefore, while structurally at the periphery of the M3-S2/M3 central gating element, the conformational freedom of S1-M1 and S2-M4 is integral in mechanical opening of the channel pore. In conclusion, my work has provided new insights into mechanisms coupling

ligand binding to ion channel gating in NMDA receptors, while also laying the groundwork for future targeting of the linkers to correct dysfunctional receptor activity.

To my mother and father

COUPLING LIGAND BINDING TO ION CHANNEL GATING IN NMDA RECEPTORS

TABLE OF CONTENTS

LIST OF FIGURES

LIST OF TABLES

ACKNOWLEDGEMENTS

Foremost, my greatest appreciation and thanks are for the lab members who directly contributed to my research. Janet Allopena expertly handled essentially all the molecular biology in my research projects. She did the mutagenesis and mRNA preparations that were the initial stages in all my projects. She further trained Priya Borker, an undergraduate student, who did some of the molecular biology work related to the project described in chapter 2. Michael Markowitz, another undergraduate student, has been currently doing whole-cell oocyte recordings under my training and guidance and has made significant advances in the experiments. While every one I mention here has been of great help, my research would not have progressed as far as it did and in the time it took without the help of these three individuals.

I emphatically thank my mentor Dr. Lonnie P. Wollmuth. His mentoring in all aspects of research—from conception of a scientific idea, experimental design and implementation to address it, analysis of the results and drawing supportable conclusions, oral and written presentations, as well as writing grants to finance all these—has been indispensable in my maturation as a scientist. On the way, he has also taught me subtler but equally important lessons in science, for example that there are no failed experiments, all experiments reveal something that otherwise would have remained hidden. Continued development of the instincts to appreciate these lessons and apply them in future endeavors is important to becoming a good scientist.

I thank all other past and current members of the Wollmuth lab who at some point or another have helped me in my work. They include Michael Prodromou, Dr. Alexandra Corrales, Dr. Martin Prieto, Jessica Helm, Gulcan Akgul, Catherine Salussolia, Rashek Kazi and Quan "Alfred" Gan. I appreciate the support of my thesis committee members – Drs. David

McKinnon, Hiro Furukawa and Mark Mayer—and thank them for it. I also thank other helping members of the Stony Brook research community including Diane Godden, Catherine Costanzo, Carron Kaufman and Dr. Michael Frohman (in the MSTP).

I thank my friends/colleagues with whom I have had extensive discussions about science and life over coffee and other drinks. They include Justin Rodriguez, Catherine Salussolia, Drs. George Zanazzi and Oladapo Yeku.

Finally my personal gratitude for making me everything that I am extends towards my family, most importantly the immediate Talukders—brother Hisham, mother Nazmun Nahar and father Dr. Mohammed.

CHAPTER 1: INTRODUCTION

NMDA receptors are ligand-gated ion channels that partly mediate rapid neuron-to-neuron signaling in the mammalian central nervous system. At their most basic level, NMDA receptors convert the excitatory chemical signal carried by the extracellularly available glutamate molecules into depolarizing electrical currents along the neuronal surface. When integrated within the nervous system circuitry, this fundamental role of NMDA receptors subserves a broad spectrum of higher order CNS functions including neurodevelopmental maturation, memory formation and pain perception. NMDA receptor activity beyond its physiological ranges can trigger and/or complicate both acute (e.g. stroke and seizure) and chronic (e.g. Parkinson's and Alzheimer's diseases) neurological, as well as psychiatric (e.g. Schizophrenia), disorders. Consequently, curtailing its pathological functions while maintaining its normal physiology by means of NMDA receptor-targeted pharmacology continues to be an active area of research. In this context, my research has focused on dissecting the mechanisms of the defining feature of NMDA receptor gating—coupling ligand binding to ion channel opening—with the ultimate goal of modulating it through novel sites and mechanisms of drug action.

NMDA RECEPTORS IN GLUTAMATERGIC SYNAPTIC TRANSMISSION

Transmission of neuron-to-neuron signaling occurs through chemical mediators, or neurotransmitters, acting within the localized area of a synapse where the two neurons connect (Fig. 1.1A & B). The neurotransmitters are released from the presynaptic neuron, diffuse across the synapse, and are detected by the postsynaptic neuron where they either excite or inhibit further electrochemical activity. Glutamate is the predominant neurotransmitter of excitatory neurotransmission and gamma-aminobutyric acid (GABA) in the brain and glycine in the spinal cord are the predominant neurotransmitters of inhibitory neurotransmission. Whereas the neurotransmitter itself determines the overall excitability of the postsynaptic, the plasma membrane-embedded types of receptors detecting these neurotransmitters set distinct tones of activity. Glutamate binding to and activation of postsynaptic glutamate receptors that are physically associated with ion channels, hence ionotropic glutamate receptors (iGluRs), initiate rapid excitatory electrical activity within the cell (Fig. 1.1B).

At a prototypical synapse, the rapid excitatory current is carried by inward cationic fluxes through the glutamate-bound channel-open iGluRs. The amplitude and kinetics of this excitatory postsynaptic current (EPSC) are determined by the biophysical properties of the combinations of iGluR subtypes, as well as their individual subunit compositions, present at the postsynaptic membrane. While the iGluR family consists of three subtypes—kainate, α-amino-3-hydroxy-S-methylisoxazole-4-propionic acid (AMPA) and *N*-methyl-D-aspartate (NMDA)—of receptors, the AMPA and NMDA are predominantly situated in excitatory postsynaptic signaling complexes (Fig. 1.1B). AMPA receptors mediate a fast and transient component of the EPSC restricted to the millisecond timescale (Mosbacher et al., 1994; Edmonds et al., 1995; Erreger et al., 2004) (Fig. 1.1C). NMDA receptors mediate a slower and persistent component of the EPSC,

lasting from tens to thousands of milliseconds (Monyer et al., 1992; Wyllie et al., 1996; Vicini et al., 1998) (Fig. 1.1C). When integrated into the nervous system circuitry, this minimal AMPA and NMDA receptor-mediated functional unit of excitatory synaptic signaling plays an essential role in higher order neurophysiological processes.

The rapid kinetics of AMPA receptors endow them the ability to induce sudden electrical changes in the neuron with important functional consequences. For example, many interneurons within a localized cortical circuitry express AMPA receptors whose contribution to the synaptic conductance time course is completed within sub-milliseconds. The resulting large and fast EPSP can trigger action potentials within a short temporal window with fast frequencies (Geiger et al., 1997). The localized circuitry containing these AMPA receptors is therefore capable of oscillatory activity thought to be important in working memory (Jonas et al., 2004; Isaac et al., 2007; Lisman). AMPA receptors also exhibit fast (in milliseconds) and strong (< 5% of peak current amplitudes) desensitization wherein current conductance through the receptors is drastically reduced even though glutamate is bound. Thus, within a single synaptic release of glutamate, AMPA receptor-mediated currents are further resolved into separate temporal windows, further speeding up information exchange (Wall et al., 2002; Zucker and Regehr, 2002).

Unlike AMPA and NMDA receptors (in general), kainate receptors function at both pre- and post-synaptic sites. Postsynaptic kainate receptors often possess slower time course (time constants of decay > 100 ms) and are activated by bursts of activity rather than a single synaptic event (Traynelis et al., 2010). At the mossy fiber-CA3 pyramidal cell synapses, kainate receptor-mediated EPSCs amplify synaptic integration and frequency-dependent spike transmission

(Sachidhanandam et al., 2009). Presynaptic kainate receptors, based on their specific subunit composition, can both facilitate and depress synaptic activity by serving as autoreceptors detecting glutamate release (Semyanov and Kullmann, 2001; Lerma, 2006, Cossart, 1998 #88). Presynaptic kainate receptors on inhibitory interneurons can distinctly modulate hippocampal gamma oscillations (Fisahn et al., 2004). In addition, kainate receptor at extrasynaptic sites can detect glutamate spilled over from the synapse and further modify the propagative electrical activity (Pinheiro and Mulle, 2006).

NMDA receptors in neurodevelopmental maturation.

Being tetrameric complexes, the constituent NMDA receptor subunits (GluN1, GluN2A-D and GluN3A-B) are regionally and developmentally expressed during development. In prenatal and very early postnatal life, NMDA receptors containing the GluN2B predominate in the cortex, hippocampus and cerebellum (van Zundert et al., 2004). Because GluN2B-containing NMDA receptors have slow deactivation kinetics, the EPSC component meditated by NMDA receptors within these brain regions is prolonged, an effect that is important for circuit formation and development. As an example, the presence of GluN2B at synaptic sites within a developing visual cortex permits the formation of ocular dominance columns and the refinement of thalamocortical connections required for future binocular vision (Erisir and Harris, 2003). In the first weeks of postnatal life, NMDA receptors in these brain regions take their adult forms with a subunit switch to GluN2A-, and in the cerebellum to GluN2C-, containing receptors. This subunit switch could be driven by agonist binding, as in hippocampal principal cells (Barria and Malinow, 2002), or sensory experience, as in thalamocortical synapses (Quinlan et al., 1999; Barth and Malenka, 2001; Lu et al., 2001). Further, GluN3A-containing NMDA receptors

maintain an immature receptor state permissive for synaptogenesis and formation of dendritic spines (Perez-Otano et al., 2001). Subsequent down-regulation of the GluN3A-containing NMDA receptors is required for strengthening and stabilization of matured synaptic connections onto adulthood (Roberts et al., 2009). As a general summary, GluN2B, GluN2D and GluN3A are the predominant subunits in the changing brain during development, whereas GluN2A and GluN2C take over in the adult brain.

NMDA receptors in learning and memory.

The cellular and electrophysiological correlate of learning and memory is thought to be a form of synaptic plasticity known as long term potentiation (LTP) (Kessels and Malinow, 2009). Simplistically, LTP describes the persistent strengthening of excitatory synaptic connections based on the pattern of previous synaptic input. Thus, 'memory' of the previous synaptic input to a localized circuit is maintained in the form of stronger connections within the same circuitry. In the Schaffer collateral input to CA1 pyramidal cells, NMDA receptors are absolutely required for the induction of LTP (or induction of memory formation). Unique to NMDA receptors, their voltage-dependent Mg^{2+} block and Ca^{2+} permeability, subserve their roles in LTP induction. When a high frequency train of stimuli is delivered to the presynaptic Schaffer collaterals (the previous input), they release glutamate that subsequently bind to iGluRs and trigger EPSC on the postsynaptic pyramidal cells. Currents fluxing through the faster AMPA receptor depolarize the postsynaptic membrane relieving Mg^{2+} block of NMDA receptors present at resting negative potentials. Now the fully active NMDA receptors permit great influxes of Ca^{2+}, which then initiate intracellular signaling cascades important in LTP induction. A final result of these events is the delivery and retention of greater numbers and varieties of AMPA receptors to the

postsynaptic membrane. The synaptic strength is therefore strengthened, as future stimulation of this synapse will generate greater postsynaptic activity through larger concentration of AMPA receptors, as well as a stereotypical pattern of activity dependent on the AMPA receptor composition. Because of their voltage-dependent Mg^{2+} block, the NMDA receptor functions as coincidence detectors of both glutamate release and membrane depolarization thereby generating mechanisms of synapse specificity, associativity and cooperativity (Traynelis et al., 2010). In certain 'silent' synapses, NMDA receptors are the only functional iGluRs, and only upon LTP induction and consequent AMPA receptor infiltration do those synapses fully mature (Kerchner and Nicoll, 2008). The longer time course of synaptic signaling mediated by GluN2B-containing NMDA receptors enhances LTP (Tang et al., 1999; Erreger et al., 2005a) and likely generates greater flexibility in intensifying and pruning synaptic connections during development.

NMDA receptors in nociception.

NMDA receptors play critical roles in the induction and maintenance of neuronal hyperexcitability triggered by noxious stimuli. Both allodynia (previously harmless stimuli now generates pain) and hyperalgesia (augmented pain response) are mediated within the spinal cord by a form of synaptic plasticity termed central desensitization (Petrenko et al., 2003). Excessive input of noxious stimuli from peripheral nerve afferents, especially the C-fibers, depolarizes the postsynaptic membrane strongly enough to relieve Mg^{2+} block of NMDA receptors. Thus, a state of NMDA receptor hyperactivity is established which persists chronically through long term transcriptional, translational and post-translational changes resulting in further enhancement of NMDA-receptor mediated signaling (Davies and Lodge, 1987; Dickenson and Sullivan, 1987). Furthermore, uniquely in the spinal cord, NMDA receptors are situated presynaptically where

they participate in feed-forward release of additional glutamate, as well as inflammatory compounds such as substance P (Petrenko et al., 2003). Inflammation out in the peripheral nervous system can also lead to increases in NMDA receptor numbers on afferent nerve fibers where they contribute to peripheral sensitization apparent in neuropathic pain (Carlton and Coggeshall, 1999). GluN2B-containing NMDA receptors appear to be especially important in both acute and chronic pain perception (Petrenko et al., 2003). In summary, NMDA receptors acting both physiologically and pathologically within the central and peripheral nervous systems transmit nociceptive signals.

NMDA RECEPTORS IN DISEASE STATES

NMDA receptors participate in pathological neuronal death through the process of glutamate-mediated excitotoxicity. Injury-driven unregulated release of glutamate triggers excessive activation of NMDA receptors and consequent inflow of excess Ca^{2+} through the NMDA receptor ion channel (Tymianski et al., 1993). The high amounts of intracellular Ca^{2+} can then induce proapoptotic signal transduction pathways ultimately causing neuronal death and dumping of the neuronal glutamate stores within the extracellular space to restart the excitotoxicity cycle on neighboring neurons (Choi, 1987). Additionally, damaging injuries to the brain can cause energy failure with neurons unable to maintain their hyperpolarized potential. The resulting depolarization relieves Mg^{2+} of NMDA receptors leading to their unopposed hyperactivation. The initial injury can be acute, as in ischemic stroke and traumatic brain injury, or part of the chronic manifestations of neurodegenerative diseases such as Parkinson's, Alzheimer's and Huntington's diseases, amyotropic lateral sclerosis and possibly multiple sclerosis. (Waxman and Lynch, 2005). In Alzhemier's disease and other dementia, dysregulation of NMDA receptor-mediated long-term plasticity may be a direct contributing factor to memory impairments (Malenka and Malinow, 2010). Glutamate-mediated excitotoxicity facilitates the growth and invasion of brain tumors, particularly malignant gliomas (Rothstein and Brem, 2001; Takano et al., 2001). Hyperactivation of NMDA receptors also generate hyperexcitable states of the nervous system prominent in seizure disorder and some form of dyskinesias (Brotchie, 2000; Kalia et al., 2008).

On the other hand, hypofunction of NMDA receptors can also contribute to disease states, most prominently schizophrenia. Reduction of normal NMDA receptor activity, whether in research studies or recreational intake of NMDA receptor antagonists such as ketamine and

PCP, can fully mimic the negative symptoms, cognitive impairments and physiologic disturbances apparent in schizophrenia (Luby et al., 1959; Krystal et al., 1994; Coyle, 2006). The NMDA receptor hypofunction hypothesis particularly implicates NMDA receptors situated on inhibitory interneurons in the prefrontal cortex (Woo et al., 1998). The resulting reduced excitatory drive of these interneurons leads to their decreased firing and subsequent decreased inhibition of their synaptically-connected downstream neurons throughout the brain. Thus, at the organ level, disinhibition of the overall brain circuitry likely manifests in clinical schizophrenia (Woo et al., 1998; Coyle, 2006). Furthermore, a number of risk genes in schizophrenia, such as G72 (Chumakov et al., 2002), GRM3 (Wroblewska et al., 1997), DTNP1 (Williams et al., 2004) and NRG1 (Petryshen et al., 2005), are involved in the glutamatergic transmission system, although their pathophysiological mechanisms are unknown.

NMDA RECEPTORS AS DRUG TARGETS

Based on their mechanisms and sites of action, drugs targeting NMDA receptors can be distinguished as competitive antagonists binding at the agonist-binding sites, non-competitive allosteric modulators binding at other extracellular sites and channel pore blockers. Most of the early attempts at clinical modulation of NMDA receptors were through competitive antagonists, such as selfotel (Davis et al., 1997; Morris et al., 1999) and gavestinel (Lees et al., 2000), and channel blockers, such as aptiganel (Albers et al., 2001) aimed at curbing glutamate-mediated excitotoxicity in acute ischemic stroke. Although, these first generation NMDA receptor drugs were neuroprotective both in vitro as well as in animal models of stroke (Waxman and Lynch, 2005), they were ultimately deemed failures in clinical trials due to unacceptable side-effects. The most prominent of the side-effects—hallucinations, drowsiness, memory and motor dysfunctions—were attributed to nonselective block of those NMDA receptors that were functional in normal CNS physiology (Birmingham, 2002; Kemp and McKernan, 2002; Kalia et al., 2008). To bypass these shortcomings, recent strategies have focused on more subtle modulation of NMDA receptor activity with some proving to be clinically successful.

One way of achieve subtle activity modulation is to target specific subunit compositions of NMDA receptors. Ifenprodil is one such drug which although not yet in clinical use is instructive on subunit-specific binding sites within the NMDA receptor ion channel complex. Ifenprodil selectively inhibits NMDA receptors containing the GluN2B subunit. It binds to an extracellular amino-terminal domain (NTD) on GluN2B from where it allosterically prevents opening of the ion channel pore despite the receptor being bound by agonists (Mony et al., 2009). The precise mechanism of action is unknown, although it might involve enhancement of the non-competitive and voltage-independent inhibition by protons (Traynelis and Cull-Candy,

1990; Mony et al., 2009). Although an NTD of similar size is present on all NMDA receptor subunits, the GluN2A and GluN2B NTDs so far appear to be sites through which endogenous (e.g., Zn^{2+} for GluN2A) and exogenous (e.g., ifenprodil for GluN2B) substances can modulate channel function, thus serving as drug targets.

The amino-adamantane derivatives, amantadine and memantine, are used clinically in Parkinson's and Alzhemier's diseases to attenuate glutamate-induced excitotoxicity (Lipton, 2005; Rezak, 2007). Part of their clinical efficacy reflects that, rather than blocking all NMDA receptors, they act in a more subtle, activity-dependent manner, affecting mainly pathologically overactive NMDA receptors (Lipton, 2007). Mechanistically, these agents have two modes of action, but the relative contributions of these modes to their clinical efficacy are unknown. Best understood is that they act as open pore blockers, blocking deep in the pore once the channel opens through endogenous mechanisms (i.e. ligand binding). Thus, they more readily block NMDA receptors that are pathologically overactive than the normally functional ones. Further, their low affinity and faster off-rates ensures rapid dissociation of NMDA receptors to permit a minimal level of activity (Traynelis and Cull-Candy, 1990; Mony et al., 2009).

In addition to their pore blocking actions, the amino-adamantane drugs exemplify a promising novel mechanism of action that controls the energetics of receptor gating. Within a thermodynamic context gating involves the energetic transfer of ligand binding into ion channel opening. These drugs, acting at sites away from where the ligands bind, can modulate gating by stabilizing receptor conformations that energetically favor a channel-closed state. They therefore facilitate closing of the ion channel and this action, independent of channel block, could underlie their high clinical efficacy, in contrast to other exclusive channel blockers, e.g. ketamine (Blanpied et al., 2005). This gating effect has been linked to a secondary binding site near the

external entrance to the channel, although its mechanistic basis is unknown (Chen et al., 1998; Sobolevsky et al., 2002; Kotermanski et al., 2009). Similar gating modulators selective for GluN2C- and GluN2D- containing NMDA receptors have recently been identified (Mullasseril et al.; Hansen and Traynelis). An exceptionally useful aspect of this mechanism of action is that gating can be bidirectionally controlled, shifting the energetic preference towards either channel-closed or open states depending on the need. Obviously, further advances in drug design will naturally follow unraveling of the molecular, structural and functional mechanisms underlying gating in NMDA receptors.

STRUCTURE/FUNCTION OF NMDA RECEPTORS

NMDA receptors, like all other members of the iGluR family, are modular proteins composed of four semi-independent domains (for a general review, see Traynelis et. al., 2010). The modular architecture is maintained both at the quaternary level of the tetrameric complexes and at the tertiary level of individual subunits (Fig. 1.2A & B). The NMDA receptor is an obligate heterotetramer consisting of two GluN1 subunits and two other subunits either of GluN2- A, B, C or D or GluN3- A or B. Expression patterns of the different GluN2 and GluN3 subunits, as well as alternately spliced forms of GluN1, are spatiotemporally regulated. For each subunit, starting at the N terminus is the amino-terminal domain (ATD) and then the ligand-binding domain (LBD), both located extracellularly. The LBD is made up of two discontinuous polypeptide segments S1 and S2, the latter of which is an extracelullar loop between transmembrane segments M3 and M4. Following the LBD is the transmembrane ion channel-forming domain (TMD) consisting of three full-pass transmembrane segments M1, M3 and M4 and a pore-loop (P-loop) M2. From the M4 transmembrane segment emerges the intracellular carboxy-terminal domain (CTD). Each one of these domains can function semi-independently and, with the exception of M4 and CTD, are likely evolutionary descendents of prokaryotic proteins with similar structures and related functions (O'Hara et al., 1993; Wo and Oswald, 1995; Wood et al., 1995; Paas, 1998; Kuner et al., 2003). Neither the ATD or the CTD are absolutely required for basic receptor function—that of ligand-induced opening of the ion channel—but they can modulate this gating process in physiologically important ways (Mohrmann et al., 2002; Gielen et al., 2009; Puddifoot et al., 2009; Hansen et al., 2010). The primary functions of these domains involve trafficking to cell surface (ATD & CTD), subunit-subunit recognition during tetrameric assembly (ATD), synaptic localization (CTD) and affecting intracellular signal

transduction pathways (CTD) (Traynelis et al., 2010; Mayer, 2011). Importantly though, the ATD and its associated linker to the LBD regulate the distinct gating energetics endowed by the specific GluN2 subunit, from the very low P_o (0.01) GluN2C/D- to the ~50-fold higher P_o (0.36-0.60) GluN2A- containing receptors (Gielen et al., 2009; Yuan et al., 2009). Structures of isolated ATDs have revealed that the ATD can dynamically adopt closed or open conformations that are mechanistically linked to the channel gate, either directly or indirectly via the intervening LBD (Jin et al., 2009; Kumar et al., 2009; Mayer, 2011). Moreover, in NMDA receptors the energetic preference of these closed versus open conformations can be tweaked by allosteric modulators like Zn^{2+} (binding to GluN2A and GluN2B ATDs) and ifenprodil, a drug that can specifically control function of GluN2B-containing NMDA receptors (Gielen et al., 2009; Karakas et al., 2009; Mony et al., 2009; Hansen et al., 2010). Nevertheless, the necessary and sufficient domains that mediate gating are the LBD and TMD (Fig 1.2C).

Gating dynamics in the ligand-binding domain.

The LBD, formed by the polypeptide segments S1 and S2, folds into a structure that resembles a clamshell or a venus fly-trap. S1 contributes mostly to the upper D1 (distal to the membrane) lobe and S2 mostly to the lower D2 (proximal to the membrane) lobe of this clamshell structure, although short segments of S1 and S2 contribute in vice-versa (Fig. 1.2C). Two D1 lobes from adjacent subunits make intersubunit contacts via both eletrostatic and hydrophobic helix-to-helix interactions, which in NMDA receptors stabilize a back-to-back heterodimer (GluN1/GluN2) arrangement (Furukawa et al., 2005). Thus, the LBD assembles as a dimer of dimers with an overall two-fold rotational symmetry. The D2 lobes that are more proximal to the TMD are relatively freer, as if suspended from D1 (Sun et al., 2002). The ligand-binding site is within the

interlobe cleft of each LBD. Unlike AMPA and kainate receptors, which use only glutamate as their agonist, NMDA receptor activation requires the binding of two different agonists: glutamate binding to GluN2 subunits and glycine binding to GluN1 and GluN3 subunits.

Multiple crystal structures of ligand- bound and unbound, as well as antagonist- and partial agonist- bound, iGluR subunits have revealed the global conformational dynamics of the LBD induced by ligand binding (Fig. 1.3). The ligand first docks at the upper surface of the interlobe cleft making direct contact with residues from the D1 lobe (Kuusinen et al., 1999; Jayaraman et al., 2000). All agonists commonly use their α-carboxyl and α-amino groups to interact with highly conserved residues primarily in the D1 lobe (Armstrong et al., 1998; Armstrong and Gouaux, 2000; Furukawa and Gouaux, 2003; Furukawa et al., 2005; Mayer, 2005a; Gill et al., 2008). Ligand specificity arises from subsequent interactions of their λ-positioned groups with divergent residues primarily in the D2 lobe (Furukawa et al., 2005; Yao et al., 2008). The D2 lobe swings upward making high affinity contacts with the ligand (Abele et al., 2000; Armstrong and Gouaux, 2000). This upward swing of the D2 lobe, through its attachment to the TMD, generates the required energy to open the ion channel pore (Fig 1.3B). Furthermore, the upward swing of the D2 lobe is made possible by the intersubunit contacts between two adjacent upper lobes. Thus, ligand-induced closure of the LBD clamshell occurs with the D2 lobe pulling upward against a stationary D1 lobe. The closed clamshell and accompanying open ion channel state of the receptor is energetically unfavorable. The receptor can return to a more favorable energetic state in one of two ways. First, it can either reopen the clamshell which consequently closes the transmembrane ion channel and initiates ligand dissociation from the LBD (Fig. 1.3A). Alternatively, at least for the related AMPA receptor, it can break the intersubunit D1-to-D1 dimer interface which moves the entire LBD with bound

ligand downward and consequently closes the channel—a ligand-bound nonconducting desensitized state of the receptor (Sun et al., 2002) (Fig. 1.3C). Recently, it was found that, in the absence of agonists, the AMPA receptor LBD is surprisingly mobile, spontaneously transitioning between the apo-like intact and desensitization-like broken D1-to-D1 dimer interface (Plested and Mayer, 2009). During gating and likely even in the apo form, these conformational dynamics at the LBD are propagated onto the ion channel.

Gating dynamics in the ion channel.

The ion channel part of the NMDA receptor is formed by the TMDs of the four subunits wrapping around a central pore with a 4-fold symmetry (Sobolevsky et al., 2009). The M3 transmembrane segment and M2 pore loop line respectively the external and internal halves of the pore. The M1 transmembrane segments surround the pore-lining segment, while the M4 transmembrane segments lies more externally making more extensive contacts with an adjacent subunit than with itself (Sobolevsky et al., 2009). The only crystal structure of an iGluR ion channel revealed the long suspected structural resemblance of the M1-M3 ion channel core to the K^+ channel (Wo and Oswald, 1995; Wood et al., 1995; Kuner et al., 2003; Sobolevsky et al., 2009). In essence, the ion channel core of an iGluR is an inverted K^+ channel without the K^+ selectivity. The evolutionary kinship between the iGluR and K^+ channels was cemented with the finding of a prokaryotic iGluR that is selectively permeant to K^+ channels (Chen et al., 1999a; Panchenko et al., 2001).

Gating in the ion channel (i.e. pore opening and closing) likely follows general dynamic patterns similar to K+ channels, although specific details are surely different. The M3 segment is the major channel gating element with its movement being directly controlled by the LBD

(Kohda et al., 2000; Jones et al., 2002; Sobolevsky et al., 2002; Yuan et al., 2005; Blanke and VanDongen, 2008). At the external mouth of the pore, the M3 segments from the four subunits make a bundle helical crossing that constitute the narrowest region of the pore. In an antagonist-bound state of an iGluR, this pore region was found to be constricted enough to sterically block ions from passing through and therefore, compounded with results from other studies, has been termed the ion channel gate (Chang and Kuo, 2008; Sobolevsky et al., 2009). Pore/gate opening most directly involves splaying apart, especially at this bundle helical crossing, of the four M3 segments away from the central pore axis. Additional pore opening movements also occur at the inner half of the pore by the four M2 pore loops, thus permitting complete transfer of cations from one side of the membrane to another. Contributions of the M1 and M4 segments to ion channel gating are less clear, but their movements are most likely not as extensive as the M3 segments. Comparison of ligand- bound and unbound isolated LBD crystal structures supports this idea, as LBD elements most proximal to the M3 segment undergoes the greatest movements upon ligand binding as compared to the LBD elements proximal to the M1, which is less mobile, and the M4, which is the least mobile, transmembrane segments (Armstrong and Gouaux, 2000) (Fig. 1.4).

Kinetic mechanisms of NMDA receptor activation.

For a single NMDA receptor, defining the kinetic mechanisms of activation gating has identified key energetic steps including intermediate states that follow ligand binding but precede full ion channel opening (Banke and Traynelis, 2003; Auerbach and Zhou, 2005; Schorge et al., 2005; Kussius and Popescu, 2009) (Fig. 1.5A & B). These states probably do not represent a single protein conformation but rather a continuum of transiently stable conformations with similar

energy profiles. In a linear gating scheme (Fig. 1.5C), $C_3 - C_2 - C_1 - O_1 - O_2$, comprising three short duration closed-time (C) components and the two aggregate open-time (O) components represents the central activation pathway, with ligand docking and initial clam-shell closure occurring prior to the receptor reaches C_3 (Kussius and Popescu, 2010). The two off-pathway longer duration closed-time components C_4 and C_5 represents the microscopic desensitized states (Dravid et al., 2008) (Fig. 1.5C). In essence, this linear gating scheme describes gating as a unified conformational wave across the quaternary structure of the protein starting with ligand binding and ending with channel opening.

Alternatively, a cyclic kinetic model of NMDA receptor activation that incorporates subunit-specific pre-open gating steps has also been advanced (Banke and Traynelis, 2003; Erreger et al., 2005a; Schorge et al., 2005) (Fig 1.5D). Immediately following ligand binding, the NMDA receptor undergoes two kinetically distinct channel closed/pre-open gating steps. In the linear model of NMDA receptor activation, the slower pre-open gating step ($C_3 \rightarrow C_2$) must occur before the faster one ($C_2 \rightarrow C_1$), whereas in the cyclic model, these sequential gating steps can occur in any order, either $C_3 \rightarrow C_s \rightarrow C_f$ or $C_3 \rightarrow C_f \rightarrow C_s$. Based on the localized effects of GluN1- and GluN2A- specific partial agonists, these fast and slow pre-open gating steps have been linked to the GluN1 and GluN2A subunits respectively. Thus, the cyclic kinetic model describes gating as proceeding through a fast GluN1-specific ($C_3 - C_f$) and a slow GluN2-specific ($C_3 - C_s$) pre-open gating steps, in any order (depicted by the loop), followed by concerted channel opening. A rapid equilibrium between a brief closed state after C_s/C_f in which both GluN1 and GluN2 are primed for pore opening steps is assumed. Furthermore, both microscopic desensitization states C_4 and C_5 are connected to the same C_3 state in this model

(Banke and Traynelis, 2003; Dravid et al., 2008). The precise molecular and structural correlates of these kinetically-defined stepwise gating transitions are yet to be discovered.

Concerted vs. subunit-independent gating.

Despite requiring two different agonists, glycine and glutamate, binding to two different subunits, GluN1/GluN3 and GluN2 respectively, NMDA receptors have been described to undergo a concerted gating mechanism (Benveniste and Mayer, 1991a; Clements and Westbrook, 1991; Schorge et al., 2005). In it, the two glycine and two glutamate molecules must first bind to their respective LBD and only then can the receptor complex progress through gating steps that ultimately culminate in opening of the ion channel pore (Fig. 1.6A). Thus, all four subunits act concertedly in opening of the channel pore. Whether any of the pre-open gating steps occur independently in a subunit (captured in the cyclic kinetic model) or concertedly across the quaternary receptor complex (captured in the linear kinetic model) is a matter of tense debate (Banke and Traynelis, 2003; Kussius and Popescu, 2009). In sharp contrast to NMDA receptors, the closely related AMPA receptor apparently undergoes subunit-independent gating (Rosenmund et al., 1998; Smith and Howe, 2000; Poon et al., 2010; Prieto and Wollmuth, 2010). In it, glutamate binding to a single subunit can trigger that pore opening actions only in that subunit manifested as a subconductance opening ion single-channel recordings (Fig 1.6B). Thus, depending on the number of activated subunits, anywhere from one to three subconductance in addition to the one full conductance levels have been reported for AMPA receptors (for a summary table, see Prieto & Wollmuth, 2010). Although it is thought that each of these conductance levels arise from pore opening actions of individual M3 segments, this has never been experimentally proven. It is possible that the subconductance levels could arise from

subunit-independent movements of other structural elements revealed in the recent AMPA receptor structure (Sobolevsky et al., 2009), such as the pre-M1 helix cuffing the channel gate (see below) or the M2 pore loops which did not crystallize well (perhaps due to crystallography artifact or inherent dynamism!)

Mechanisms coupling ligand binding to ion channel gating.

Ligand-induced structural changes in the LBD are physically coupled to opening/closing of the ion channel by way of three linkers—S1-M1, M3-S2 and S2-M4—connecting the LBD and TMD in a subunit (Fig. 1.2). These linkers provide the crucial medium for transfer of gating energetics between the LBD and the ion channel. The M3-S2 linker, due to its connection to the major pore-lining and channel gating element – the M3 segment, most directly carries this gating energy. Indeed, M3-S2 couples the ligand-induced conformational changes in the LBD to pore opening outward movements, either translational or rotational, of the M3 segment (Jones et al., 2002; Sobolevsky et al., 2002; Chang and Kuo, 2008). On the other hand, the peripheral S1-M1 and S2-M4, through their interactions with M3-S2 and other proximal structures, may modulate the gating process (Krupp et al., 1998; Villarroel et al., 1998; Yelshansky et al., 2004; Schmid et al., 2007; Talukder et al., 2010). As such, these linkers represent unexplored drug targets through which receptor activity can be regulated in a non-competitive manner (Balannik et al., 2005), separate from the mostly failed approaches of competitive and allosteric modulators and pore blockers (Lipton, 2006; Kalia et al., 2008).

Recently, a moderately high resolution look at the linker structures in an AMPA receptor has revealed some key features of their arrangements (Sobolevsky et al., 2009). In the homomeric GluA2-containing AMPA receptor structure, the linkers were observed to take on

two distinct conformations that mediate the 2-fold extracellular to 4-fold transmembrane symmetry mismatch. In the NMDA receptor, the two different linker conformations were postulated to be subunit-specific, with GluN1 adopting the A/C and GluN2 the B/D conformations. The functional consequences of these differences remain unknown, but if they exist in the NMDA receptor, likely translates into distinct glycine-mediated GluN1 and glutamate-mediated GluN2 gating steps.

Furthermore, the structure revealed short α-helical segments within the S1-M1 (pre-M1 helix) and S2-M4 (pre-M4 helix) linker. The pre-M1 helix appears to be ideally positioned to affect gating. It lays parallel to the membrane with its N-terminal and C-terminal ends in contact with the outer tips of M1 and M4 transmembrane segments. More importantly the four pre-M1 helices are snugly apposed with the M3 bundle-helical crossing, essentially forming a cuff around the M3 ion channel gate. Thus, for the gate to open, the pre-M1 helices must swing outward allowing for the pore opening movements of M3. Whether this movement of pre-M1 helix occurs simultaneously with or distinguishably prior to (a pre-open gating step) the M3 movements remains to be seen.

My thesis research has focused in on these LBD-TMD linkers to define both structurally and kinetically the mechanisms coupling ligand binding to ion channel gating in NMDA receptors. In chapter 2 of this thesis dissertation, I discuss my findings related to the modulatory roles the S1-M1 and S2-M4 linkers play in NMDA receptor gating. Specifically, I have identified localized positions within these linkers that can influence the energetics of gating and hypothesized the possible mechanisms in which they can do so. Intriguingly, I have defined potential sites and mechanisms of drug actions targeting the linkers and working as 'gating' modulators. In chapter 3, I describe my work addressing the importance of the conformational

freedom of M3-S2 relative to S2-M4 in activation gating. Specifically, I find that the relative gating movements of M3-S2 and S2-M4 in the GluN1 and GluN2A subunits are equivalent and that they occur concertedly across all four subunits during opening of the ion channel pore. The same approach that I have used successfully in my second project (chapter 3) can now be used to address the conformational gating dynamics of other structural elements, most excitingly of pre-M1 helix, as well as localize their possible roles in kinetically defined stepwise gating transitions.

FIGURES

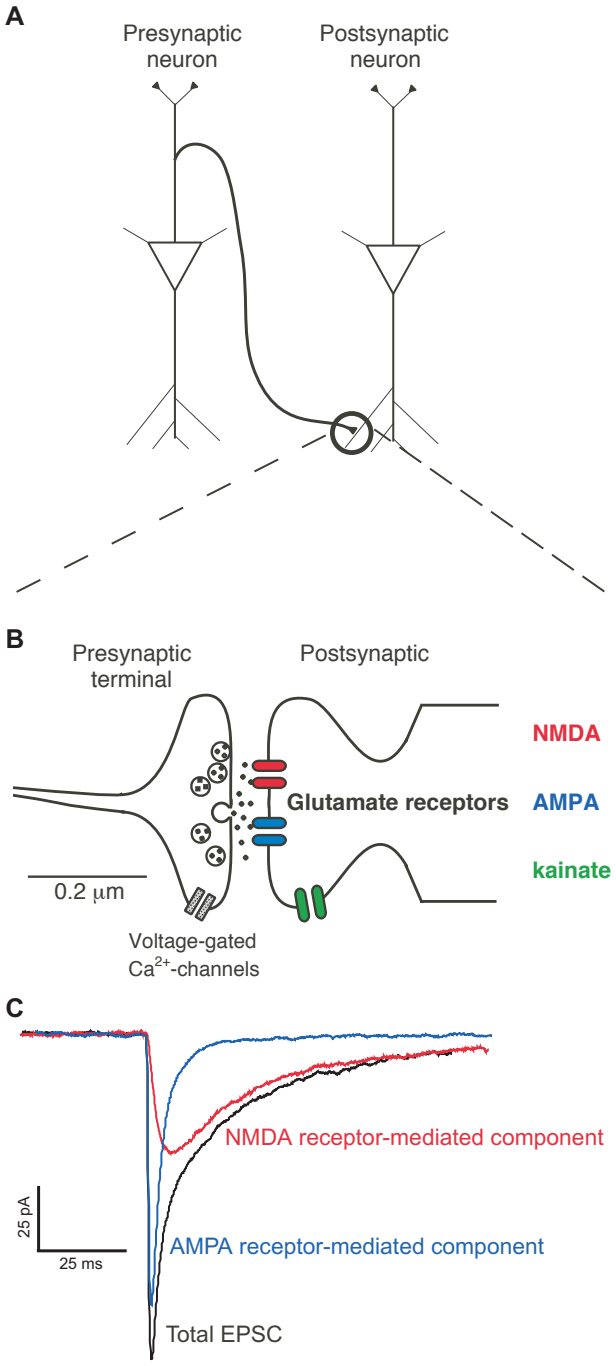

Figure 1.1. Glutamatergic synaptic transmission.

(A) Pictorial representation of a synaptically connected pair of neurons.

(B) The pre- and post- synaptic terminals of the two neurons shown in A. Incoming presynaptic action potentials activate voltage-gated Ca^{2+} channels, which triggers the membrane fusion of glutamate-filled vesicles. These synaptically-released glutamate then activate iGluRs embedded in the post-synaptic membrane. At most excitatory postsynaptic sites in the brain, the AMPA and NMDA receptors are situated at the synapse, whereas kainate receptors are situated extrasynaptically and also presynaptically (not shown).

(C) AMPA and NMDA receptor-mediated EPSCs at a synapse between a pyramidal and multipolar interneuron in the visual cortex. The NMDA receptor component was isolated by applying the AMPA receptor-specific antagonist CNQX. The fast and slow time-course of the AMPA and NMDA receptor-mediated current respectively is clearly contrasted. Unpublished data from L. P. Wollmuth.

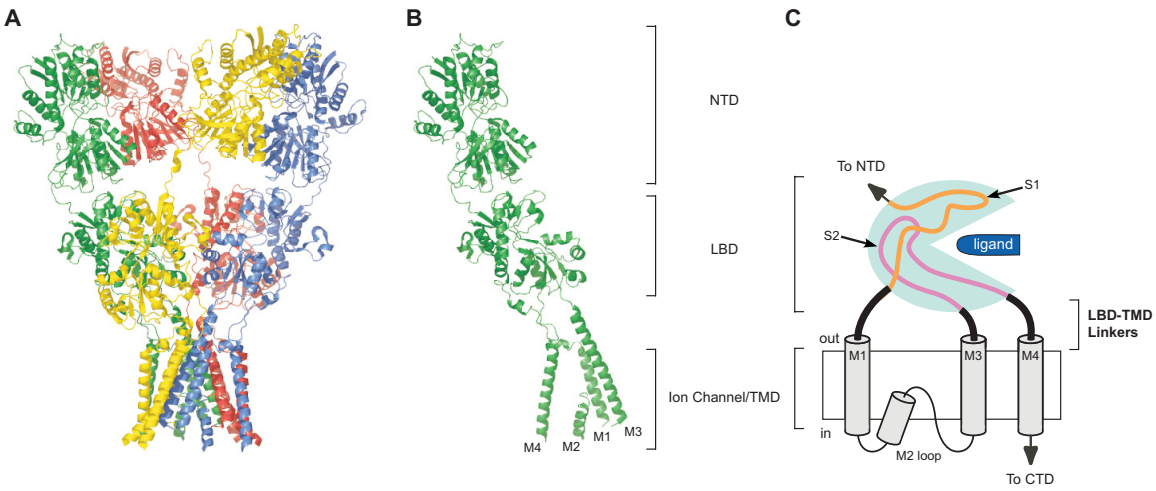

Figure 1.2. Structure of an IGluR.

Crystal structure at 3.6 Å of a homotetrameric GluA2 AMPA receptor (A) and one of its subunits (B) (PDB code 3KG2), as well as a schematic representation of a subunit (C). The receptor complex organizes in layers with the extracellular amino-terminal (NTD) and ligand-binding (LBD) domains and transmembrane ion channel-forming domain (TMD). The intracellular carboxy-terminal domain is absent from this crystal structure. From Sobolevsky et. al., 2009.

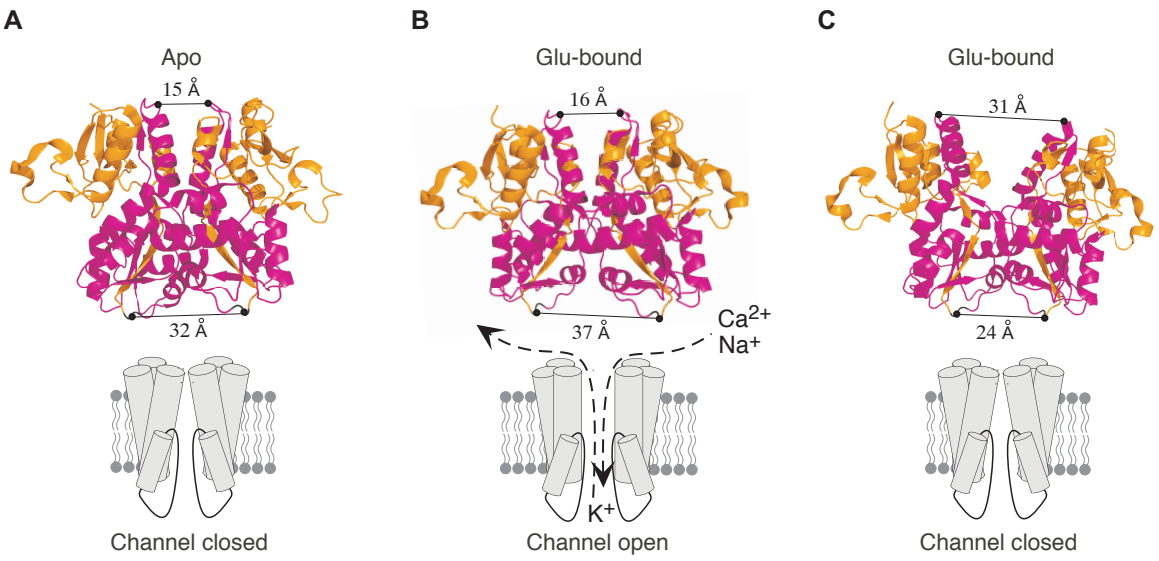

Figure 1.3. Global conformational changes during iGluR gating.

Ribbon (top) and schematic (bottom) representations of a dimeric LBD and associated TMDs respectively in various conformation states of an iGluR: resting (apo; PDB code 1FTO) (A), active (PDB code 1FTJ) (B) and desensitized (PDB code 2I3V). In the LBD S1 and S2 segments are colored as orange and magenta respectively. Distances between the inter-dimer interface at the upper lobe and membrane-proximal parts of the associated lower lobes are indicated.

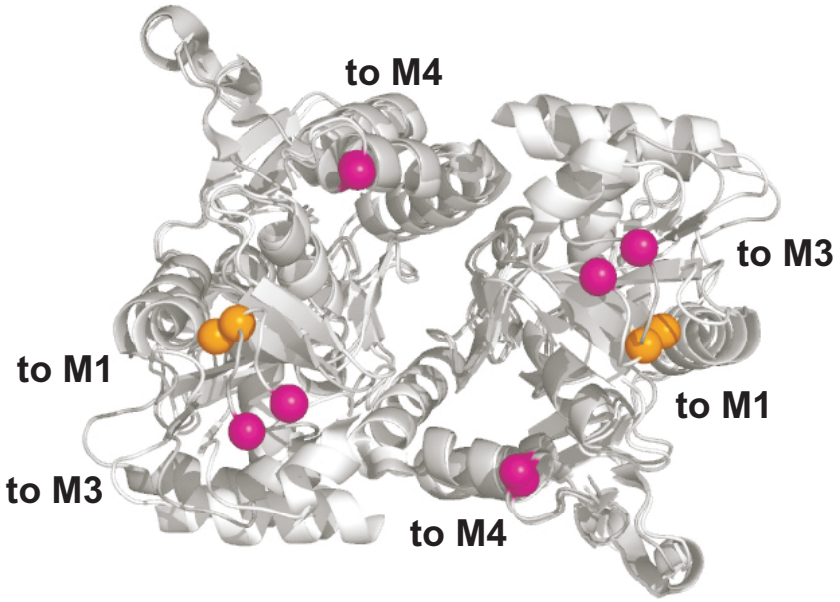

Figure 1.4. Conformational movements in the LBD leading to ion channel opening.

Superposed crystal structures of an apo (PDB code 1FTO) (white) and a glutamate-bound (PDB code 1FTJ) (gray) iGluR LBD dimer. The most membrane proximal LBD elements leading into M1, M3 and M4 transmembrane segments are shown as colored balls and labeled accordingly.

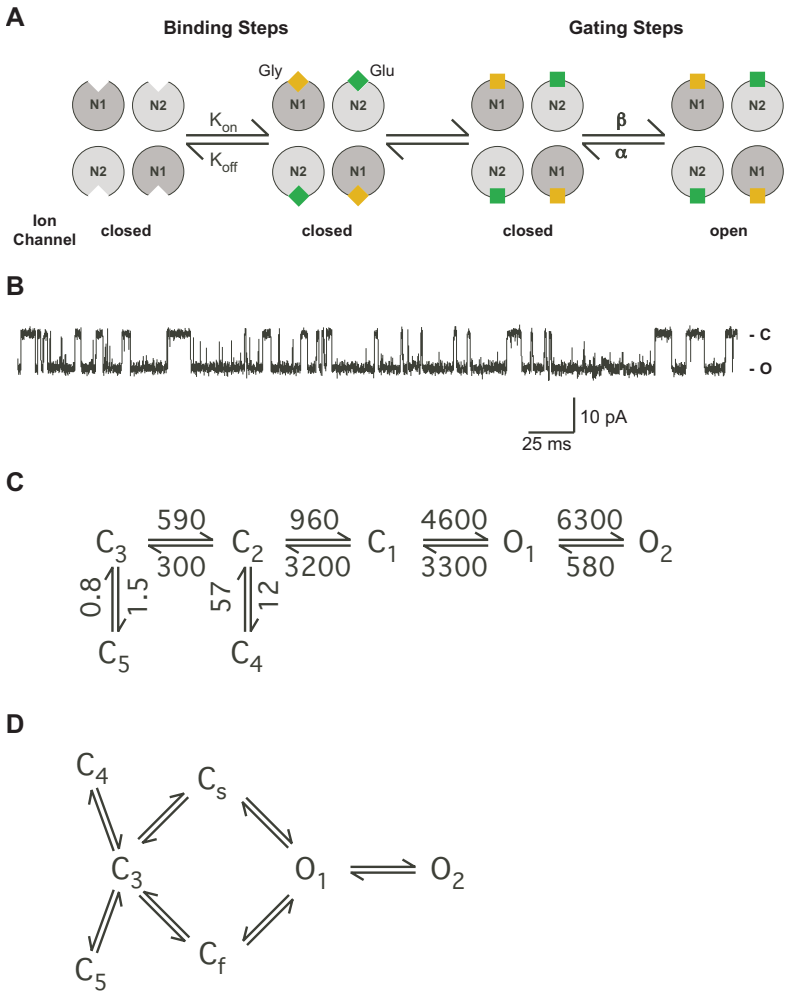

Figure 1.5. Kinetic mechanisms of activation in NMDA receptors.

(A) A global model of NMDA receptor gating. The ligand-binding steps constitute the binding of two glycine and two glutamate molecules to GluN1 and GluN2 subunits respectively. Only after the four agonists bind do the gating steps initiate, progress though multiple intermediate states and culminate in ion channel pore opening.

(B) Gating steps in an NMDA receptor. A cell-attached single-channel recording of GluN1/GluN2A NMDA receptor under saturating agonist concentrations (for more details see Fig. 3.4A). Multiple closed and open periods with distinct durations can be seen.

(C) A linear state model (Kussius and Popescu, 2009) of NMDA receptor activation with the rate constants (s^{-1}) of transitions averaged from fits of individual single channel recordings of GluN1/GluN2A containing NMDA receptors (see chapter 3). The central activation pathway, $C_3 - C_2 - C_1 - O_1 - O_2$, comprises multiple fully liganded channel-closed (C) and channel-open (O) state transitions. The off-pathway C_4 and C_5 are states related to microscopic desensitization. Ligand docking at the LBD and initial LBD closure around the ligand occurs prior to state C_3.

(D) A cyclic state model (Banke and Traynelis, 2003) of NMDA receptor activation. The $C_3 - C_s$ and $C_f - O_1$ transitions are equivalent and describe the slow pre-open gating transition suggested to be GluN2-specific. The $C_3 - C_f$ and $C_s - O_1$ transitions are equivalent and describe the fast pre-open gating transition suggested to be GluN1-specific. These putative subunit-specific transitions are followed by a very short duration pre-open state from where rapid concerted channel opening occurs. The $C_3 - C_4$ and $C_3 - C_5$ transitions represent processes related to microscopic desensitization.

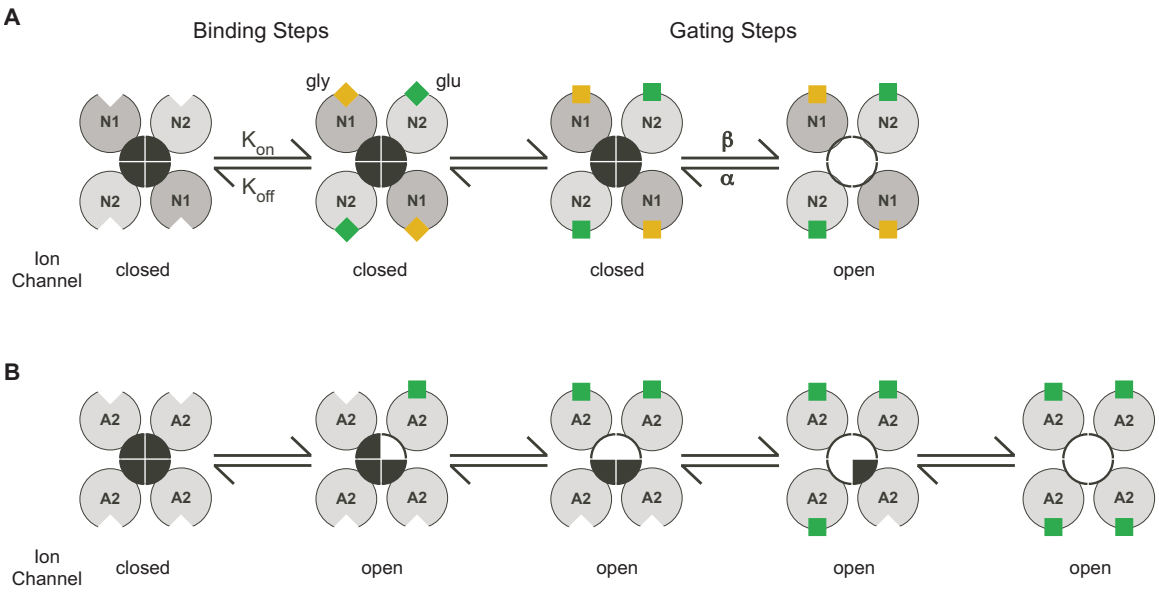

Figure 1.6. Concerted vs. subunit-independent gating in iGluRs.

(A) Pore opening in the NMDA receptor activation first requires binding of all four agonists, two glycine and two glutamate molecules binding to GluN1 and GluN2 respectively.

(B) In contrast, pore opening in AMPA receptors can occur partially with individual glutamate molecules binding to and triggering channel activation in individual subunits, which in single-channel electrophysiology manifest as subconductance current levels.

CHAPTER 2: SPECIFIC SITES WITHIN THE LIGAND-BINDING DOMAIN AND ION CHANNEL LINKERS MODULATE NMDA RECEPTOR GATING

ABSTRACT

Gating in the NMDA receptor is initiated in the extracellular ligand-binding domain (LBD) and is ultimately propagated via three linkers—S1-M1, M3-S2 and S2-M4—to the ion channel. M3-S2 directly couples LBD movements into channel gating, but the functional and structural contributions of S1-M1 and S2-M4 to the overall gating process are unknown. A scan of substituted cysteines in and around the NMDA receptor S1-M1 and S2-M4 with a bulky cysteine-reactive reagent identified numerous positions that showed potentiation of glutamate-activated as well as leak currents. As indexed by MK801, an open channel blocker, this potentiation was due to an increase in open probability, an interpretation confirmed for a subset of positions with single channel recordings. The magnitude of this gating effect, acting through S1-M1 or S2-M4, was dependent on the intrinsic gating properties of the NMDARs, being more effective in the inherently low open probability GluN2C- than the higher open probability GluN2A- subunit containing receptors. For the majority of these potentiation positions, we propose that alteration of gating arises from steric destabilization of contact interfaces where close apposition of the contacting partners is necessary for efficient channel closure. Our results therefore indicate that the NMDA receptor S1-M1 and S2-M4 linkers are dynamic during gating and can modulate the overall energetics of this process. Furthermore, the results conceptualize a mechanistic, as well as a possible structural, framework for pharmacologically targeting the linkers through non-competitive and subunit-specific modes of action.

INTRODUCTION

NMDA receptors (NMDAR), along with AMPA and kainate receptors, are ion channels gated by glutamate, the major excitatory neurotransmitter in the mammalian central nervous system. Glutamate-mediated signaling is essential for basic neuron-to-neuron signaling and higher order nervous system processes including learning, memory and pain perception (Cull-Candy and Leszkiewicz, 2004; Sudhof and Malenka, 2008). When aberrant, glutamate-mediated signaling, particularly involving the NMDAR, can trigger and/or complicate numerous acute (e.g., stroke & epilepsy) and chronic (e.g., Alzheimer's and Parkinson's) disease states, as well as psychiatric conditions (e.g., Schizophrenia) (Krystal et al., 2003; Waxman and Lynch, 2005).

A hallmark of NMDAR function is gating – the coupling of ligand binding/unbinding to ion channel opening/closing. The core structural components of this process are the extracellular ligand-binding domain (LBD) (S1 and S2) and the channel-forming transmembrane domain (M1-M4) (Fig. 2.1) (Mayer, 2005b; Oswald et al., 2007; Sobolevsky et al., 2009). Three peptide linkers—S1-M1, M3-S2 and S2-M4—couple the ligand-binding and transmembrane domains (Fig 2.1). M3-S2, by connecting to the pore-lining and major transmembrane gating element M3, is central to gating (Jones et al., 2002; Sobolevsky et al., 2002; Chang and Kuo, 2008). On the other hand, the peripheral S1-M1 and S2-M4, through their interactions with M3-S2 and other proximal structures, may modulate the gating process (Krupp et al., 1998; Villarroel et al., 1998; Yelshansky et al., 2004; Schmid et al., 2007). As such, these linkers represent unexplored drug targets where receptor activity can be regulated in a non-competitive manner (Balannik et al., 2005), separate from the mostly failed approaches of competitive and allosteric modulators and pore blockers (Lipton, 2006; Kalia et al., 2008).

A functional NMDAR has four subunits, typically two glycine-binding GluN1s and two glutamate-binding GluN2s. GluN2 has four isoforms (A-D), each imparting distinct biophysical properties to the intact receptor and having diverse spatiotemporal distributions within the CNS (Cull-Candy and Leszkiewicz, 2004; Paoletti and Neyton, 2007). A recent homotetrameric AMPAR structure (PDB ID 3KG2) revealed the general arrangement and conformations of the LBD-TM linkers. Notably, the linkers were shown to mediate the symmetry mismatch between the extracellular (2-fold) and transmembrane (4-fold) domains by taking on two different conformations. In the NMDAR, the two conformations are apparently subunit-specific (Sobolevsky et al., 2009). Nevertheless, there are limitations in relating specific linker positions in this AMPAR structure to their NMDAR counterparts due to variability in their lengths, amino acid composition and low resolution of certain linkers in the structure (supplementary Fig. 2.1). In addition, a single structural snapshot does not identify functionally important elements of gating.

Taking advantage of substituted cysteines, we identify specific positions encompassing the NMDAR S1-M1 and S2-M4 that can modulate gating. This modulation is subunit-specific, being dependent on the inherent gating properties as determined by the expressed GluN2 isoform (GluN2C or GluN2A). We propose that most of these positions are located at sites of transient gating-dependent interactions whose stabilization or destabilization can shift overall gating energetics towards the channel- open or closed states, respectively.

MATERIALS AND METHODS

Materials.

MTS reagents, 3-(Triethylammonium)propyl Methanethiosulfonate Bromide (PTrEA), [2-(Trimethylammonium)ethyl] Methanethiosulfonate Bromide (MTSET) and 2-Aminoethyl Methanethiosulfonate Hydrobromide (MTSEA), were purchased from Toronto Research Chemicals (Downsview, Ontario, Canada). The GluN1 glycine-site antagonist, 5, 7-Dichlorokynurenic acid (DCKA), was purchased from ToCris Bioscience (Ellisville, MO, USA). The GluN2 glutamate-site antagonist, DL-2-amino-phosphonopentanoic acid (APV), and the NMDA receptor channel blocker, MK801, were purchased from Sigma Chemicals (St. Louis, MO, USA).

Mutagenesis and expression.

Cysteine substitutions in the GluN1(K526-L533 in S1-M1 and S782-A888 in S2-M4) and GluN2C(R518-P525 in S1-M1 and N781-S789 in S2-M4) subunits were generated using PCR-based methods. Various cysteine-substituted GluN1 and GluN2C subunits were made previously: GluN1 positions D534-L544 (S1-M1), A635-R641 (M3-S2) and T789-A796 (S2-M4) (Beck et al., 1999); GluN2C positions P642-R645 (M3-S2) (Watanabe et al., 2002); and GluN2C positions S526-W537 (S1-M1), A630-V641 (M3-S2) and K790-G798 (S2-M4) (Sobolevsky et al., 2007). Mutations were initially made in clones present in a pSp64T-derived vector. Subsequently, a fragment encompassing the mutation was subcloned back into the wild-type template. All constructs were sequenced over the entire length of the replaced fragment. cRNA was transcribed for each expression construct using SP6 RNA polymerase (Ambion Inc.). The cRNA was examined electrophoretically on a denaturing agarose gel. Dilutions of RNA

(0.01-0.1 μg/μl) were prepared in order to achieve optimal expression. Wild-type and mutant GluN1 and GluN2C subunits were co-expressed in *Xenopus laevis* oocytes. Oocytes were prepared, injected and maintained as previously described (Sobolevsky et al., 2002). Recordings were made 2-5 days after injections.

In GluN2A, an endogenous cysteine (C399) reacts with MTS reagents resulting in ~ 30% inhibition of current amplitudes. Therefore, all of our studies involving GluN2A were done using a GluN2A construct in which this cysteine was mutated to an alanine (C399A) (Choi et al., 2001), referred to here as GluN2A'.

Whole-cell Current Recordings and Data Analysis.

Whole-cell currents of *Xenopus* oocytes were recorded at room temperature (20º C) using two microelectrode voltage clamp (TEVC) (DAGAN TEV-200A, DAGAN Corp.) with Cell Works software (*npi* electronic). Microelectrodes were filled with 3 M KCl and had resistances of 1-4 MΩ. To maximize solution exchange rates, we used a narrow flowthrough recording chamber with a small volume of ~70 ul. When recording GluN1-GluN2C, the external solution consisted of (in mM): 115 NaCl, 2.5 KCl, 0.18 $CaCl_2$ and 5 HEPES (pH 7.2, NaOH), unless otherwise noted. When recording GluN1-GluN2A', $BaCl_2$ was substituted for $CaCl_2$ (to prevent Ca^{2+}-dependent desensitization) and 100 μM EDTA (to minimize Zn^{2+}-mediated modification) was added to the external solution. All reagents, including glutamate (200 μM), glycine (20 μM), APV (100 μM), DCKA (10 μM), and MTS reagents, were applied with the bath solution.

Data analysis was done using Igor Pro (Wavemetrics, Inc.) and Microsoft Excel. For analysis and illustration, leak currents were subtracted from total currents. Results are presented as mean +/- SEM ($n \geq 4$). An ANOVA or Student's *t*-test was used to define statistical

differences. The Dunnet test was used for multiple comparisons. Significance was assumed $P < 0.05$.

Experimental Protocols.

NMDA receptor cysteine-substituted mutant channels were probed from the extracellular side with MTS reagents. MTS reagent-containing solutions were prepared, stored, and applied as previously described (Sobolevsky et al., 2002).

Steady-State Reactions. Steady-state reactions were quantified at a holding potential of -60 mV (see Figs. 2.2A-D). Baseline glutamate-activated current amplitudes (I_{pre}) were established by three to five 15-s applications of glutamate and glycine. All agonist or any other reagent applications were separated by 30 to 120 sec washes in glutamate-free solution. PTrEA (1 mM) was applied for 60 secs either in the presence of agonists or in their absence (but in the presence of the competitive antagonists APV and DCKA). After the PTrEA exposure, current amplitudes (I_{post}) were determined again using three to five agonist applications. MTSET (1 mM) or MTSEA (1 mM) was applied only in the presence of agonists. The change in glutamate-activated current amplitude, expressed as a percentage (% change), was calculated as: $= (1 - I_{post}/I_{pre}) \times 100$. In certain instances, we corrected for observed current rundown by fitting a single exponential function to a minimum of three pre-MTS reagent glutamate-activated current amplitudes.

MK801 inhibition. MK801 is an irreversible (on the time-scale of tens of minutes) open channel blocker at hyperpolarized potentials (Huettner and Bean, 1988) and correspondingly its rate/extent of block has been used previously to index P_o (Huettner and Bean, 1988; Jahr, 1992;

Rosenmund et al., 1995; Chen et al., 1999b). We quantified the rate of MK801 inhibition of open channels using the protocol shown in Fig. 2.6A-B. A continuous MK801 application in the presence of agonists was started after glutamate-activated currents had reached steady-state (typically 15-30 secs) or after PTrEA had potentiated glutamate-activated currents to steady-state levels (typically 45-75 secs). Through an initial trial-and-error process for each cysteine-substituted receptor, we adjusted the concentration of MK801 to reach maximal block within 4-10 mins: 300 nM for GluN2C(A630C); 200 nM for GluN1(P787C); 150 nM for GluN2C(E635C); 25 nM for GluN2C(S533C); and 50 nM for the remaining cysteine-substituted receptors. Resulting changes in current amplitude were fitted with a single exponential function. The reciprocal of the time constant (τ) of this fit multiplied by the concentration of MK801 defined the apparent 2nd order rate constant for block: $k = 1/(\tau[\text{MK801}])$. We used the rate of MK801 whole-cell current inhibition to index relative P_o, not an absolute P_o which could be complicated since, in addition to open channel block, MK801 might also interact with the gating machinery (Dilmore and Johnson, 1998). Moreover, for GluN1-GluN2C, (+)MK801 (the stereoisomer we use) does not have the paradoxical pH dependence of increasing the affinity of channel block despite lowering P_o that (-)MK801 exhibits (Dravid et al., 2007).

Reaction Rates. Reaction rates in the presence of glutamate and glycine (k_+) and in their absence but in the presence of APV and DCKA (k_-) were determined using "pulsive" protocols (see Fig. 2.9A & B), as described in detail in Sobolevsky et. al., (2002). Changes in current amplitude were fitted with a single exponential. The reciprocal of the time constant (τ) of this fit multiplied by the concentration of the MTS reagent defined the apparent 2nd order rate constant for chemical modification k_+ or $k_- = 1/(\tau\,[C])$.

Single Channel Recordings and Analysis.

Prior to recording, oocytes were bathed in a hypertonic solution consisting of (in mM): 200 K-aspartate, 20 KCl, 5 EGTA, and 10 HEPES (pH 7.4, KOH) for 5-15 mins and then manually devitellinized. Oocytes were then placed in the recording chamber under the continuous flow of a bathing solution (in mM): 115 NaCl, 2.5 KCl, 0.50 $CaCl_2$, 1 $MgCl_2$ and 5 HEPES (pH 7.2, NaOH). Currents in outside-out patches, isolated from these oocytes, were recorded at room temperature (20-23º C). The recording external solution, which was applied using a single barrel application pipette, was the same as the bathing solution but without added $MgCl_2$; to this solution, we added 0.5 mM glycine and 1 mM glutamate (pH 7.2, NaOH) with or without PTrEA (1 mM). The internal pipette solution contained (in mM): 10 KCl, 90 Kgluconate, 2 MgATP, 5 Phosphocreatine, 1 BAPTA and 10 HEPES (pH 7.4, KOH).

Microscopic currents were recorded using an Axopatch 200B amplifier (Molecular Devices, Sunnyvale, CA) with PatchMaster software (HEKA Elektronik, Lambrecht, Germany) and were initially filtered at 10 kHz using a 4 pole low-pass Bessel filter and digitized at 50 kHz. All recordings were made at –80 mV. Pipettes were pulled from thick-walled borosilicate glass, coated with Sylgard (Dow Corning, Midland, MI) and fire polished immediately before use. Pipette resistances were 5-25 MΩ when filled with the pipette solution and measured in the bathing solution. The pipette holder was cleaned daily with 70% ethanol and stored in Drierite overnight. The level of the batch solution was kept as low as possible. A typical experiment consisted of at least three continuous control pre-PTrEA 30 second applications of agonists, followed by a 1 min exposure to agonists+PTrEA (1 mM), and then back to continuous agonist application until the patch became unstable. Although patches certainly contained multiple

channels (the exact number was unknown but presumably was between 1-8), GluN1-GluN2C receptors have a very low P_o (0.01) (Dravid et al., 2008), making double openings extremely rare (< 2% of the time). If double openings were more prominent in the baseline recording, we terminated the experiment.

Currents were exported from PatchMaster to Igor Pro for initial processing including subtraction of mean baseline current, resampling and additional filtering. Records were then exported from Igor Pro to QuB (www.qub.buffalo.edu) for idealization. Idealized records were then exported back to Igor Pro and/or ChannelLab (Synaptosoft, Inc., Decatur, GA) for further analysis.

Idealization of records using QuB. Currents were resampled at 25 kHz and digitally refiltered at 5 kHz to a final frequency of ≈4.5 kHz. Idealization was done, with an imposed 'dead time' of 40 μs (resolution of 80 μs), using the SKM method (Qin, 2004) with a model that had two open classes and one closed class (Stern et al., 1992; Dravid et al., 2008), all interconnected. The amplitude and standard deviation for the single closed state (baseline) was defined using the 'grab' function in QuB. We initially also used the 'grab' function to estimate amplitudes of the two open classes for wild type and mutant receptors. The current amplitudes were qualitatively comparable. Nevertheless, to reduce variability due to the specific starting values 'grabed', we set the current amplitudes of the two open classes to –3.2 and –1.8 pA, based on previously published values for single channel conductance sublevels for recombinant GluN1-GluN2C receptors expressed in oocytes (Stern et al., 1992). The initial standard deviations of these open classes were set to that for baseline. We then allowed the mean current levels and standard deviations to be reestimated during idealization.

Current amplitudes for the two conductance levels (lower and higher) were derived from all-point histograms (QuB). Mean lifetimes were derived from single exponential fits to dwell-time histograms of the identified conductance levels. Two exponentials were fit to dwell time histograms of composite open times (ChannelLab). Patch P_o was determined from the total open time (low + high conductance) divided by the total time of the recording. We did not correct for missed events, which would be about equivalent for both before and after PTrEA.

RESULTS

To identify key positions in the NMDAR linkers that can influence gating , we took advantage of substituted cysteines in and around the GluN1 and GluN2C linkers (Fig. 2.1C). We screened these substituted cysteines, one at a time, with the cysteine-reactive reagent 3-(Triethylammonium)propyl Methanthiosulfonate bromide (PTrEA), anticipating that, given its positive valence and large size, it might in certain instances affect gating movements of the linkers.

Accessibility scan of the GluN1 and GluN2C linkers.

The protocol used to determine the effect of PTrEA on whole-cell glycine- and glutamate-activated (referred to as glutamate-activated) current amplitudes for cysteine-substituted NMDARs is illustrated in Fig. 2.2. We compared current amplitudes before (I_{pre}) and after (I_{post}) exposure to extracellular PTrEA (1 mM, thick lines) applied in the continuous presence of agonists (Fig. 2.2A-C). We also determined PTrEA accessibility in the absence of agonist, but in the presence of the competitive antagonists DCKA (at the GluN1 site) and APV (at the GluN2 site) to minimize channel opening (Fig. 2.2D). Since NMDARs composed of GluN1 and GluN2C subunits do not undergo any apparent desensitization (Krupp et al., 1996), we assume that, during PTrEA application, the cysteine-substituted GluN1-GluN2C receptors exist primarily in the open and closed states (in the presence of agonists) or in the closed state (in the absence of agonists but presence of antagonists). Similar exposures of wild-type GluN1-GluN2C receptors to PTrEA produced no significant changes in current amplitudes indicating that possible modifications of endogenous cysteines do not affect receptor function.

In terms of whole-cell glutamate-activated currents, three distinct outcomes were observed following PTrEA exposure to cysteine-substituted GluN1-GluN2C receptors: no significant change (Fig. 2.2A), inhibition (Fig. 2.2B) or potentiation (Fig. 2.2C & D). Figs. 2.3-2.5 summarize the mean percent change (% change) in glutamate-activated current amplitudes of wild-type and mutant GluN1-GluN2C receptors containing substituted cysteines in and around S1-M1 (Fig. 2.3), M3-S2 (Fig. 2.4) or S2-M4 (Fig. 2.5) with PTrEA applied either in the presence (PTrEA+, left) or absence (PTrEA-, right) of agonists. Unfilled bars indicate cysteine-substituted positions where PTrEA application did not significantly change glutamate-activated current amplitudes. Filled bars showing either current inhibition (+ % change) or potentiation (- % change) indicate positions where % change was significantly different from that observed in wild-type GluN1-GluN2C. GluN1(S535C) and GluN2C(L529C) (Fig. 2.3A & B), denoted by the symbol X, showed no detectable glutamate-activated currents. Current amplitudes in GluN2C(L791C) (denoted by asterisk in Fig. 2.5B) never reached steady-state (up to 4 min agonist application, data not shown), but they were clearly altered in response to PTrEA. PTrEA-induced current potentiation for GluN2C(I793C) (denoted by double asterisks in Fig. 2.5B) never reached steady-state (up to 5 mins and 4 mM PTrEA application was attempted, data not shown). Panel C in Figures 2.3-2.5 shows a summary of the effects of PTrEA, when applied in the presence of agonists, on the positions tested (adjacent circle): no effect- open circle; inhibition- black circle; and potentiation- red circle. Positions where leak currents, i.e. currents in the absence of agonists, were significantly altered following PTrEA [e.g., GluN2C(S789C), Fig. 2.2C; supplemental Table 2.1] are highlighted in green.

Interpretation of PTrEA-induced effects on cysteine-substituted positions.

Due to their extracellular location, the GluN1-GluN2C linkers are widely accessible, with most cysteine-substituted receptors undergoing significant PTrEA-induced changes in glutamate-activated current amplitude (inhibition or potentiation, 68 of 87 positions tested). Additionally, some of the seemingly inaccessible positions, i.e. the white positions [e.g., GluN1(P642C) and GluN2C(I633C), both in M3-S2, Figs. 2.4A & B], might be accessible, but reaction with PTrEA did not affect glutamate-activated current amplitudes (silent reaction). Overall, the linkers showed limited differences in reactivity when PTrEA was applied either in the presence or absence of agonists. This lack of discrete state-dependence probably reflects the extracellular location of the linkers, with no physical barriers (i.e. activation gate, membrane lipids, etc.) preventing global access, but it does not preclude the possibility of local state-dependent restrictions on accessibility below the limits of resolution of the steady-state protocol.

Of the positions that do undergo significant PTrEA-induced changes in glutamate-activated current amplitudes, notable are those that show potentiation following PTrEA (red positions in Figs. 2.3C, 2.4C and 2.5C). Previously it was proposed, albeit untested, that potentiation following modification by MTS reagents reflects a gating effect with the overall energetics shifted towards channel opening (Yuan et al., 2005; Sobolevsky et al., 2007). Consistent with this idea, eight of the 18 potentiation positions showed significant PTrEA-induced increases in leak current (supplemental Table 2.1), suggesting constitutive channel opening following PTrEA (note only nine total positions showed significant PTrEA-induced increases in leak currents). Surprisingly, the potentiation positions are prominent in S1-M1 and S2-M4—regions typically not associated with channel gating.

To address the linkers' possible role in gating, we considered the basis for PTrEA-induced changes in current amplitudes by focusing mainly on potentiation positions. Macroscopic

whole-cell currents (I_{wc}) are defined by the equation, $I_{wc} = N\gamma P_o$, where N is the number of surface receptors, γ is the single channel conductance and P_o is the channel's open probability. Within the seconds-to-minutes timescale of PTrEA reaction and consequent modification of current amplitudes, it is unlikely that N changes. Hence, a change in whole-cell current following reaction to PTrEA (or any other MTS reagent) is the net effect of changes in γ (a conductance effect) and P_o (a gating effect), $\Delta I_{wc} = \Delta\gamma + \Delta P_o$.

The rate of channel block by MK801 becomes faster in receptors showing PTrEA-induced current potentiation,

Initially, to test whether an increase in P_o underlies PTrEA-induced current potentiation, we measured rates of whole-cell current inhibition by the largely irreversible NMDA receptor open channel blocker MK801 (Huettner and Bean, 1988). Since access to the MK801 blocking site in the pore depends on channel opening, the rate of MK801 block in wild-type and cysteine-substituted/PTrEA-treated receptors should be proportional to P_o, assuming that MK801's interaction with its blocking site is not greatly perturbed (see Material & Methods and supplemental Fig. 2.2).

Figure 2.6A illustrates MK801-mediated inhibition of glutamate-activated whole-cell current in wild-type GluN1-GluN2C. NMDAR P_o is highly dependent on the GluN2 subtype (Chen et al., 1999b; Gielen et al., 2009), with GluN2C-containing receptors ($P_o \sim 0.01$) (Dravid et al., 2008) having a ~40-fold lower P_o than GluN2A-containing receptors ($P_o \sim 0.36$-0.50) (Erreger et al., 2004; Gielen et al., 2009). Accordingly, the rate of MK801 current inhibition (see Materials and Methods), as determined by the fit of a single exponential function to the time course of MK801 inhibition of glutamate-activated current (Fig. 2.6C, dashed overlay) was dramatically slower

for GluN1-GluN2C (k = 2.68 x 10^5 ± 7000 $M^{-1}s^{-1}$, n = 8) than for GluN1-GluN2A' (k = 7.44 x 10^6 ± 1300000 $M^{-1}s^{-1}$, n = 13, see below and also Gielen et al., 2009).

We compared the rate of MK801 current inhibition for all GluN1- and GluN2C- potentiation positions without (open circle) and following (filled circles) PTrEA (Figs. 2.6B-D). We did not undertake these and subsequent experiments for two S2-M4 potentiation positions: GluN1(T789C) (Fig. 2.5A), because its pre-PTrEA current amplitude was small (I_{pre} < 30 nA), making it difficult to obtain a reliable measure of the rate of MK801 inhibition; and GluN2C(I793C), because PTrEA-induced current potentiation did not reach steady-state (Fig. 2.5B, double asterisks). Additionally, all three M3/M3-S2 potentiation positions, GluN1(A635C), GluN2C(A630C) and GluN2C(E635C), showed significantly reduced steady-state MK801 inhibition either before and/or after PTrEA application, along with additional inconsistencies, including a notable rebound of current at the end of the MK801 application (supplemental Fig. 2.2). Because these deviations suggest that MK801 block itself was disrupted (Yuan et al., 2005; Chang and Kuo, 2008), we did not analyze these M3/M3-S2 potentiation positions further.

For certain positions in S1-M1 and S2-M4, the cysteine substitution itself significantly altered the rate of MK801 inhibition from that of wild-type ($k \approx$ 2.68 x 10^5): GluN1(P787) at S2-M4 (k = 2.72 x 10^4 ± 2000, n = 6), GluN2C(S533C) at S1-M1 (6.26 x 10^5 ± 85000, n = 7) and GluN2C(D792C) at S2-M4 (4.95 x 10^5 ± 85000, n = 5) (Figs. 2.6C & D, denoted by asterisks). Following PTrEA, all tested GluN1- and GluN2C- potentiation positions showed a significant increase in the rate of MK801 inhibition (Figs. 2.6C & D) suggesting that their open probability (P_o) was increased. Surprisingly, the relationship between the increase in P_o and the corresponding potentiation of current amplitudes showed a poor correlation (R^2 = 0.37) when the

GluN1- and GluN2C- potentiation positions were pooled together (Fig. 2.6E, GluN1 + GluN2C). However, when the GluN1- and GluN2C- potentiation positions were considered separately, the resulting correlation drastically improved, with R^2 values of ~0.8 for either GluN1 or GluN2C (Fig. 2.6E). We do not fully understand this difference between the subunits but it may be a manifestation of subunit-specific contributions to channel gating (e.g., (Banke and Traynelis, 2003; Blanke and VanDongen, 2008). Nevertheless, the key point here is that the strong correlation within a subunit strongly supports the idea that potentiation is being driven mainly by an increase in P_o. The use of MK801 to index a relative P_o is further supported by results with PTrEA-induced inhibition positions (supplemental Fig. 2.3).

Single channel activity in a patch increases following PTrEA exposure to receptors containing potentiation positions.

Although the MK801 results support the idea that potentiation reflects an increase in P_o, there could be some unanticipated systematic effect of PTrEA on the rate of MK801 block. To further verify that PTrEA-induced potentiation is driven by an increase in P_o, we measured single channel activity from outside-out patches isolated from *Xenopus* oocytes for wild type receptors and a subset of potentiation positions before and after PTrEA (Fig. 2.7). We selected one potentiation position in GluN1 S1-M1 (S531), one in GluN2C S1-M1 (V523) and one in GluN2C S2-M4 (S788). Patches certainly contained multiple receptors and we refer to the total time the patch spent in an open state (lower plus higher conductances) as the 'Patch P_o' (see Materials & Methods). For wild type receptors, the two conductance levels were comparable in amplitude to those reported previously in oocyte patches (Stern et al., 1992) though the mean lifetimes, especially for the higher conductance level, were somewhat longer (supplemental

Table 2.2). As with macroscopic experiments, PTrEA had no notable effects on single channel currents of wild-type receptors, though there was a slight but insignificant trend towards a reduced patch P_o ($P_{o,post}/P_o$ = 0.72 ± 0.04, n = 3) (Fig. 2.7B, right). The three receptors with cysteine-substituted potentiation positions before PTrEA were indistinguishable from wild-type receptors (supplemental Table 2.2). In contrast, following PTrEA, all three potentiation positions showed a significant increase in patch activity [$P_{o,post}/P_o$, GluN1(S531C), 3.64 ± 0.67; GluN2C(V523C), 2.13 ± 0.23; GluN2C(S788C), 3.02 ± 0.46, n = 3 for each] (Figs. 2.7A & B, right). For GluN2C(V523C) and GluN2C(S788C), PTrEA did not affect the amplitude of either the lower- or higher-conductance levels (Fig. 2.7B, left). For GluN1(S531C), however, along with an increase in P_o, PTrEA also significantly reduced the amplitude of the higher conductance (γ_{post}/γ, 0.91 ± 0.02) (Fig. 2.7B). Analysis of open-time distributions before and after PTrEA showed no significant alterations (Fig. 2.7C), suggesting that the increase in P_o was due to a decrease in closed time rather than an increase in open time. Overall, in agreement with the MK801 results, the single channel recordings indicate that PTrEA induces a strong increase in open probability, consistent with the idea that current potentiation arises mainly if not exclusively (at least for the three tested positions) from a gating effect of increasing channel P_o.

GluN1- potentiation positions show reduced PTrEA-induced current potentiation when co-expressed with GluN2A'.

Wild-type GluN1-GluN2C receptors have a low P_o (~0.01) (Dravid et al., 2008). As judged by MK801 inhibition kinetics, all GluN1-GluN2C cysteine-substituted potentiation positions yield receptors with P_o in a similarly low range (Figs. 2.6C & D). Following their reaction with PTrEA, all of these potentiation positions showed significant increases in relative P_o (Figs. 2.6C

& D and 7). On the other hand, wild-type GluN1-GluN2A inherently has a high P_o (~0.36 - 0.50) (Erreger et al., 2004), making further increases in P_o limited (it can increase a maximum of ~2-3-fold to reach P_o = 1). If whole-cell current potentiation is a gating effect arising from an increased P_o, we reasoned that GluN1-potentiation positions, identified based on co-expression with GluN2C, would show an attenuated degree of PTrEA-induced current potentiation when co-expressed with GluN2A' (a mutant GluN2A subunit where an endogenous cysteine was mutated to alanine, see Materials and Methods). Figs. 2.8A–C show the effect of PTrEA on whole-cell currents for the same GluN1-potentation positions co-expressed with either GluN2C (Figs. 2.8A & B, left panels) or GluN2A' (Figs. 2.8A & B, right panels). As expected, PTrEA-induced potentiation for all GluN1-potentiation positions (Fig. 2.8C) was significantly reduced when co-expressed with GluN2A' (e.g., GluN1(R783C)-GluN2A', Fig. 2.8A) and in some instances was reversed to current inhibition (e.g., GluN1(S531C)-GluN2A', Fig. 2.8B).

Two GluN1 cysteine-substituted positions, S531C and D534C, showed PTrEA-induced current inhibition when co-expressed with GluN2A' (Figs. 2.8B & C). Interestingly, GluN1(S531C), when coexpressed with GluN2C underwent dual PTrEA-induced effects of increase in P_o and decrease in γ (Fig. 2.7B). We reasoned that this inhibition of GluN1(cys)-GluN2A' receptors was due to a reduction in γ, an effect masked in NR2C-containing receptors because of their greater increase in P_o driving net whole-cell current potentiation. To test this, we measured the rates of MK801-mediated inhibition of currents in GluN1(S531C)-GluN2A' and GluN1(D534C)-GluN2A' without (open circles) and following (filled gray circles) reaction to PTrEA (Figs. 2.8D & E). As a reference, we also measured the rate of MK801 current inhibition for GluN1-GluN2A' (Fig. 2.8E). Following PTrEA, the rate of MK801 current inhibition for GluN1 S531C and D534C, coexpressed with GluN2A' was not significantly altered (k_{post}/k values = 0.98 ± 0.2

and 1.63 ± 0.4, respectively), in contrast to what occurred when they were co-expressed with GluN2C (Fig. 2.6C). Thus, the absence of any observable PTrEA-induced changes in P_o, as judged from MK801 inhibition kinetics, suggests that a reduction in γ underlies whole-cell current inhibition for these two GluN1 positions co-expressed with GluN2A'.

Overall, these results are consistent with PTrEA-induced current potentiation reflecting mainly a gating effect—an increase in P_o. Intriguingly, they also suggest that such modulation of NMDAR gating, mediated by the linkers, is dependent on the receptor's intrinsic P_o, as determined by the expressed GluN2 isoform (GluN2C versus GluN2A). Finally, these results highlight that PTrEA-induced changes in whole-cell currents are the weighted sum of changes in gating (P_o) and conductance (γ).

PTrEA accessibility to the potentiation positions is typically reduced in the channel-closed state.

PTrEA-induced potentiation of currents in GluN1-GluN2C cysteine-substituted receptors is driven by an apparent gating effect, but what is its structural basis? Many alternatives could be envisioned including that PTrEA in some way increases the rigidity of a specific linker, increasing the efficacy of coupling the conformational change in the LBD to channel opening. Another possibility, the 'closed-state contact' hypothesis, is that potentiation positions are located at points of contact with other structural elements—possibly other linkers, proximal parts of the LBD, transmembrane segments and/or membrane lipids (Sobolevsky et al., 2007). The bulky PTrEA side-chain in such a contact interface would therefore sterically (and/or perhaps electrostatically) limit close (though not necessarily tight) apposition of the contacting partners. If this contact interface is part of an energetically stable closed state, then the energetics of

activation gating would be shifted towards channel opening after PTrEA, resulting in an increased P_o and current potentiation.

If the 'closed-state contact hypothesis' is correct, positions at such interfaces should show restricted accessibility in the closed compared to the open state. None of the potentiation positions in and around S1-M1 (Fig. 2.3) and S2-M4 (Fig. 2.5) showed discrete binary state-dependence to PTrEA, but these steady-state reactivity experiments (Figs. 2.2-2.5) have low resolution for determining state-dependent accessibility. We therefore measured modification rates for PTrEA applied in the presence of agonists, when the channels are open and closed (Fig. 2.9A, left), or in their absence, when the channels are presumably closed (Fig. 2.9A, right). For these experiments, we focused on positions that showed >100% steady-state potentiation because of the complications of measuring reaction rates for less robust current potentiation. For 6 of 8 tested positions (S531C & P787C in GluN1 and R518C, V523C, S788C & S789C in GluN2C), modification rates for PTrEA were significantly slower in the absence of agonist (k_-, unfilled circles) than in their presence (k_+, filled circles) (Figs. 2.9B & C, left), with k_+/k_- ratios ranging from ~3 to ~130 (Figs. 2.9B & C, right). The reduced accessibility in the absence of agonists for these potentiation positions support the notion that they are at contact interfaces in the closed state. For the two other positions, modification rates for PTrEA were either not significantly different [GluN1(K526C), Fig. 2.9B] or actually faster [GluN2C(E530C), Fig. 2.9C] in the absence than the presence of agonists, suggesting that other mechanisms besides the 'closed-state contact' may underlie PTrEA-induced changes in gating.

Degree of whole-cell current potentiation is dependent on the size of the reactive reagent.

An additional prediction of the 'closed-state contact' hypothesis is that reagents less bulky than PTrEA would have reduced steric effects and would produce less dramatic increases in P_o, and correspondingly would elicit attenuated degrees of current potentiation. We therefore compared the effects of three differently sized (but same valence and general structure) MTS reagents—PTrEA, MTSET and MTSEA, from large to small respectively (Fig. 2.10A)—on currents for GluN1- and GluN2C- potentiation positions. Because this assay is less dependent on initial (pre-MTS) current amplitudes, we were able to test all S1-M1 and S2-M4 potentiation positions. In general, with smaller-sized reagents (i.e. MTSET and MTSEA), the main phenotypes were either an incremental reduction in potentiation (e.g. GluN2C(S789C) in S2-M4, Fig. 2.10B) or a reversal to net inhibition (e.g. GluN1(S531C) in S1-M1, Fig. 2.10C). Such size-dependent PTrEA/MTSET/MTSEA patterns occurred for nine of 13 potentiation positions tested (positions S531C, D534C, R783C & P787C in GluN1 and R518C, V523C, S533C, S788C & S789C in GluN2C, Figs. 2.10D & E) and are consistent with the idea that these potentiation positions are located at closed-state dependent contact interfaces. Notably, all six potentiation positions showing reduced PTrEA accessibility in the closed state (Fig. 2.9) also showed size-dependence consistent with the 'closed-state contact' hypothesis (Fig. 2.10).

Of the remaining four positions, GluN2C(E530C) in S1-M1 showed strong but not significantly different degrees of current potentiation for all three reagents (Fig. 2.10E), suggesting that charge rather than steric effects may underlie current potentiation. Positions K526C in GluN1 (Fig. 2.10D) and M787C in GluN2C (Fig. 2.10E) did not show any size-dependent PTrEA/MTSET/MTSEA pattern. Additionally, position D792C in GluN2C did show a size-dependent pattern, although it was opposite to our prediction with the degree of current potentiation increasing with larger reagents (Fig. 2.10E). Based on the homologous position in

GluA2, it is likely that the membrane environment is confounding MTS accessibility in an unknown manner.

DISCUSSION

Gating in ionotropic GluRs involves the transduction of structural changes in the LBD initiated by ligand binding/unbinding into physical movements of the ion channel culminating in dilation/constriction of the central pore (Sun et al., 2002; Erreger et al., 2004; Mayer, 2006; Hansen et al., 2007). The transduction machinery between the ligand-binding and transmembrane domains is comprised of the linkers S1-M1, M3-S2 and S2-M4. While M3-S2 is central to the transduction process, our experiments indicate that S1-M1 and S2-M4 can also affect or modulate gating. Further, we identify specific positions in and around S1-M1 and S2-M4 that are important to the energetics of this process and are apparently located at key contact interfaces in the channel-closed state.

PTrEA reaction at potentiation positions in and around S1-M1 and S2-M4 shifts gating equilibrium towards the open state.

Of the 87 positions encompassing the GluN1 and GluN2 linkers tested, 18 of them underwent persistent PTrEA-induced potentiation of whole cell-currents (Figs. 2.2-2.5), with 15 of these potentiation positions located in the S1-M1 and S2-M4 linkers. All of the S1-M1 and S2-M4 potentiation positions showed a significantly faster rate of block by the open channel blocker MK-801 following PTrEA than before it (Fig. 2.6), suggesting that current potentiation is due to an increase in P_o. Confirming this, three potentiation positions [GluN1(S531C), GluN2C(V523C), GluN2C(S788C)] tested with single channel recordings all showed a significant increase in P_o following PTrEA (Fig. 2.7). Thus, PTrEA-induced potentiation of whole-cell currents arises mainly if not exclusively—assuming MK801 is a valid (relative) index of P_o—from a gating effect of an increase in the time the receptor spends in the open state,

indicating that the dynamics of the S1-M1 and S2-M4 linkers are important components of the NMDAR gating process.

An increase in P_o could arise in one of two ways: either by destabilization of the closed state or stabilization of the open state. Analysis of single channel recordings of receptors containing potentiation positions showed that following PTrEA, they had an increased P_o (Figs. 2.7A & B) with no significant changes in open time durations (Fig. 2.7C). Thus, at least for these positions the increase in P_o most likely arises from a destabilization of the closed state. Additionally, PTrEA-induced potentiation positions were often associated with significant increases in leak currents (supplemental Table 2.1). Although we did not explore in detail these changes in leak currents, they most likely reflect constitutively open PTrEA-reacted NMDARs (Yuan et al., 2005; Schmid et al., 2007; Sobolevsky et al., 2007), presumably due to a destabilized closed state. However, for those potentiation positions not directly tested with single channel recordings, we cannot rule out that increases in P_o arise from stabilization of the open state.

Structural basis underlying PTrEA-induced increases in P_o.

The structural basis underlying PTrEA-induced increases in P_o is certainly not the same for all potentiation positions, but identifying these mechanisms will help define elementary gating steps following ligand binding but preceding ion channel opening. One structural mechanism we considered is that certain potentiation positions are located at dynamic contact interfaces in the closed state and that the introduction of a bulky side-chain at these positions sterically disrupts the stability of this state, thus shifting gating equilibrium towards the open state (the 'closed-state contact' hypothesis).

Consistent with this hypothesis, we found that most tested potentiation positions showed a reduced degree of access in the closed as compared to the open state (Fig. 2.9). Additionally, the degree of potentiation for nine out of the 13 positions was reduced with decreasing MTS reagent size (Fig. 2.10), suggesting that steric constraints are important to the gating effect (see supplemental Table 2.3 for a summary of all potentiation positions). Notable for these experiments is that positions tested for both state- and size- dependence showed consistent patterns: either they showed dependencies in both parameters [e.g., GluN1(S531C)] or they showed dependencies in neither parameters [e.g., GluN1(K526C)]. Thus, based on two independent experimental approaches, a subset of the potentiation positions (Fig. 2.11, red arrowheads) appear to be located at contact interfaces in the channel-closed state. These contact interfaces could be important to receptor function because of specific and local interactions (e.g., electrostatics) between the contacting partners in the closed state or they may be part of the transient state-dependent positioning of the overall linkers/transmembrane segments during gating.

Although there is uncertainty in relating specific positions in the NMDAR linkers to those in the AMPAR structure (supplemental Fig. 2.1), there are some intriguing 'hotspots' of potentiation positions. One notable hotspot comprises the adjacent serines in GluN2C S2-M4, S788 and S789 (Fig. 2.11). In the closed-state AMPAR structure (PDB ID 3KG2), the analogous positions T784 and S785 are located within 4 Å of the extracellular end of the highly conserved SYTANLAAF motif in M3/M3-S2 of an adjacent subunit. This motif contains the 'Lurcher' position, substitution of which in NMDARs have strong effects on gating (Jones et al., 2002; Yuan et al., 2005), and the channel's activation gate (Chang and Kuo, 2008) (Sobolevsky et al., 2009). However, reflecting the potential complexity in identifying interactions in the linkers,

these S2-M4 positions are also proximal (< 8 Å) to M3/M3-S2 in the same subunit and M1/S1-M1 in an adjacent subunit. Thus, even with an available structure, identifying gating-dependent contacting partners will be challenging. Nevertheless, identifying them and defining their relative dynamics during gating will be essential in elaborating mechanisms coupling LBD conformational changes to ion channel opening/closing.

Certain positions showed discrete state-dependent accessibility (i.e., apparently accessible in the open but not in the closed state) to PTrEA suggesting that they are at dynamic contact interfaces, yet PTrEA did not induce current potentiation (e.g., GluN2C(P531C), Fig. 2.3B). One possibility is that modification at these positions produced a stronger conductance effect (decrease in γ) outweighing any gating effect (increase in P_o), thus resulting in net inhibition. Alternatively (or in addition to), the contact interface at these positions may make only minor contributions to the overall energetics of the closed state. This latter alternative is intriguing since it suggests that potentiation positions are specifically identifying linker elements (or structures) that are critical to gating.

PTrEA-induced gating effects are specific to the GluN2 subunit and dependent on the intrinsic P_o of the NMDAR.

GluN1-potentiation positions, defined by co-expression with GluN2C, showed reduced degrees of PTrEA-induced current potentiation when co-expressed with GluN2A' (Fig. 2.8). NMDAR P_o is GluN2 subunit-specific (Chen et al., 1999b; Gielen et al., 2009; Yuan et al., 2009). GluN2A-containing NMDARs have a relatively high intrinsic P_o (0.36 - 0.50) (Erreger et al., 2004) whereas for GluN2C-containing NMDARs it is much lower (~0.01) (Dravid et al., 2008). Hence, for GluN2A-containing receptors, the energetics of channel gating are already shifted more

towards the open state than for GluN2C- containing receptors, limiting the potential for further increases. In contrast, for GluN2C-containing receptors, where channel opening is intrinsically disfavored, there exists greater energetic 'room' to increase P_o. Thus, the inherent biophysical gating properties of NMDARs dictate the directionality and extent of linker-mediated modulation of gating.

Novel sites and mechanism of modulating NMDAR function.

NMDARs are implicated in diverse neurological and psychiatric diseases (Kalia et al., 2008). However, since they are ubiquitous in the CNS and subserve numerous physiological functions, selective targeting of dysfunctional NMDARs is essential for any clinically useful drug. Indeed, competitive antagonists at either the GluN1 glycine-binding site or the GluN2 glutamate-binding site have been abandoned in clinical trials (Kalia et al., 2008) mainly due to their indiscriminate actions on all NMDARs. In contrast, allosteric modulators at the N-terminal domain, such as the GluN2B-specific ifenprodil, show promise in subunit-specific targeting, although their clinical utility is yet unknown (Paoletti and Neyton, 2007). At the ion channel, several classes of pore blockers are used for limited purposes, e.g. ketamine for anesthesia and memantine for moderate-to-severe Alzheimer's disease (Lipton, 2006).

Here we identify the NMDAR linker region as a novel pharmacologic target wherein drug action, in a noncompetitive mechanism, could modulate gating. The linkers are extracellularly exposed, as evidenced from their wide accessibility to PTrEA (Figs. 2.3-2.5). More specifically, targeting of S1-M1 and S2-M4, which are remote from the central axis of the pore and do not directly control channel gating (unlike M3-S2), may offer more subtle means of modulating NMDAR function, potentially lessening side-effects. Finally, since the proposed

mechanism of drug action at the linkers regulates gating energetics, any modulation of receptor activity is dictated by the inherent gating properties of the NMDAR, which themselves are highly dependent on the specific GluN2 subunit. This concept can be used to attain subunit-specificity in drug action and exploit the spatiotemporal localization of the different GluN2 subunits in the CNS. Hence, NMDAR activity can be strongly potentiated for GluN1-GluN2C whereas it can be strongly inhibited for GluN1-GluN2A. Intriguingly, memantine and amantadine, two drugs currently in clinical use and known to function as pore blockers, might also have gating effects by interacting with the linkers as secondary sites of action (Blanpied et al., 2005; Chen and Lipton, 2005; Kotermanski et al., 2009).

FIGURES

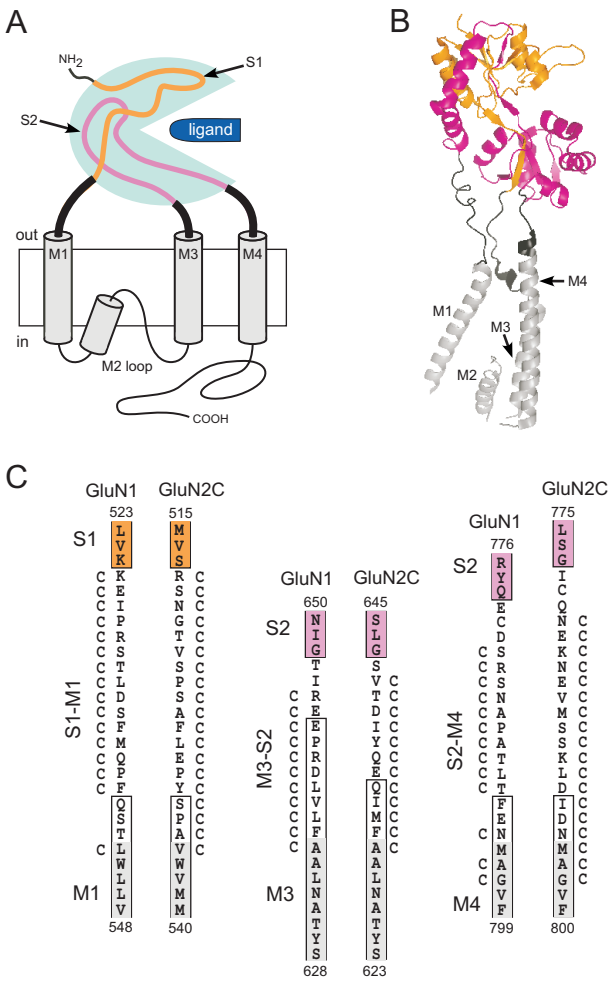

Figure 2.1. The linkers S1-M1, M3-S2 and S2-M4 connect the extracellular LBD to the transmembrane segments in a glutamate receptor subunit.

(A) Schematic representation of the functional core of an ionotropic glutamate receptor (iGluR) subunit. The extracellular ligand-binding domain (LBD), shown in cyan, is composed of lobes S1 (shown in orange) (N terminal to M1) and S2 (shown in magenta) (between M3 and M4). The hydrophobic segments M1, M3 and M4, as well as the M2 pore loop, are shown as gray cylinders. Thick black bars indicate regions in and around the linkers S1-M1, M3-S2 and S2-M4 where cysteines were substituted.

(B) Ribbon representation of a single GluR subunit ($GluA2_{cryst}$, subunit A, PDB ID 3KG2), viewed from the side and oriented with the extracellular solution above. The LBD, the linkers and the transmembrane segments are shown with colors as in A.

(C) Sequence of the regions encompassing the three linkers in the GluN1 and GluN2C subunits. The proximal parts of the presumed hydrophobic segments M1, M3 and M4 (Schmid et al., 2007) are highlighted in gray. The boxed regions around these hydrophobic segments show the proximal α-helical extent of the transmembrane segments as revealed by GluA2cryst (Sobolevsky et al., 2009). GluN1 is assumed to take the A/C conformation, while GluN2C the B/D conformation. The proximal parts of S1 and S2 are highlighted in orange and magenta, respectively. Positions substituted with cysteines and tested for PTrEA reactivity are indicated (see Materials and Methods). Certain positions, specifically those without an adjacent 'C,' were not tested because MTS reagents did not persistently alter their current amplitudes (Beck et al., 1999). Numbering is for the mature protein.

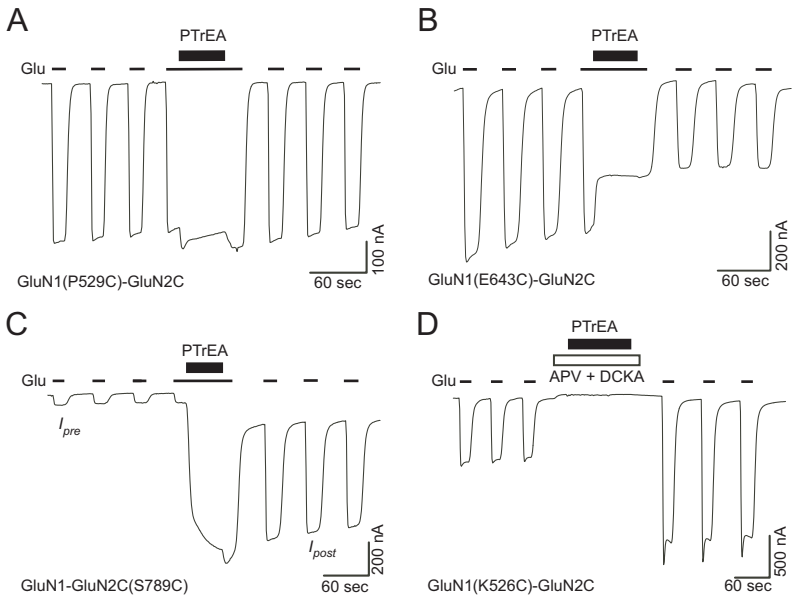

Figure 2.2. Steady-state recording protocols to assay accessibility of substituted cysteines to PTrEA.

Examples of whole-cell currents recorded from *Xenopus* oocytes expressing GluN1(P529C)-GluN2C (A), GluN1(E643C)-GluN2C (B), GluN1-GluN2C(S789C) (C) or GluN1(K526C)-GluN2C (D). Currents were elicited by glycine (20 μM) and glutamate (200 μM) (thin lines labeled with 'Glu') at a holding potential of -60 mV. (A-C) PTrEA (1 mM) (thick lines) was applied for 60 secs in the continuous presence of agonists. (D) PTrEA was applied for 60 secs in the absence of agonists, but in the presence of the competitive antagonists DCKA (10 μM) and APV (100 μM) (open box). I_{pre} and I_{post} (C) refers to current amplitudes measured before and after application of PTrEA, respectively. PTrEA produced either no effects on glutamate-activated current amplitudes (A), current inhibition (B) or potentiation (C & D). For certain mutants, leak current was also significantly changed following PTrEA application (C).

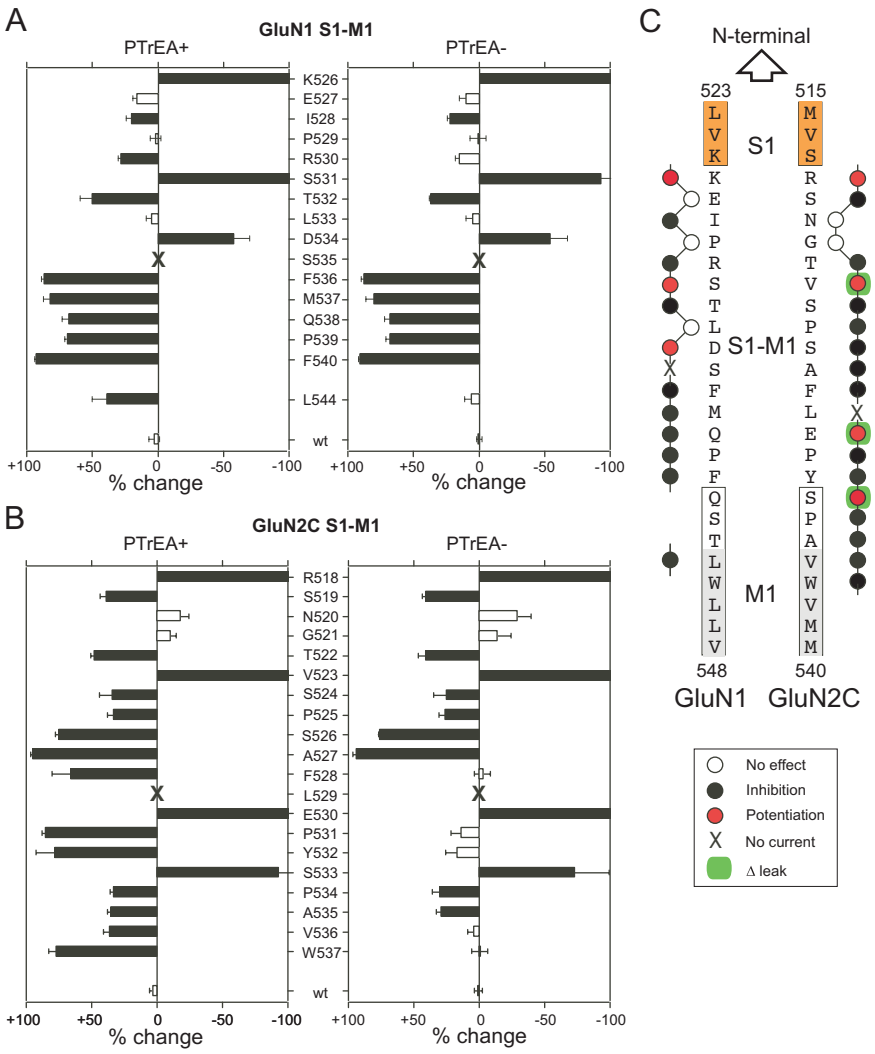

Figure 2.3. Effects of PTrEA on substituted cysteines in and around the GluN1 and GluN2C S1-M1 linkers.

(A & B) Mean percent change (± 2SEM) in glutamate-activated current amplitudes measured before (I_{pre}) and after (I_{post}) exposure of wild-type and cysteine-substituted GluN1 (A) or GluN2C (B) subunits to PTrEA in the continuous presence (PTrEA+, left) or absence (PTrEA-, right) of agonists. Left and right pointing bars indicate inhibition and potentiation, respectively. For positions with percent change = -100, potentiation was stronger than 100%. Filled bars indicate

that the value of % change is statistically different from that of wild-type GluN1-GluN2C ($P < 0.05$).

(C) Summary of discrete effects of PTrEA, applied in the presence of agonists, on substituted cysteines in and around the GluN1 and GluN2C S1-M1 linkers. Adjacent circles indicate that positions were tested for reactivity with PTrEA: unfilled circles, no effect on glutamate-activated current; black circles, current inhibition; red circles, current potentiation. X, no detectable glutamate-activated current; green highlight, significant PTrEA-induced change in leak current.

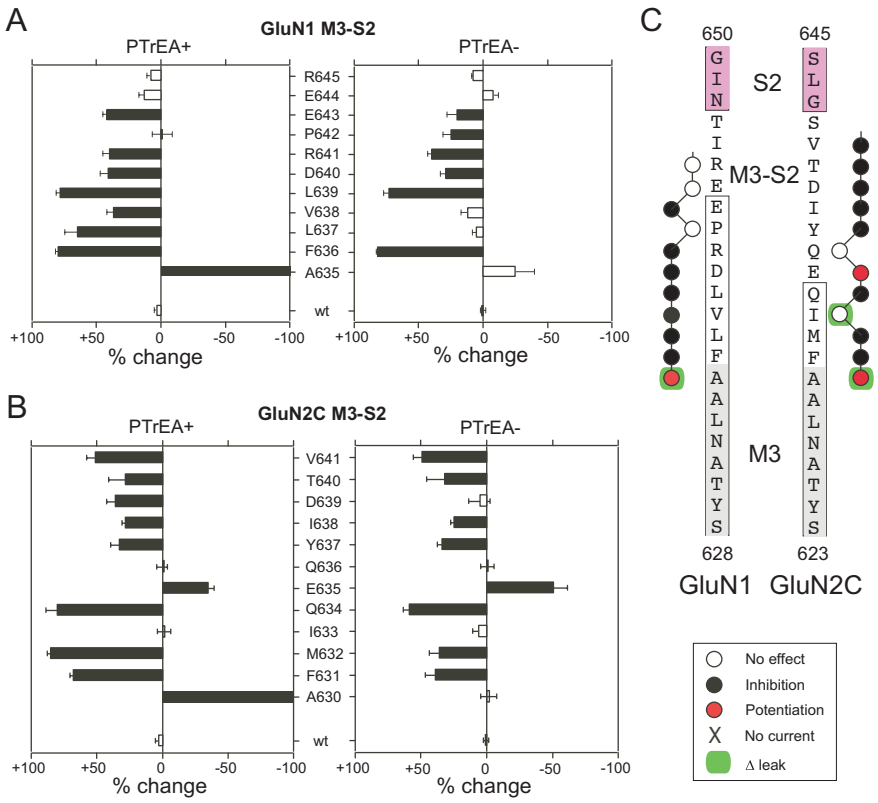

Figure 2.4. Effects of PTrEA on substituted cysteines in and around the GluN1 and GluN2C M3-S2 linkers.

Same as Fig. 2.3, but for M3-S2.

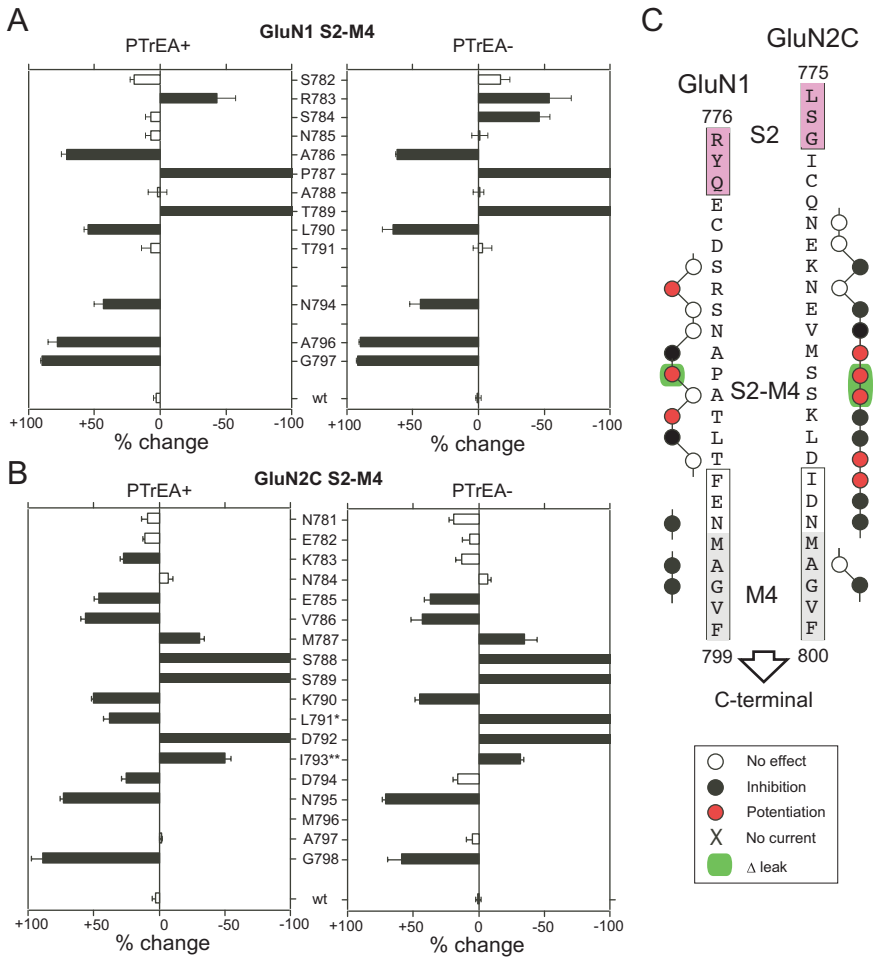

Figure 2.5. Effects PTrEA on substituted cysteines in and around the GluN1 and GluN2C S2-M4 linkers.

Same as Fig. 2.3, but for S2-M4.

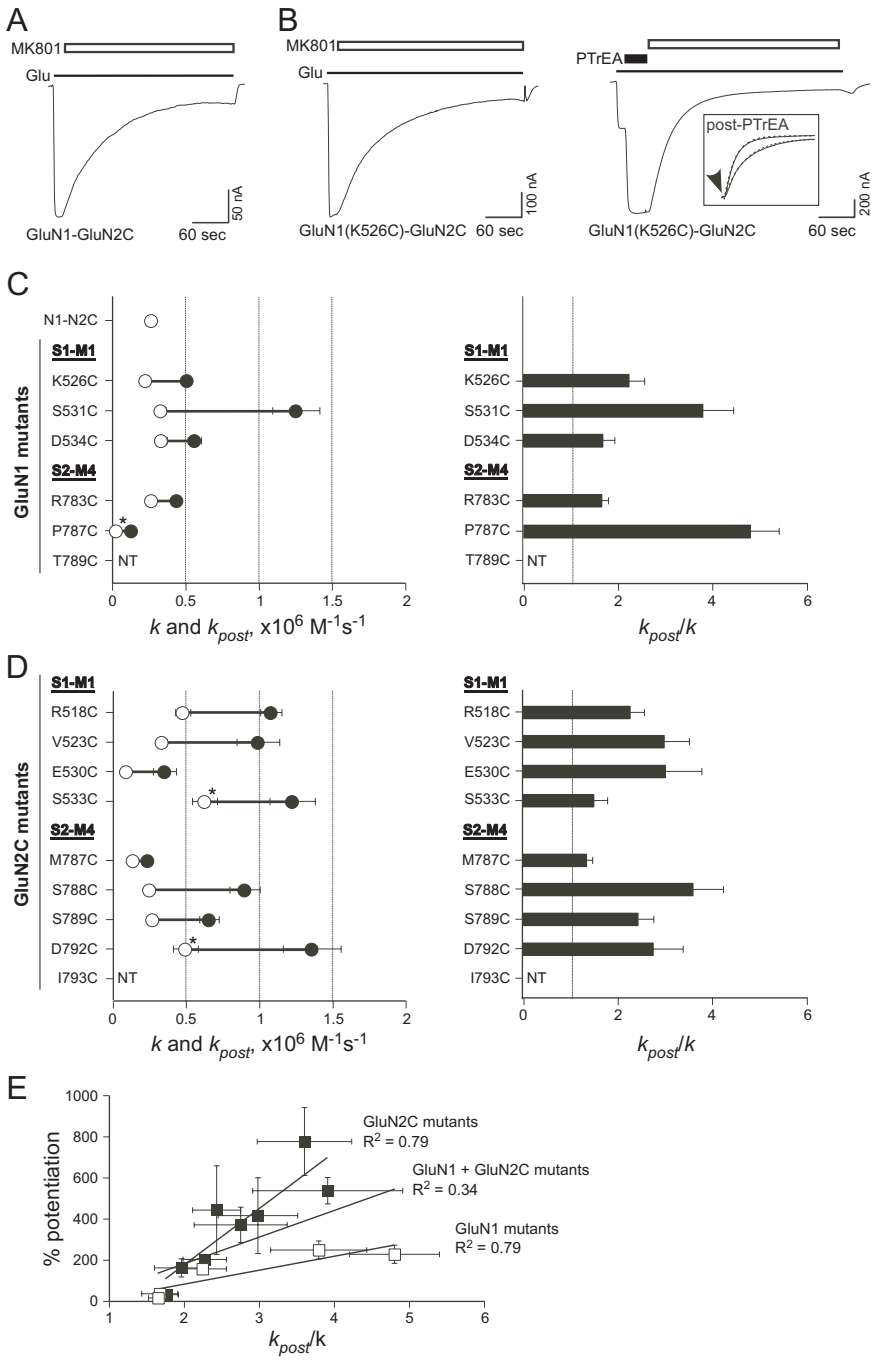

Figure 2.6. MK801 current inhibition as an index of P_o.

(A) MK801 inhibition of glutamate-activated currents of wild-type GluN1-GluN2C. After glutamate-activated currents (Glu, thin line) had reached steady-state, 50 nM MK801 (unfilled bar) was applied in the presence of agonists until steady-state inhibition was attained. (B)

MK801 inhibition of glutamate-activated current of GluN1(K526C)-GluN2C without (left) or following (right) PTrEA application (solid bar). When PTrEA was used, MK801 appplication was initiated once PTrEA-induced potentiation had reached steady-state. Inset, the MK801-mediated decays of normalized currents without and following PTrEA (post-PTrEA) were fitted with a single-exponential function (dashed overlays) to determine the time constant τ of inhibition. Arrowhead indicates onset of MK801 inhibition.

(C & D, left) Summary of rate constants of MK801 inhibition without (k, unfilled circles) and following (k_{post}, filled circles) PTrEA for GluN1- (C) and GluN2C- (D) potentiation positions. The rate of MK801 inhibition (k) of wild-type GluN1-GluN2C is shown in C. Potentiation positions in M3/M3-S2 are not included in this analysis (see text and supplementary Fig. 2.2). Asterisks denote positions where the cysteine substitution itself significantly altered the rate of MK801 inhibition as compared to wild-type GluN1-GluN2C. NT denotes positions not tested because of small current amplitudes [GluN1(S789C)] or incomplete reaction with PTrEA [GluN2C(I793C)]. In some instances error bars are smaller than the symbols.

(C & D, right) The ratio k_{post}/k for GluN1- (B) and GluN2C- (C) potentiation positions. Dotted line indicates $k_{post}/k = 1$. Filled bars indicate positions where the rate of MK801 inhibition following PTrEA was significantly different from that without PTrEA ($P < 0.05$).

(E) Correlation between k_{post}/k and % potentiation of whole-cell glutamate-activated current with three linear regressions shown: GluN1 (unfilled squares) and GluN2C (filled squares) positions pooled together (GluN1 + GluN2C) and each subunit considered separately. R^2 value for each respective fit is shown.

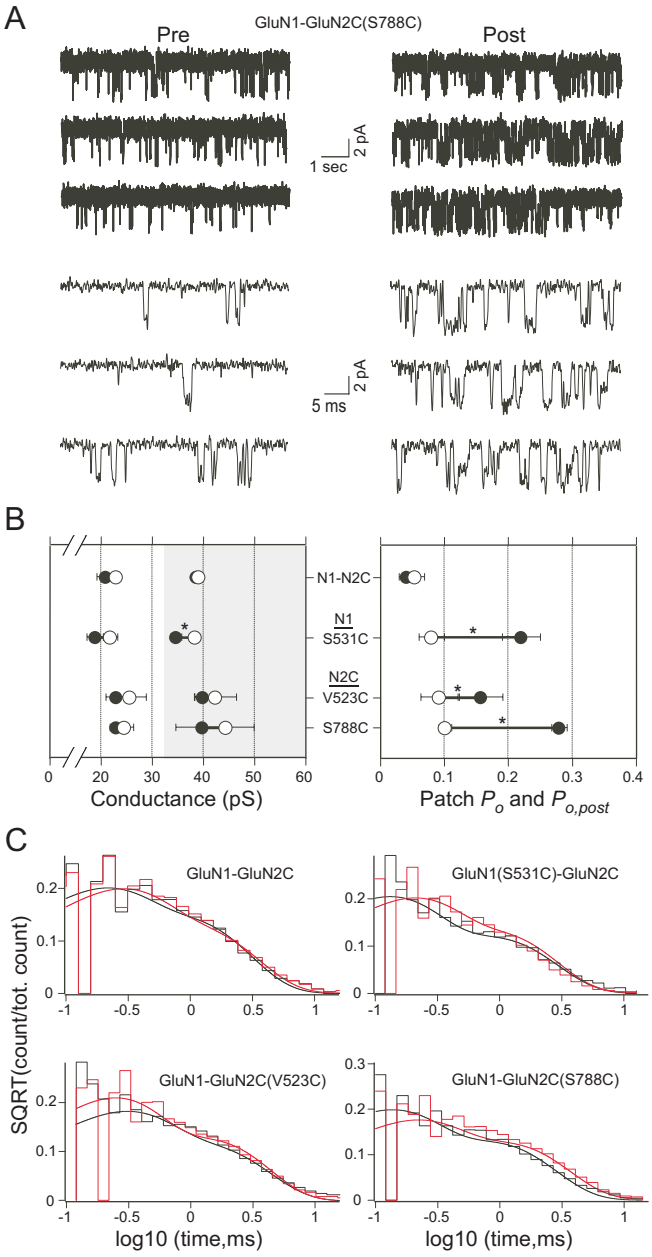

Figure 2.7. The effect of PTrEA on single channel currents.

(A) An example outside-out patch from an oocyte injected with GluN1-GluN2C(S788C) showing glutamate-activated single channel activity before (Pre) and after (Post) PTrEA. For display, currents were digitally refiltered at 5 kHz (top) or at 2 kHz (bottom) after being collected at 10 kHz. Holding potential was –80 mV.

(B) Mean values of conductance (left panel) and Patch P_o (right panel) before (open circles) and after (filled circles) PTrEA (n = 3 for each receptor; see also supplemental Table 2.2). In the conductance graph, the light and shaded parts show the arbitrary ranges for the lower- and higher- conductance levels, respectively. Asterisks denote statistical significance ($P < 0.05$) in the post/pre ratio from that of the wild-type GluN1-GluN2C.

(C) Composite open time histograms before (black) and after (red) PTrEA. The data were fit with two exponential components (for values see supplemental Table 2.2).

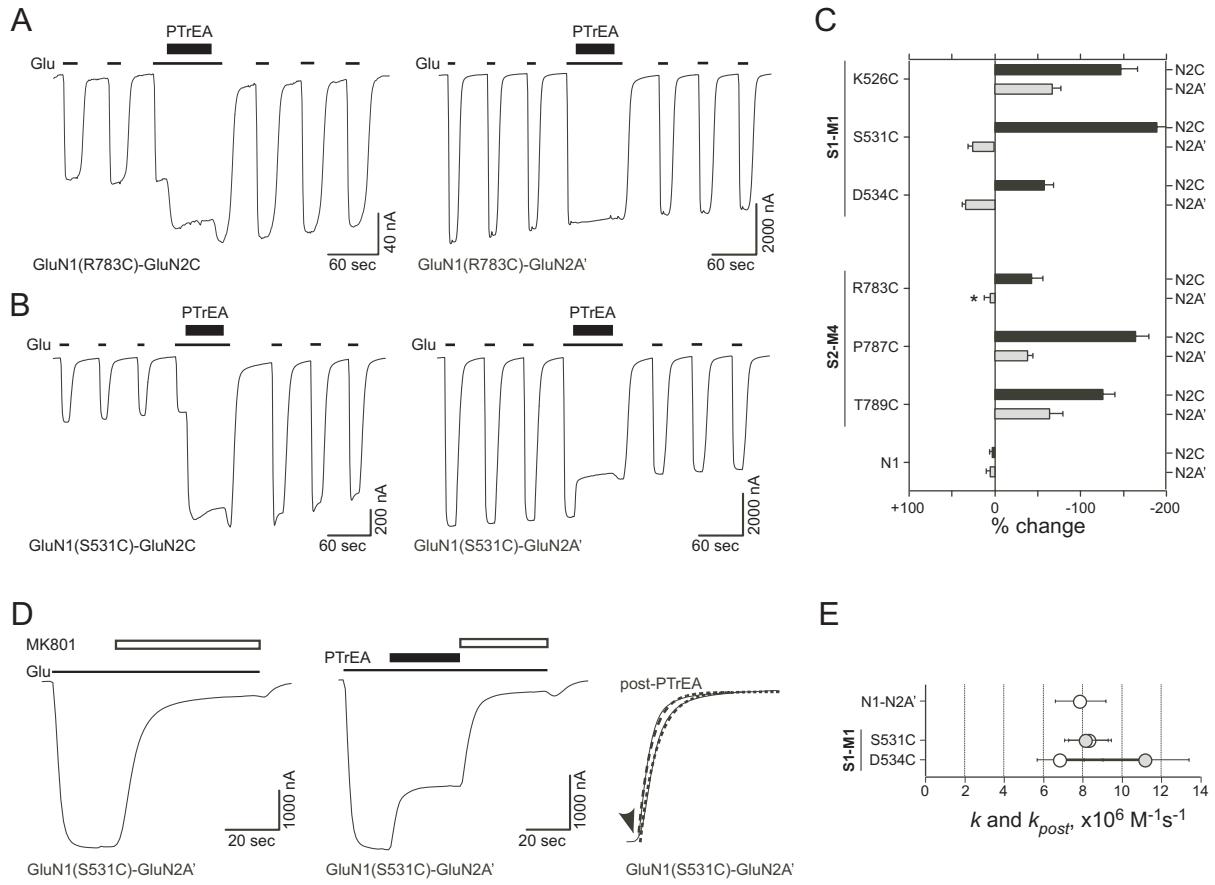

Figure 2.8. Steady-state reaction of PTrEA to GluN1-potentiation positions co-expressed with GluN2C or GluN2A'.

(A & B) Example recordings showing effects of PTrEA on glutamate-activated current amplitudes for the same GluN1 potentiation positions co-expressed with either GluN2C (left) or GluN2A' (right). The protocol used is identical to that in Fig. 2.2 (see Materials and Methods). For GluN1-GluN2A' NMDARs, we replaced Ca^{2+} with Ba^{2+} and added EDTA to the external solution to limit Ca^{2+}-dependent desensitization and Zn^{2+}-mediated modulation, respectively. We recorded a limited number of identical cysteine-substituted GluN1 positions, co-expressed with GluN2C in the Ba^{2+}- and EDTA- containing solution and found no significant influence of the differing solutions on PTrEA-induced effects (data not shown).

(C) Mean % change (± 2SEM) of glutamate-activated current amplitudes following PTrEA for the GluN1- potentiation positions co-expressed with either GluN2C (black bars) or GluN2A' (gray bars). Asterisk denotes % change not significantly different from the respective control wild-type GluN1-GluN2C or GluN1-GluN2A' receptors.

(D) Rate of MK801 current inhibition for GluN1(S531C)-GluN2A'. MK801 (50 nM, unfilled bars) was applied in the continuous presence of agonists (thin black line, Glu) either without (left) or following (middle) PTrEA. Same protocols and conditions as in Fig. 2.6B.

Single exponential fits to MK801-mediated decay of normalized currents are shown at right.

(E) Rate constants k (without PTrEA, unfilled circles) and k_{post} (following PTrEA, filled circles) of MK801 current inhibition for the two GluN1 positions that showed significant PTrEA-induced current inhibition when co-expressed with GluN2A' (from C), as well as for GluN1-GluN2A'.

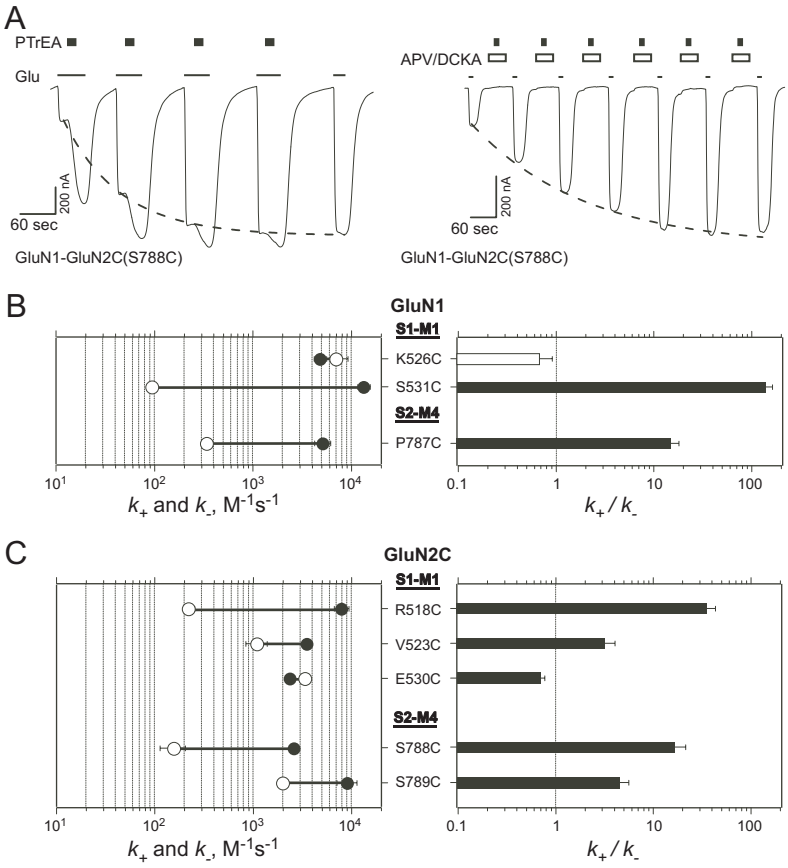

Figure 2.9. PTrEA modification rates for potentiation positions.

(A) Pulsive protocol to assay PTrEA (black bars) modification rates of GluN1-GluN2C(S788C) in the presence (left) or absence (right) of agonists (thin line). (Left) 25 μM PTrEA was applied in the continuous presence of agonists in four 15 sec pulses for a cumulative 60 secs exposure. (Right) 200 μM PTrEA was applied in the absence of agonist, but in the continuous presence antagonists DCKA and APV (open box), in six 15 sec pulses for a cumulative 90 secs exposure. Dashed lines denote single exponential fits of current amplitudes as a function of the cumulative time of PTrEA exposure that defines the rate constants of chemical modification in the presence (k_+) or absence (k_-) of agonists.

(B and C, left) Mean values of k_+ (filled circles) and k_- (open circles) (± 2SEM) for GluN1- (B) and GluN2C- (C) potentiation positions. In some instances, error bars are smaller than the symbols.

(B and C, right) k_+/k_- for GluN1- (B) and GlunN2C- (C) potentiation positions. Filled bars indicate positions where PTrEA modification rates in the presence and absence of agonists were significantly different ($P < 0.05$). Dotted line indicates $k_+/k_- = 1$.

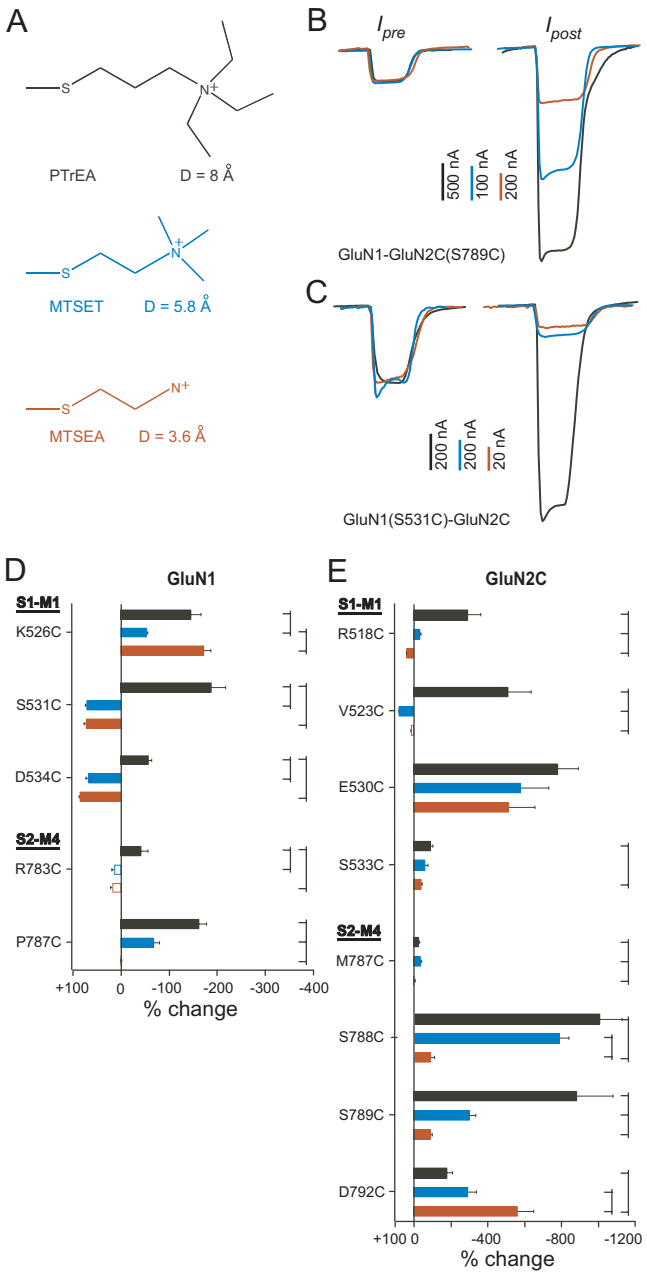

Figure 2.10. Steady-state reaction of potentiation positions with variably-sized MTS reagents.

(A) Chemical structures of the three differently-sized MTS reagents tested: PTrEA (black), MTSET (blue) and MTSEA, (brown). The diameters of each side-group (Lu et al., 1999) are shown. All reagents have the same valence (+1) and general structure.

(B & C) Glutamate-activated currents for cysteine-substituted GluN1-GluN2C receptors before (I_{pre}) and after (I_{post}) reaction with MTS reagents: PTrEA, black; MTSET, blue; MTSEA, brown. The protocol used was identical to that shown in Fig. 2.2. For comparison of MTS-induced changes in current amplitude, current amplitudes (I_{pre}) before MTS reagent application were normalized.

(D & E) Mean % change (± 2SEM) in current amplitude following steady-state exposure of GluN1 (D) or GluN2C (E) potentiation positions to PTrEA (black), MTSET (blue) or MTSEA (brown) in the continuous presence of agonists. Filled bars indicate that the value of % change is statistically different from that of wild-type GluN1-GluN2C channels ($P < 0.05$). Symbols to the right of bars indicate statistically significant differences ($P < 0.05$) between the variably-sized reagents.

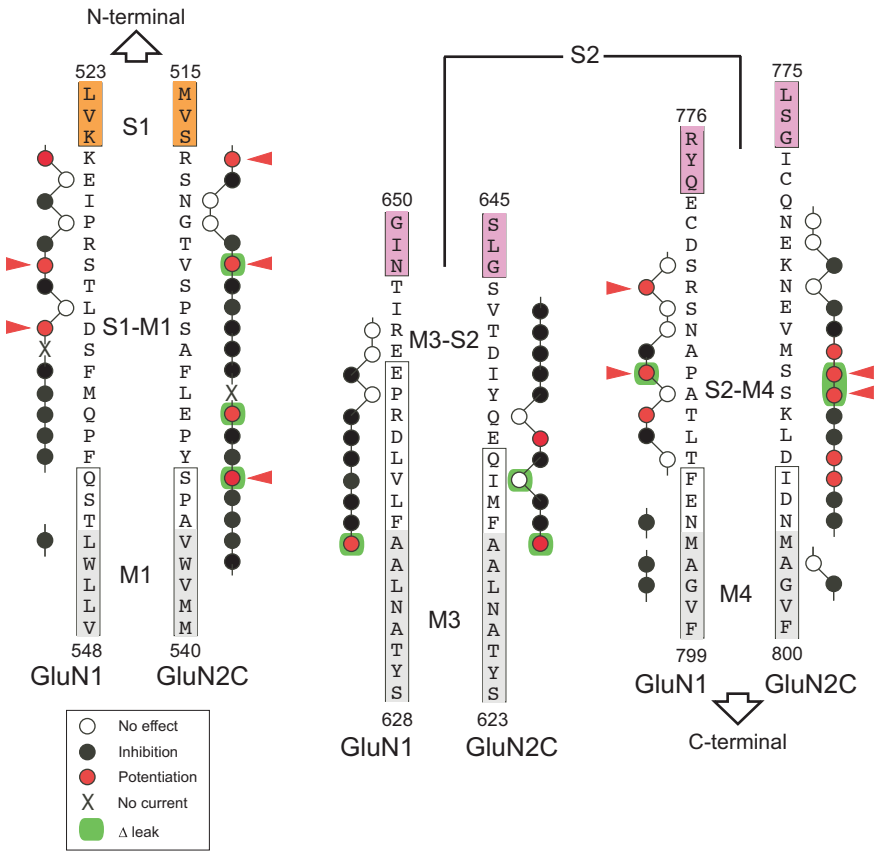

Figure 2.11. Summary of linker positions affecting gating.

Summary of discrete effects of PTrEA, applied in the presence of agonists, on substituted cysteines in and around the GluN1 and GluN2C linkers. Adjacent circles indicate that positions were tested for reactivity with PTrEA : unfilled circles, no effect on glutamate-activated current; black circles, current inhibition; red circles, current potentiation. X, no detectable glutamate-activated current; green highlight, significant PTrEA-induced change in leak current (from Figs. 2.3C, 2.4C & 2.5C). Also highlighted here are the nine potentiation positions proposed to be at transient contact interface in the closed state (red arrowheads).

SUPPLEMENTAL INFORMATION

Comparison of the LBD-TM linkers in GluR subunits (suppl. Fig. 2.1).

Supplemental Figure 2.1 shows a sequence alignment of the LBD-TM linkers (as well as adjacent parts of S1, S2 and TM segments) of the 18 mammalian GluR subunits. The major structural motifs derived from the crystal structure of a largely intact homotetrameric (GluA2) AMPA receptor (Sobolevsky et. al., 2009) are shown above the alignment. For the linker region, using the AMPAR structure as an absolute guide for the other subunits—especially NMDAR subunits—has certain limitations. First, there are notable gaps in the NMDAR sequence, as compared to that of the AMPAR. While this occurs at positions 11 (GluN1) and 8 (GluN2) in S1-M1, these gaps are extremely prominent in the S2-M4 linker. Indeed, it seems likely that the pre-M4 helix in NMDAR subunits is either not present or has a much different character. Second, there is widespread sequence variation between AMPAR (which obviously show much more similarity to kainate receptor subunits) and NMDAR subunits. While there certainly are points of similarity [e.g., at the C-terminal end of the pre-M1 helix, AMPAR and GluN2 subunits all have a negatively charged residue (position 17) followed by a proline (position 18)], notable differences also occur. For example, at the N-terminal end of the pre-M1 helix for the same subunits, position 12 is a valine (AMPAR subunits) versus the structurally rigid proline (GluN2 subunits) and position 13 is a bulky, hydrophobic phenylalanine (AMPAR subunits) versus a polar serine (GluN2 subunits). How these variations in amino acid composition affect the local structure is unknown. Finally, it should also be noted that the overall resolution of the new structure was 3.6 Å and that the density of the linkers was low making the specific positioning of side chains/residues uncertain (though their general arrangement is clear).

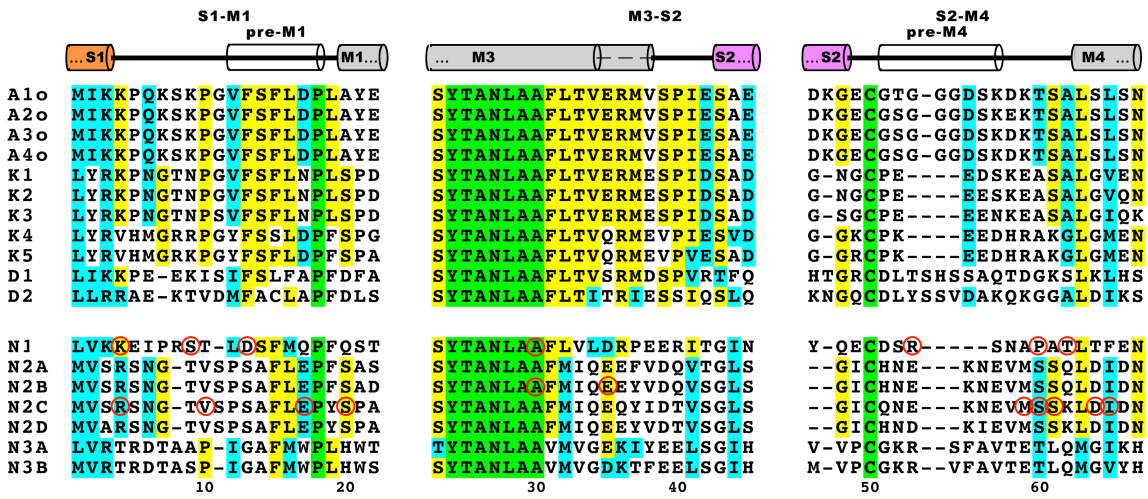

Supplemental Figure 2.1. Sequence alignments of LBD-TMD linkers in ionotropic glutamate receptor subunits.

Sequences were aligned using ClustalW 1.81 (UCSD Biology Workbench). Residues highlighted in green are conserved across all subunits; those highlighted in yellow are identical whereas those highlighted cyan are similar to the other subunits in at least 50% of the subunits. The following similarity matrix was used (single amino acid code): NQ, ED, KR, IVLM, FYW, GA, TS. All sequences are from rat. Protein accession numbers: GluA1 (P19490), GluA2 (P19491), GluA3 (P19492), GluA4 (P19493), GluK1 (P22756), GluK2 (P42260), GluK3 (P42264), GluK4 (Q01812), GluK5 (Q63273), GluD1 (Q62640), GluD2 (Q62640), GluN1 (P35439), GluN2A (Q00959), GluN2B (Q00960), GluN2C (Q00961), GluN2D (Q62645), GluN3A (Q62800) and GluN3B (Q8VHN2).

For the schematic above the alignment (derived from the AMPAR structure, Sobolevsky et al., 2009; PDB ID 3KG2), the color scheme is the same as in Fig. 2.1 (S1, orange, S2, magenta; transmembrane segments, gray; linkers, solid black line), and the dashed line for M3/M3-S2 indicates the helical extension of the A/C subunits whereas the corresponding region in the B/D subunits is extended. For the NMDAR, GluN1 is presumed to take on the A/C conformation,

while GluN2s the B/D conformation (Sobolevsky et. al., 2009). The gray and white cylinders represent the transmembrane and extracellular juxta-membrane helical segments, respectively. Residues in red circles are potentiation positions identified in the manuscript. Numbering at the bottom of the alignment starts with the first residue shown (in S1) and proceeds continuously through the alignment.

Supplemental Table 1. Positions showing significant changes in leak current following reaction with PTrEA in the presence of agonists.

Position	*D leak* %	N	Designation
S1-M1			Fig. 2.3C
GluN2C(V523C)	-67 ± 34%	6	Red
GluN2C(S526C)	9 ± 4%	4	Black
GluN2C(E530C)	-27 ± 6%	4	Red
GluN2C(S533C)	-12 ± 4%	4	Red
M3-S2			Fig. 2.4C
GluN1(A635C)	-32 ± 4%	9	Red
GluN2C(A630C)	-23 ± 2%	4	Red
GluN2C(I633C)	-23 ± 3%	7	White
S2-M4			Fig. 2.5C
GluN1(P787C)	-11 ± 2%	9	Red
GluN2C(S788C)	-35 ± 24%	5	Red
GluN2C(S789C)	-60 ± 24%	5	Red

Listed are cysteine-substituted channels where the change in the leak current (*D leak %*) following PTrEA, applied in the presence of agonists, was significantly different than that in wild type receptors (*D leak* = 1 ± 1%, n = 9). All mutant channels shown in Figs. 2.3, 2.4 and 2.5 were included in this analysis. Values shown are mean ± 2SEM.

The extent of MK801 block is significantly altered only in receptors containing substitutions in the M3-S2 linker (suppl. Fig. 2.2).

Alteration of MK801 inhibition kinetics in a given receptor can index relative P_o assuming the mechanism of MK801 block is not significantly altered either by the cysteine-substitution itself or following PTrEA. One way we assayed for any perturbation of MK801 block was to quantify the fractional block of whole-cell current before and after PTrEA by MK801. We find that for all S1-M1 and S2-M4 linker potentiation positions, the extent of current inhibition is not significantly different from that in wild-type GluN1-GluN2C receptors (open bars, supplemental Fig. 2.2B & C). In contrast, M3/M3-S2 potentiation positions showed multiple signs of altered MK801 block including current rebound with removal of MK801 (supplemental Fig. 2.2A), significantly reduced extent of inhibition compared to wild type (black bars, supplemental Fig. 2.2B & C), and consistent double exponential fits to MK801 inhibition, e.g. GluN2C E635C (data not shown). Not surprisingly, all three positions are located within or near M3, the major gating element and physically close to the site of MK801 channel block (Kashiwagi et al., 2002). We suspect that, as previously reported with other positions in M3 (Yuan et al., 2005), these cysteine-substituted/PTrEA-reacted M3/M3-S2 potentiation positions perturb the structural determinants of MK801 interaction within the pore. We therefore did not explore these M3/M3-S2 positions further. In contrast, for S1-M1 and S2-M4 potentiation positions, the absence of any apparent changes in MK801 block suggests, with caveats, that the mechanism of MK801 block deep in the pore is unaffected.

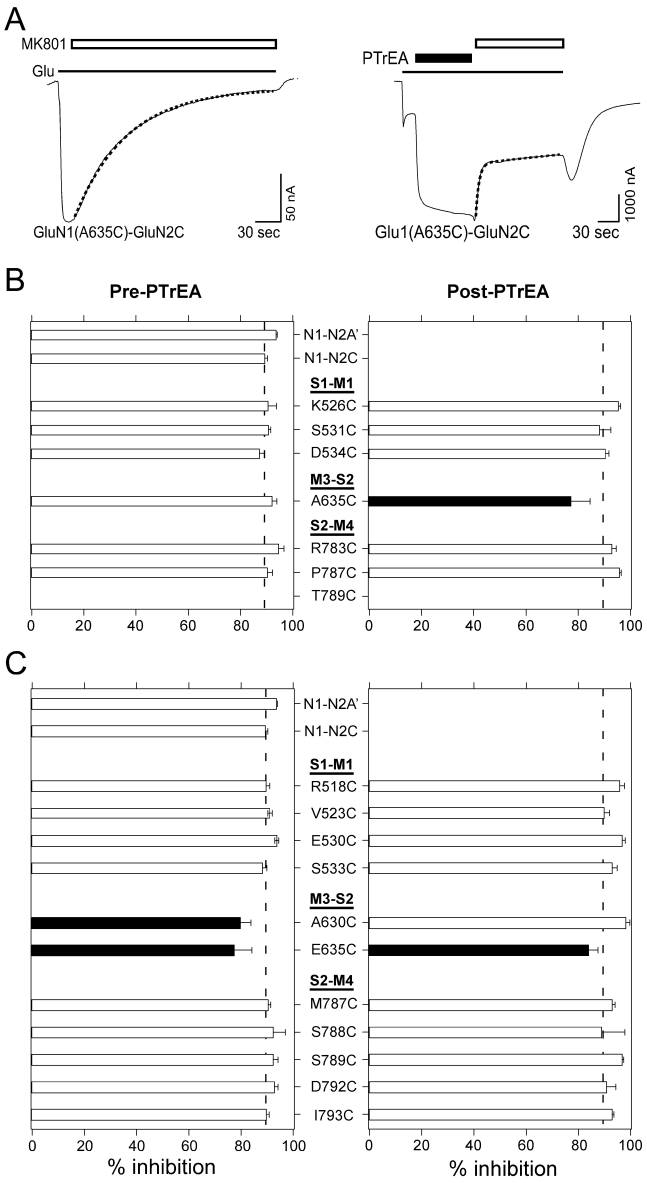

Supplemental Figure 2.2. Extent of MK801-mediated current inhibition in wild type and cysteine-substituted receptors.

The extent of MK801 current inhibition for all cysteine-substituted/ PTrEA-reacted potentiation positions in the GluN1 and GluN2C S1-M1 and S2-M4 linkers are comparable to wild-type. In contrast, potentiation positions in M3/M3-S2 linkers showed multiple signs of altered MK801 block including current rebound at removal of MK801 (A), reduced extent of inhibition (B & C),

and consistent double exponential fits to MK801 inhibition, e.g. GluN2C E635C (data not shown).

(A) Extent of MK801-mediated current inhibition in GluN1(A635C)-GluN2C receptors reached ~93% (left recording), a value comparable to wild-type GluN1-GluN2C receptors (Fig. 2.6A). Following reaction to PTrEA, the extent of MK801 inhibition was significantly reduced (right) and, at the end of MK801 exposure, a significant rebound of current (not seen in wild-type or other mutants) was observed. Dashed overlays indicate 1st order exponential fits to MK801 inhibition.

(B & C) Mean percent MK801-mediated inhibition (+/- 2SEM) of currents without (pre-PTrEA) and following (post-PTrEA) PTrEA for GluN1 (B) and GluN2C (C) potentiation positions. Filled bars indicate positions where extent of MK801 inhibition was significantly different from that of wild-type GluN1-GluN2C ($p < 0.05$).

MK801 block kinetics in cysteine-substituted receptors that show PTrEA-induced current inhibition (suppl. Fig. 2.3).

To test whether other factors, such as an interaction between the positively-charged MK801 and PTrEA, confound MK801-based estimates of relative P_o, we measured the rates of MK801 inhibition for a limited number of positions that showed PTrEA-induced current inhibition (supplemental Fig. 2.3). The net PTrEA-induced inhibition of current amplitudes could be driven by a gating effect (decrease in P_o) and/or a conductance effect (decrease in g). Of the four positions tested, one, GluN2C V786, showed a significant decrease in the rate of MK801 inhibition following PTrEA (supplemental Fig. 2.3B). For the other three positions, GluN1 R641, GluN2C T522 and GluN2C E785, PTrEA had no significant effect on rates of MK801 inhibition (supplemental Fig. 2.3A & B). These results indicate that PTrEA reaction with sites at the linkers does not generally increase the rate of MK801 inhibition (as occurs with potentiation positions). Rather the rate of MK801 block is altered in a manner consistent with changes in macroscopic currents: inhibition positions show either a reduced rate of MK801 block (possibly reflecting a reduced P_o) or no change (suggesting a reduction in conductance underlies PTrEA-induced whole-cell current inhibition), whereas potentiation positions show exclusively an increased rate (Fig. 2.6).

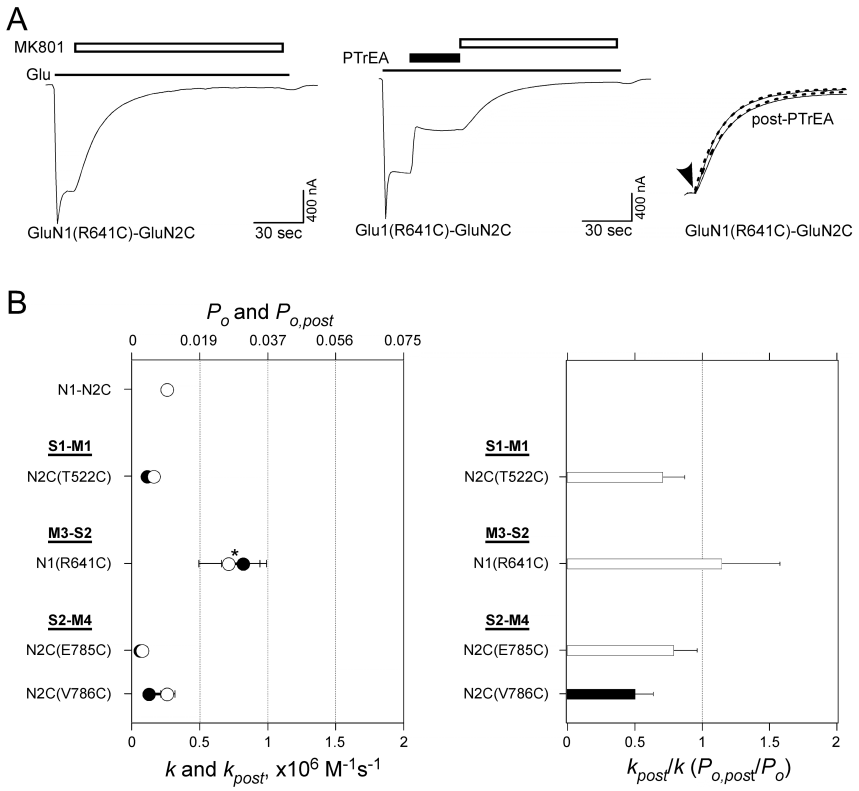

Supplemental Figure 2.3. MK801 block kinetics in cysteine-substituted receptors that show PTrEA-induced current inhibition.

Rate of MK801 inhibition of currents following PTrEA reaction with example GluN1- and GluN2C- inhibition positions (see Figs. 2.3-2.5) is either unchanged (A & B) or significantly reduced (GluN2C V786C, B).

(A) MK801 current inhibition in GluN1(641C)-GluN2C without (left) and following (middle) PTrEA. Single exponential fits to MK801-mediated inhibition of normalized currents are denoted by dashed overlays (right).

(B, left) Rates of MK801 inhibition without (k, unfilled circle) and following (k_{post}, filled circles) PTrEA. Asterisks denote positions where the cysteine substitution itself significantly the altered rate of MK801 inhibition from wild-type GluN1-GluN2C. In some instances error bars are smaller than the symbol.

(B, right) Ratio k_{post}/k. Dashed line indicates $k_{post}/k = 1$. Filled bar indicates positions where rate of MK801 inhibition following PTrEA was significantly different from that without PTrEA. Note that GluN2C-inhibition position V786C shows a significant reduction in P_o following PTrEA, suggesting that the net inhibition of whole-cell amplitudes is due in part to a gating effect.

Single channel recordings of wild type and cysteine-substituted GluN1-GluN2C receptors (suppl. Table 2).

We recorded single channels from wild-type and cysteine-substituted GluN1-GluN2C receptors in the presence of 0.5 mM Ca^{2+} (see Materials and Methods). In our recordings, we always found two conductance levels for wild type (as well as mutant) receptors (supplemental Table 2), as has been reported previously (Stern et al., 1992; Dravid et al., 2008). The values of these conductance levels (lower, 23.0 ± 0.4 pS and higher, 39.2 ± 0.7 pS) are comparable to those reported previously from oocytes in 1 mM Ca^{2+} (19 & 35 pS; (Stern et al., 1992) but smaller than those recorded from HEK 293 cells (28 & 45 pS; (Dravid et al., 2008). The mean open times were dependent on the conductance level with the lower conductance having a mean open time of 0.25 ± 0.04 ms and the higher conductance 1.09 ± 0.19 ms. This differs from earlier reports which found that the mean open time was independent of the conductance level (Stern et al., 1992; Dravid et al., 2008). Several factors could contribute to this. For one, we did not correct for missed events. In addition, the idealization by QuB may have missed rapid transitions to the lower conductance level (though for the present experiments we are mainly interested in the total open time). Nevertheless, visual inspection of the main conductance levels indicated that the QuB idealization was quite good and that no obvious events (closures or transitions into the lower conductance level) were missed in the longer open events.

Supplemental Table 2. Single channel parameters of wild-type and cysteine-substituted GluN1-GluN2C receptors tested before and after PTrEA in outside-out patches.

		N1-N2C		N1(S531C)-N2C		N1-N2C(V523C)		N1-N2C(S788C)	
PRE-PTrEA		mean	SEM	mean	SEM	mean	SEM	mean	SEM
Lower	*I* (pA)	-1.84	0.02	-1.75	0.07	-2.06	0.15	-1.97	0.08
	g (pS)	23.0	0.4	21.9	1.45	25.7	3.2	24.6	1.8
	area	26%	4%	33%	2%	40%	4%	27%	4%
	MOT (ms)	0.25	0.04	0.21	0.03	0.35	0.11	0.14	0.02
	occupancy (s)	0.82	0.22	2.60	0.92	2.98	0.78	2.40	0.39
	# of events	2598	819	8448	2363	7790	2248	10359	1444
Higher	*I* (pA)	-3.14	0.03	-3.08	0.03	-3.40	0.19	-3.56	0.26
	g (pS)	39.2	0.7	38.5	0.69	42.5	4.1	44.5	5.5
	area	74%	4%	67%	2%	60%	4%	73%	4%
	MOT (ms)	1.09	0.19	0.71	0.03	0.93	0.23	0.75	0.11
	occupancy (s)	1.88	0.36	5.49	1.80	4.93	1.73	6.19	0.24
	# of events	2206	638	6474	1915	5779	2017	8355	1195
	TOT (s)	2.70	0.58	8.09	2.71	7.90	2.46	8.59	0.50
	total time (s)	64	9.4	87.78	14.46	87.5	1.2	89.39	9.38
	Patch P_o	0.054	0.015	0.08	0.02	0.09	0.03	0.10	0.01
	t_{fast} (ms)	0.16	0.03	0.15	0.01	0.22	0.07	0.11	0.02
	t_{slow} (ms)	1.10	0.20	0.86	0.04	1.15	0.31	0.82	0.11
POST-PTrEA									
Lower	*I* (pA)	-1.68	0.08	-1.51	0.08	-1.87	0.08	-1.84	0.06
	g (pS)	21.0	1.8	18.9	1.7	23	2	23.0	1.2
	Area1	42%	5%	44%	1%	41%	2%	27%	4%
	MOT (ms)	0.35	0.04	0.29	0.02	0.42	0.09	0.19	0.03
	occupancy (s)	1.54	0.53	8.17	1.14	6.50	1.42	10.07	1.93
	# of events	3360	943	22705	3499	13732	3463	34982	5501
Higher	*I* (pA)	-3.11	0.04	-2.79	0.05	-3.20	0.08	-3.19	0.24
	g (pS)	38.8	0.8	34.8	1.1	40	2	39.9	5.2
	SD	58%	5%	56%	1%	59%	2%	73%	4%
	MOT (ms)	0.88	0.18	0.57	0.08	0.82	0.19	0.80	0.08
	occupancy (s)	2.28	1.00	10.54	1.65	10.12	2.17	22.08	3.06
	# of events	2784	1030	17317	2954	11092	2711	27490	5013
	TOT (s)	3.83	1.52	18.71	2.78	16.62	3.43	3.83	1.52
	total time (s)	74.81	12.55	93.34	15.80	104.92	9.44	112.47	15.01
	Patch P_o	0.04	0.01	0.22	0.03	0.16	0.03	0.28	0.01
	t_{fast} (ms)	0.20	0.06	0.21	0.01	0.19	0.02	0.14	0.03
	t_{slow} (ms)	1.10	0.14	0.84	0.07	1.06	0.15	0.94	0.10
POST/PRE Ratio									
	lower g	0.91	0.04	0.86	0.03	0.92	0.02	0.94	0.02
	MOT	1.51	0.13	1.50	0.13	1.68	0.32	1.30	0.06
	higher g	0.99	0.01	0.91	0.02	0.95	0.03	0.90	0.02
	MOT	0.78	0.05	0.79	0.08	0.99	0.13	1.12	0.11
	Patch P_o	0.72	0.04	3.64	0.67	2.13	0.23	3.02	0.46

Single channel recordings were done as described in text (n = 3 for each receptor) at a holding potential of -80 mV. MOT, mean open time. TOT, total open time. τ_{fast} and τ_{slow} were derived from 2nd order exponential fits to dwell time histograms (e.g. Fig. 2.7C).

Supplemental Table 3. Summary of observed effects on potentiation positions.

		SS Pot.	Δ Leak	MK801 $k_{post}/k > 1$	Patch P_o pst/pre > 1	Mod. Rts $k_+/k_- > 1$	SS Pot. Size Dep.
GluN1		Figs. 2-5	Figs. 2-5	Fig. 2.6	Fig. 2.7	Fig. 2.9	Fig. 2.10
S1-M1	K526C	Yes (>100%)	No	Yes	-	No	No
	S531C	Yes (>100%)	No	Yes	Yes	Yes	Yes
	D534C	Yes	No	Yes	-	-	Yes
M3-S2	A635C*	Yes (>100%)	Yes	-	-	-	-
S2-M4	R783C	Yes	No	Yes	-	-	Yes
	P787C	Yes (>100%)	Yes	Yes	-	Yes	Yes
	T789C[$]	Yes (>100%)	No	-	-	-	-
GluN2C							
S1-M1	R518C	Yes (>100%)	No	Yes	-	Yes	Yes
	V523C	Yes (>100%)	Yes	Yes	Yes	Yes	Yes
	E530C	Yes (>100%)	Yes	Yes	-	No	No
	S533C	Yes	Yes	Yes	-	-	Yes
M3-S2	A630C*	Yes	Yes	-	-	-	-
	E635C*	Yes (>100%)	No	-	-	-	-
S2-M4	M787C	Yes	No	Yes	-	-	No
	S788C	Yes (>100%)	Yes	Yes	Yes	Yes	Yes
	S789C	Yes (>100%)	Yes	Yes	-	Yes	Yes
	D792C[†]	Yes (>100%)	No	Yes	-	-	No
	I793C[#]	Yes	No	-	-	-	-

Listed are the cysteine-substituted receptors in the present study for which PTrEA induced whole-cell current potentiations. A dash (-) indicates properties not tested. *M3/M3-S2 potentiation positions were not studied in detail due to their apparent disruption of MK801 block (supplementary Fig. 2.2). [$]GluN1(T789C) was not explored beyond steady-state PTrEA accessibility (Fig. 2.5) due to small control current amplitudes. [†]GluN2C(D792C) was not tested for PTrEA modification rates. [#]GluN2C(I793C) was not explored beyond steady-state PTrEA accessibility (Fig. 2.5) because it showed incomplete reaction to PTrEA.

CHAPTER 3: LOCAL CONSTRAINTS IN EITHER THE GLUN1 OR GLUN2 SUBUNIT EQUALLY IMPAIR NMDA RECEPTOR PORE OPENING

ABSTRACT

The defining functional feature of NMDA receptors is activation gating—the energetic coupling of ligand binding into opening of the associated ion channel pore. NMDA receptors are obligate heterotetramers typically composed of glycine-binding GluN1 and glutamate-binding GluN2 subunits that gate in a concerted fashion requiring all four ligands to bind for subsequent opening of the channel pore. In an individual subunit, the extracellular ligand-binding domain, composed of discontinuous polypeptide segments S1 and S2, and the transmembrane channel-forming domain, composed of M1-M4 segments, are connected by three linkers: S1-M1, M3-S2 and S2-M4. To study subunit-specific events during pore opening in NMDA receptors, we impaired activation gating via intrasubunit disulfide bonds connecting the M3-S2 and S2-M4 in either the GluN1 or GluN2A subunit, thereby interfering with the movement of the M3 segment, the major pore lining and channel gating element. NMDA receptors with gating impairments in either the GluN1 or GluN2A subunit were dramatically resistant to channel opening, but when they did open showed only a single conductance level indistinguishable from wild type. Importantly, the late gating steps comprising pore opening to its main long-duration open state were equivalently affected regardless of which subunit was constrained. Thus the NMDA receptor ion channel undergoes a pore opening mechanism in which the intrasubunit conformational dynamics at the level of the ligand-binding/transmembrane domain linkers, are tightly coupled across the four subunits. Our results further indicate that conformational freedom of the linkers between the ligand-binding and transmembrane domains is critical to the activation gating process.

INTRODUCTION

Representative crystal structures of ligand-gated ion channels from multiple families are now available (Jiang et al., 2002; Hilf and Dutzler, 2008; Kawate et al., 2009; Sobolevsky et al., 2009). Nevertheless, the dynamics of their activation gating—the series of conformational changes that couple binding of ligands to opening of the ion channel pore—remain unresolved. Ionotropic glutamate receptors (iGluRs), including the NMDA receptor subtype, mediate fast excitatory synaptic transmission integral to central nervous system function. Kinetic studies of NMDA receptors have identified key energetic steps, including various intermediate states, in the activation gating process (Wyllie et al., 1996; Banke and Traynelis, 2003; Auerbach and Zhou, 2005; Schorge et al., 2005; Dravid et al., 2008; Kussius and Popescu, 2009). These kinetic mechanisms therefore provide a template to define the dynamics of gating in NMDA receptors, though the structural events underlying the kinetic steps are unknown.

A single iGluR subunit contains four modular domains, the extracellular amino-terminal (ATD) and ligand-binding (LBD) domains, a transmembrane domain (TMD) and an intracellular C-terminal domain (CTD) (Oswald et al., 2007; Traynelis et al., 2010; Mayer, 2011). The core domains necessary and sufficient for activation gating are the LBD (composed of S1 and S2) and TMD (composed of M1-M4) (Fig. 3.1A). These core domains are coupled by three short polypeptide linkers (S1-M1, M3-S2 and S2-M4) that mediate ligand-induced conformational changes in the LBD to opening of the channel pore. In the tetrameric assembly of an iGluR, the four M3 transmembrane segments form the pore and constitute the main channel gating element (Kohda et al., 2000; Jones et al., 2002; Qian and Johnson, 2002; Sobolevsky et al., 2002; Yuan et al., 2005; Blanke and VanDongen, 2008; Chang and Kuo, 2008). Homologous to the evolutionarily linked K^+ channel (Wo and Oswald, 1995; Wood et al., 1995; Chen et al., 1999a;

Panchenko et al., 2001; Kuner et al., 2003; Sobolevsky et al., 2009), opening of the channel pore in iGluRs involves, in some form, movements of the M3 segments away from the central axis of the pore (Fig. 3.1B). The M3-S2 linker that connects the LBD to the M3 segment must therefore be a central element of the gating machinery coupling conformational dynamics at the LBD to pore opening.

In the only intact iGluR structure of a homomeric AMPA receptor, the LBD-TMD linkers mediate an unprecedented symmetry mismatch between the LBD (2-fold symmetry relative to central axis of receptor) and the ion channel (4-fold symmetry) by adopting different conformations in adjacent subunits (Sobolevsky et al., 2009). If this symmetry mismatch also exists in the NMDA receptor, it is likely to have important gating consequences because the functional unit within the receptor is thought to be a heterodimer containing a glycine-binding GluN1 and a glutamate-binding GluN2 subunits (Furukawa et al., 2005). Due to the different linker arrangements, the energetic mechanisms coupling ligand binding to pore opening may differ within an NMDA receptor heterodimer. Still, in an intact NMDA receptor, all four subunits must bind their respective ligands for subsequent pore opening to occur (Benveniste and Mayer, 1991a; Clements and Westbrook, 1991; Schorge et al., 2005), although the physical mechanism and structural basis for this concerted gating process is unknown.

To investigate subunit dependent mechanisms driving pore opening in NMDA receptors, we identified means to physically constrain the M3-S2 linker by disulfide crosslinking it with the S2-M4 linker within specific NMDA receptor subunits, either GluN1 or GluN2A. Using single channel recordings and kinetic analysis to define energetic effects on gating, we find that constraining M3-S2 in either GluN1 or GluN2A strongly reduced channel open probability. The most dramatic effect was on the late gating steps mediating pore opening where a long-lived,

energetically stable open state was nearly abolished. In these late gating steps, we found a tight coupling across all NMDA receptor subunits—full pore opening would not occur unless all four subunits undertook their own intrasubunit gating actions. Thus concerted gating in NMDA receptors requires equivalent intrasubunit movements of M3-S2 relative to S2-M4 occuring together across both GluN1 and GluN2 subunits.

METHODS

Mutagenesis and expression.

Cysteine substitutions in the rat GluN1a (accession # P35439) and GluN2A (Q00959) subunits were generated using PCR-based methods (Sobolevsky et al., 2007). As a reference and background for mutagenesis, we used a GluN2A construct in which a reactive cysteine near the N terminus of S1 was mutated to an alanine (C399A). *Xenopus* oocytes were prepared, injected with cRNA and maintained as previously described (Sobolevsky et al., 2007). Recordings were made 2-5 days after injection. For mammalian cell expression, human embryonic kidney 293 (HEK 293) cells, were co-transfected with cDNA for GluN1 and GluN2A subunits, as well as a vector for enhanced green fluoresecent protein (pEGFP-Cl, Clontech), at a ratio of (in μg) 1:1:1, using Fugene 6 (Roche). Recordings were made 24-72 hours after transfection.

Macroscopic current recordings and analysis.

Macroscopic currents of *Xenopus* oocytes were recorded at room temperature (20-23º C) using two microelectrode voltage clamp (TEVC) (DAGAN TEV-200A, DAGAN Corp.) with Cell Works software (*npi* electronic). Microelectrodes were filled with 3 M KCl and had resistances of 1-4 MΩ. The external solution consisted of (in mM): 115 NaCl, 2.5 KCl, 0.18 $BaCl_2$, 5 HEPES and 100 μM EDTA (pH 7.2, NaOH), unless otherwise noted. All reagents including glycine (20 μM) and glutamate (200 μM), competitive antagonists for GluN1, 5, 7-Dichlorokynurenic acid (DCKA, 10 μM) and for GluN2, DL-2-amino-5-phosphonopentanoic acid (APV, 100 μM), and the reducing agent dithiothreitol (DTT, 4 mM) were applied with the bath solution. All reagents were obtained from Roche or Sigma-Aldrich.

Steady-state reactions. Steady-state reactions were quantified at a holding potential of -60 mV. Baseline glutamate-activated current amplitudes (I_{pre}) were established by three to five 15-s applications of glutamate and glycine. All agonist or any other reagent applications were separated by 30 to 120 sec washes in agonist-free solution. DTT (4 mM) was applied for 2 mins in the absence of agonist, but in the presence of the competitive antagonists DCKA (for GluN1) and APV (for GluN2). We found that DTT more effectively potentiated current amplitudes under these conditions than when applied in the presence of agonists (data not shown). After DTT exposure, current amplitudes (I_{post}) were determined using three to five agonist applications. The change in glutamate-activated current amplitude, expressed as a percentage (% change), was calculated as: = $(I_{post} - I_{pre})/I_{pre}$ x 100. In certain instances, we corrected for observed current rundown by fitting a single exponential function to a minimum of three pre-DTT glutamate-activated current amplitudes.

MK801 inhibition. MK801 is an irreversible (on the time-scale of tens of minutes) open channel blocker at hyperpolarized potentials (Huettner and Bean, 1988). MK801 inhibition was assessed with either 1 μM (Fig. 3.3A-C) or 25 nM (Fig. 3.3D-H) MK801 after agonist-induced current amplitudes had reached steady-state. The change in glutamate-activated current amplitude, expressed as a percentage (% change), was calculated as: = $(I_{post} - I_{pre})/I_{pre}$ x 100. For DTT and antagonist treatments, % change was calculated relative to the current amplitudes preceding these treatments but following MK801 block. The kinetics of MK801 inhibition were fitted with either single- or bi-exponential functions. A higher order exponential function was used only when it qualitatively minimized the residual currents (I_{res}) of these fits (see lower graphs in Fig. 3.3D & E).

Single Channel Recordings and Analysis.

Single channel recordings were made at steady-state using the cell-attached configuration on HEK 293 cells. Currents were acquired using an Axopatch 200B amplifier, filtered at 10 kHz (four-pole Bessel filter) and digitized at 50 kHz (ITC-16 interfaced with Patchmaster). The bath solution consisted of (in mM): 150 NaCl, 2.5 KCl and10 HEPES (pH 7.2, NaOH). Although gating in NMDA receptors can be modulated by external [H^+] (Erreger et al., 2005a), we used pH 7.2 rather than a high pH to allow direct comparison between the HEK cell and oocyte recordings. Pipettes electrodes were pulled from thick-walled borosilicate glass (Warner Instruments) and fire-polished immediately before use. The pipettes were filled with an external solution (pipette) consisting of the bath solution supplemented with 1 mM EDTA, 0.1 mM Gly and 1 mM glutamate. Final resistances were 10-40 MW when filled with pipette solution and measured in the bath solution. A voltage of +100 mV was applied through the recording pipette to elicit inward sodium currents. In certain instances, patches were broken into the whole-cell configuration to note the resting V_m, which was typically from -11 to -30 mV, after the recording period had ended.

For experiments assessing the effect of DTT on NMDA receptor single-channel actvity, we paralleled the DTT application protocol used to efficiently reduce the disulfide bonds in our whole-cell oocyte recordings (see Fig. 3.2C). We pretreated the NMDA receptor-transfected HEK cells with 4 mM DTT, 10 μM DCKA and 100 μM APV in our bath solution and then came in with the patch pipette (containing the agonists, but no DTT) under positive pressure to form the cell attached seal. For whole-cell recordings in oocytes, current amplitudes of the double-cysteine substituted receptors gradually decreased over time following washout of DTT,

presumably due to disulfide bond reformation (data not shown). However, for the single-channel recordings, the DTT-induced high activity levels remained constant even in recordings lasting up to 50 mins. We do not understand this apparent lack of disulfide bond reformation in the cell-attached mode, but it may reflect that the glass pipette does not provide an absolute oxidizing environment.

Data (in .dat format) were transferred to QuB (http://www.qub.buffalo.edu) for analysis. Each recording was visually inspected in its entirety for multiple simultaneous openings, signal-to-noise fluctuations, high-frequency artifacts and baseline drifts. For GluN1/GluN2A receptors without DTT and all receptors with DTT, the recordings consisted of long clusters of activity separated by seconds-long periods of zero-activity, making it straight-forward to detect > 1 channel in the patch as simultaneous openings. In these cases, given the high P_o (0.5 – 0.98) of GluN2A containing receptors and the minutes-long duration (with 10,000 – 320,000 events) of recordings without any apparent multiple openings, these recordings certainly contained only a single channel in the patch. For recordings of GluN1(R645C,S784C)/GluN2A and GluN1/GluN2A(Q642C,K785C) without DTT (P_o < 0.02), it was more challenging to detect single channel patches. First many patches were recorded but excluded from analysis due to obvious simultaneous openings of multiple channels. Of the remaining patches, only minutes long recordings (with 2500 – 52000 events) without any apparent simultaneous openings were further analyzed. According to Colquhoun and Hawkes (Colquhoun and Hawkes, 1990), a two channel patch containing channels with a P_o of 0.01 is expected to undergo at least one double-opening every 200 single-opening events. Among our analyzed GluN1(R645C,S784C)/GluN2A and GluN1/GluN2A(Q642C,K785C) recordings, the least number of events recorded in a patch

without any apparent double opening was 2675. Therefore, we are reasonably confident that we analyzed patches containing only a single channel.

Further processing was done to eliminate occasional obvious brief noise spikes (e.g. high amplitude, stereotypical exponential-like decay, etc) by matching them to the level of adjacent events using the 'erase' function in QuB. Long periods of high noise were deleted with the remaining flanking segments separated as discontinuous segments. Baseline drift was corrected by resetting baseline to zero current levels. Processed data were idealized using the SKM algorithm following filtering to 12 kHz with a Gaussian digital filter. A conservative dead-time of 0.15 ms was imposed across all recording files. The idealization protocol may have missed very fast events and we did not correct for such missed events. Still, our goal was not to define an absolute kinetic mechanism of NMDA receptor gating, but rather to compare kinetic mechanisms across conditions. For our analysis, we assume that missed events were largely equal across different experimental conditions.

Kinetic analysis was performed using the MIL algorithm in QuB. State models with increasing open and closed states were constructed and fitted to the recordings until log-likelihood (LL) values improved by less than 10 LL units/added state. We used a linear fully-liganded state model containing 3 closed states, 2 desensitized states and 2-4 open states (see Figs. 3.7A & 3.8A), of NMDA receptor gating (Kussius and Popescu, 2009). All recordings of GluN1/GluN2A and double-cysteine substituted receptors were best fit by 5 closed and 2-4 open states (all additional open states branched out of the first one). The open-time components, comprising one common short duration (O_1) and up to three long duration (O_{2-4}) intervals arise from modal gating of NMDA receptors (Popescu and Auerbach, 2003). The long open events O_3 and O_4 did not occur in every patch either of WT or double-cysteine substituted receptors. In

addition, for the double-cysteine substituted receptors, the overall number of modal shifts to these long open states was low, simply due their low (P_o < 0.03). Therefore, we could not perform any statistical analysis of shifts in modal gating. Rather, for ease of analysis and comparison, we aggregated the 2-4 open-time components into two, one short duration (O_1) and one long duration (O_2), components (Fig. 3.7A). Time constants and the relative areas of each component, the transition rate constants, as well as mean closed time (MCT) and mean open time (MOT) were averaged for each receptor without and with DTT pretreatment and compared to each other.

Statistics.

Data analysis was done using Igor Pro (Wavemetrics, Inc.), QuB and Microsoft Excel. For analysis and illustration, leak currents were subtracted from total currents. Results are presented as mean +/- SEM. An ANOVA was used to define statistical differences. The Tukey or Dunnett tests were used for multiple comparisons of means. Significance was defined at $P < 0.05$.

Biochemistry.

2-3 days after injection of ~10 ng of cRNA per oocyte, ten healthy oocytes expressing WT GluN1/GluN2A or cysteine substituted GluN1/GluN2A receptors were selected for membrane purification. For a positive control, we used GluN1(N521C,L777C)/GluN2A(E516C,L780C) receptors that form disulfide bond-stabilized intersubunit dimers (Furukawa et al., 2005). Oocytes were washed with 1x phosphate buffer saline (PBS), lysed in 1 mL lysis buffer (20 mM Tris and 0.5 mM N-Ethylmaleimide (NEM)) and centrifuged (3,000 rpm, 3 mins, 4ºC) to separate out the yolk. Recovered supernatant was centrifuged (40,000 rpm, 10 min, 4ºC). The

pellet was washed with 1 ml PBS and re-centrifuged (40,000 rpm, 10 min, 4ºC). The resulting pellet was resuspended in 87 µl solubilization buffer (20 mM Tris, 0.5 mM NEM, 50 mM NaCl and 1/1,000 protease inhibitor cocktail) without detergent and bath sonicated in ice water 4 times (15 sec on/15 sec off). Detergents (1 % Triton X-100 and 0.3 % sodium deoxycholate (monohydrate)) was added to the solubilization buffer to a final volume of 100 µl and incubated with gentle agitation at 4º C for 1 hour. Solubilized proteins were centrifuged (40,000 rpm, 20 min, 4º C) and the recovered supernatant contained the purified membrane fraction.

Membrane fractions were run on a 5 % SDS-PAGE gel under non-reducing conditions. Proteins were transferred to 0.45 mm nitrocellulose membranes by semi-dry transfer (BioRad, Hercules, CA) using Bjerrum-Schafer-Nielsen buffer. Membranes were probed with either mouse anti-NMDAR1 (1:300, Millipore) or rabbit anti-NMDAR2A (1:300, Millipore). Blots were developed with Western Blotting Luminol Reagent (Santa Cruz Biotechnology) and exposed to chemiluminesence Biomax Film (Kodak, Cedex, France).

RESULTS

Intrasubunit disulfide crosslinking of the M3-S2 and S2-M4 linkers in GluN1 and GluN2A NMDA receptor subunits.

In an iGluR subunit, the M3-S2 linker connects the LBD to the M3 transmembrane segments, the main channel gating element (Fig. 3.1). To dissect out subunit-dependent mechanisms of pore opening in NMDA receptors, we sought to constrain the gating movements of M3-S2. We therefore substituted cysteines in M3-S2 as well as S2-M4 (connecting the LBD to M4) to generate intrasubunit disulfide bonds (Fig. 3.2). Our experimental design used spontaneously formed disulfide bonds rather than oxidizing agent-induced formation of disulfide bonds because the latter can more readily trap receptors in rarely visited conformations. We tested multiple pairs of M3-S2 and S2-M4 cysteine-substituted positions in GluN1 (Fig. 3.2A) and GluN2A (Fig. 3.2B) anticipating that spontaneously formed disulfide bonds could be broken by the reducing agent dithiothreitol (DTT) and that, if these constraints affected gating, treatment with DTT would yield significant changes in current amplitudes.

For each subunit we identified a pair of positions displaying the anticipated phenotype: for GluN1 R645 in M3-S2 and S784 in S2-M4 and for GluN2A Q642 in M3-S2 and K785 in S2-M4. Exposure of the double-cysteine substituted receptors GluN1(R645C,S784C)/GluN2A or GluN1/GluN2A(Q642C,K785C) (hereafter referred to as GluN1(C,C) and GluN2A(C,C), respectively) to extracellularly applied DTT significantly potentiated whole-cell current amplitudes (% potentiation, mean ± SEM; 151 ± 28 %, n = 11 and 102 ± 14 %, n = 8, respectively) compared to GluN1/GluN2A (5.6 ± 3.5 %, n = 5) (Fig. 3.2C & D). (Note that DTT most effectively potentiated current amplitudes of the double-cysteine substituted receptors when

it was applied in the presence of competitive antagonists, see Methods). In contrast, NMDA receptors containing a corresponding single-cysteine substitution showed no significant DTT-induced current potentiation (Fig. 3.2D). We therefore conclude that DTT-induced current potentiation in the double cysteine-substituted receptors results from reduction of spontaneously formed disulfide bonds between substituted cysteines. The observed disulfide crosslinking between M3-S2 and S2-M4 was within a single subunit (intrasubunit) rather than between like subunits (e.g., substituted cysteine in M3-S2 of one GluN1 crosslinking with substituted cysteine in S2-M4 of the other GluN1 subunit), since, in contrast to the positive control, no dimers were detected for either GluN1(C,C)/GluN2A or GluN1/GluN2A(C,C) (Fig. 3.2E).

NMDA receptors with crosslinked GluN1 or GluN2A subunits are resistant to persistent pore block by MK801.

As an initial assessment of whether constraining the M3-S2 linkers affects gating, we used MK801, an irreversible open channel pore blocker (Huettner and Bean, 1988; Jahr, 1992). Treatment of GluN1/GluN2A, GluN1(C,C)/GluN2A or GluN1/GluN2A(C,C) with a high concentration (1 μM) of MK801 strongly inhibited current amplitudes (% inhibition: 95 ± 0.2 %, n = 4, 94 ± 1.4 %, n = 4 & 92 ± 0.9 %, n = 9, respectively) (Fig. 3.3A-C). Surprisingly, however, the remaining MK801-resistant current for GluN1(C,C)/GluN2A and GluN1/GluN2A(C,C) was significantly potentiated by DTT applied in the presence of competitive antagonists (% potentiation: 704 ± 88 %, n = 4 and 453 ± 35 %, n = 8, respectively), compared to that in GluN1/GluN2A (86 ± 15 %, n = 4) (Fig. 3.3A-C). This observed effect was specific to DTT as application of antagonists alone on MK801-treated GluN1(C,C)/GluN2A or GluN1/GluN2A(C,C) receptors did not produce significant current potentiation (Fig. 3.3C).

Thus, a population of double-cysteine substituted receptors is resisitant to persistent pore block by MK801 but sensitive to DTT-induced current potentiation. In conjunction with the later single channel results, we conclude that this MK801-resistant component of double-cysteine substituted receptors is the portion of cell-surface receptors containing intact DTT-sensitive crosslinks. In contrast, the portion of cell-surface receptors that undergo pore block MK801 likely contains uncrosslinked disulfides. Application of the strong oxidizing reagent Copper(II):Phenanthroline did not affect the pre-DTT current amplitudes (data not shown), suggesting that the uncrosslinked disulfides exist as superoxide species, such as as -SOH, $-SO_2H$ and $-SO_3H$ forms (Cline et al., 2004).

To investigate further these redox-heterogenous populations of cell-surface receptors, we quantified the rate of MK801 block of WT and GluN1(C,C)/GluN2A receptors. A low concentration of MK801 (25 nM) inhibited whole-cell current amplitudes of WT receptors, the rate of which was well-described by a single exponential function (time constant τ = 6.8 ± 0.6 secs, n = 5) (Figs. 3D & G). In contrast, MK801-mediated (25 nM) decay of whole-cell current amplitudes of GluN1(C,C)/GluN2A was best fitted (see Methods) with a biexponential function (τ_f = 14.8 ± 1.4 secs, τ_s = 70.3 ± 5.2, n = 4) (Figs. 3E & G). DTT treatment of GluN1(C,C)/GluN2A did not affect the kinetics of the bioexponential components of MK801 inhibition (τ_f = 12.5 ± 0.9 secs, τ_s = 71.9 ± 11, n = 5) (Figs. 3F & G) but reversed their fractional contributions (post-DTT: τ_f = 37.7 ± 1.9 %, τ_s = 62.3 ± 6.4 %, vs. pre-DTT: τ_f = 82.1 ± 1.9 %, τ_s = 17.3 ± 1.9 %) (Fig. 3H), resulting in an increase in the overall rate of MK801 block (Fig. 3F).

We interpret these data as follows. For GluN1(C,C)/GluN2A cell-surface receptors, τ_f, which approaches the faster single exponential function in WT receptors, underlies MK801 block of the uncrosslinked double-cysteine substituted receptors. Conversely τ_s represents MK801 block of

the crosslinked receptors. Prior to DTT, the uncrosslinked and crosslinked receptors account for ~ 40 % and ~ 60 % of the macroscopic current amplitudes. DTT treatment breaks the disulfide bonds in the crosslinked receptors, resulting in ~ 80 % of the macroscopic currents now being carried by uncrosslinked receptors. This biophysical assessment of the properties of MK801 block reveals that the heterogenous population of cell-surface double-cysteine substituted receptors significantly complicate the macroscopic current profile of these receptors. To more cleanly study the gating effects of the intrasubunit crosslinks, we therefore used single channel recordings

Constraining relative movements of M3-S2 and S2-M4 in either GluN1 or GluN2A with intrasubunit disulfide crosslinks dramatically impairs NMDA receptor activation gating.

Fig. 3.4, left shows representative steady-state single channel recordings of GluN1/GluN2A (A), GluN1(C,C)/GluN2A (B) or GluN1/GluN2A(C,C) (C) receptors acquired in the cell-attached mode on transiently transfected HEK cells. For each receptor, a parallel set of recordings was made from separate HEK cells pre-treated with DTT (Fig. 3.4, right) (see Methods). Currents were recorded in the cell-attached mode at a pipette potential of +100 mV with saturating concentrations of glycine (0.1 mM) and glutamate (1 mM) in the pipette. The recordings shown as well as all others used for subsequent analysis were done on patches that contained a single channel (see Methods).

Qualitatively, the double-cysteine substituted receptors, compared to WT GluN1/GluN2A, displayed considerably reduced single channel activity, with only flickery short duration openings apparent (Fig. 3.4B & C, left). Strikingly, the predominant long duration openings typical in WT receptors were essentially absent in double-cysteine substituted receptors (Fig.

3.4, left, bottom traces). Nevertheless, there were similarities between the single channel activity profiles; like GluN1/GluN2A, the double-cysteine substituted receptors showed: (1) bursts of activity separated by long periods of no activity, (2) no obvious sub-conductance levels, and (3) comparable unitary current amplitudes. These similarities suggest that basic NMDA receptor gating behavior was intact in the double-cysteine substituted receptors. Importantly, the observed gating differences in the double-cysteine substituted NMDA receptors were mainly, if not exclusively, due to the intrasubunit disulfide crosslinks since with DTT treatment the double-cysteine substituted receptors, like WT, showed comparable high frequency and long duration channel openings (Fig. 3.4, right).

Table 3.1 summarizes the quantified single channel properties for WT and crosslinked NMDA receptors. Importantly, crosslinking M3-S2 and S2-M4 in either GluN1 or GluN2A did not affect unitary current amplitudes. Rather, the constraints drastically reduced equilibrium channel open probability (eq. P_o) (~ 30- and 75- fold, respectively) compared to GluN1/GluN2A. This reduction in eq. P_o resulted mainly from a decrease in mean open time (MOT) with a corresponding increase in mean closed time (MCT). Interestingly, while MOT was similarly affected, MCT was differentially affected in GluN1(C,C)/GluN2A and GluN1/GluN2A(C,C), hinting at subunit-specific contributions to gating transitions restricted to channel closed periods.

Following exposure to DTT, GluN1/GluN2A, GluN1(C,C)/GluN2A and GluN1/GluN2A(C,C) showed similar eq. P_o, MCT and MOT (Table 3.1). This result indicates that the low levels of gating activity in untreated double-cysteine substituted receptors was due to the physical constraint of the disulfide crosslinks between M3-S2 and S2-M4, an effect that can be fully reversed by breaking the disulfide bonds with DTT. Thus, constraining relative movements of M3-S2 and S2-M4 in either GluN1 or GluN2A deters NMDA receptor activation gating. DTT

treatment increased single channel activity, specifically MOT, in WT receptors (Table 3.1). Since activity in GluN1/GluN2A, GluN1(C,C)/GluN2A, and GluN1/GluN2A(C,C) was comparable following DTT treatment, DTT must be having this same effect on the double-cysteine substituted receptors. Nevertheless, the focus of the present study is on the gating effects of intrasubunit crosslink rather than any additional effects of DTT on wild type or double-cysteine substituted receptors. Hence, we restricted our analysis of the single-channel results to within the DTT-untreated and separately within the DTT-treated sets of recordings, not between them.

In summary, the physical constraint produced by the intrasubunit disulfide crosslinks in either GluN1 or GluN2A dramatically impaired pore opening. Thus the conformational freedom of the M3-S2 and S2-M4 linkers is critical to the energetics of the gating process coupling ligand binding to ion channel pore opening. Further, when pore opening does occur in receptors with gating constraints in either subunit, they are of a single conductance level indistinguishable from WT receptors, suggesting that even though gating is constrained in only two of the four subunits, the two unconstrained subunits cannot gate independently.

Gating impairments in either GluN1 or GluN2A similarly impact multiple channel-open and closed dwell time components.

To examine in more detail the effects of the subunit-specific gating constraints, we characterized the durations and relative areas of the individual components within the channel closed and open dwell time histograms (Fig. 3.5). The kinetics of NMDA receptor activation contain at least four closed- and two open- time components (Gibb and Colquhoun, 1992; Banke and Traynelis, 2003; Popescu and Auerbach, 2003; Auerbach and Zhou, 2005). The analyzed single channel

records of GluN1/GluN2A (Fig. 3.5A), GluN1(C,C)/GluN2A (Fig. 3.5B) or GluN1/GluN2A(C,C) (Fig. 3.5C) were best fit with 5 closed- and 2-4 open- time components (see Methods), suggesting that the basic kinetic mechanism of activation gating is unaffected by the intrasubunit disulfide crosslinks. Although 2-4 open-time components, comprising one common short duration and up to three long duration intervals arising from modal gating of NMDA receptors (Popescu and Auerbach, 2003) could be fitted to our single-channel data set for each receptor, we collapsed them into two components, one short and one long duration, for ease of analysis and comparison. For WT, the short duration openings (t_{O1}: 0.12 ± 0.01 ms) covered only a small fraction of the channel open time (a_{O1}: 6 ± 1.1%), whereas the long duration openings represented the predominant open-time component (τ_{O2} & a_{O2}: 8.7 ± 0.9 ms & 94 ± 1.1 %) (Table 3.2). Either GluN1 or GluN2A intrasubunit crosslinks most profoundly affected gating by severely shortening the duration of the longer open-time component (τ_{O2}) (N1(C,C)/N2A, 1.6 ± 0.2 ms; and N1/N2C(C,C), 1.9 ± 0.9 ms) (Fig. 3.6A, left). While the shorter open-time component (t_{O1}) was intact, its mean duration (0.25 ± 0.05 ms; and 0.45 ± 0.09 ms, respectively) was increased by the intrasubunit crosslinks (Fig. 3.6A, left).

Of the 5 closed-time components, the GluN1 and GluN2A intrasubunit crosslinks increased the same two long duration components (τ_3 & τ_4) (τ_3: N1/N2A, 4.2 ± 0.4 ms; N1(C,C)/N2A, 38.1 ± 8.6 ms; and N1/N2A(C,C), 55.5 ± 9 ms; & τ_4: 26.9 ± 5.6 ms; 208 ± 45 ms; and 154 ± 27 ms, respectively) (Fig. 3.6B, top). The relative area shifted away from the shorter duration (a_1 & a_2) and towards the longer duration (a_4 & a_5) closed-time components (Fig. 3.6B, bottom). Intriguingly, the shortest duration closed-time component (τ_1) was prolonged, albeit modestly, exclusively by the GluN1 intrasubunit crosslinks (0.14 ± 0.005 ms; 0.25 ± 0.04 ms; and 0.11 ± 0.01 ms, respectively) with its relative area (a_1) reduced to significantly different degrees by the

crosslinks in the different subunits (20.4 ± 1.5%; 12.6 ± 1.4% and 3.7 ± 0.3%, respectively) (Fig. 3.6B). In summary, constraining relative movements of M3-S2 and S2-M4 in either GluN1 or GluN2A decreases long channel openings and consequently increases receptor dwell times in long duration channel-closed states.

The GluN1 and GluN2A subunits contribute equally to pore opening steps.

To define subunit-specific contributions to pore opening steps, we fitted a previously described linear model of NMDA receptor activation (Fig. 3.7A) (Popescu and Auerbach, 2003; Auerbach and Zhou, 2005; Kussius and Popescu, 2009) to the idealized sequence of single channel closed and open times using the maximum interval likelihood (MIL) method (see Methods). Since all single channel recordings were done under saturating agonist concentrations, full occupancy of the agonist-binding sites was assumed and thus explicit agonist binding steps were excluded from the model. The linear scheme $C_3 - C_2 - C_1 - O_1 - O_2$, comprising the three shortest duration closed-time components (τ_3, τ_2 & τ_1) and the two aggregate open-time components (τ_{O1} & τ_{O2}), represents the central activation pathway. C_5, comprising the longest duration closed-time component (τ_5), represents the main microscopic desensitized state (Dravid et al., 2008). C_4, the other long duration closed time component (τ_4), is perhaps also a desensitization-related state (Dravid et al., 2008). This sequential activation gating scheme, with the indicated connectivity of the off-pathway desensitization-related states (Fig. 3.7A), fitted best the idealized data from each single channel record as determined by the highest log(likelihood) value, with rate constants for GluN1/GluN2A receptors within the range of previously published values using comparable recording conditions and configurations (Kussius and Popescu, 2009).

In comparing the rate constants, the GluN1 and GluN2A intrasubunit crosslinks had widespread and largely overlapping effects on the NMDA receptor activation mechanism (Fig. 3.7). All the central activation transitions, $C_3 \rightarrow C_2 \rightarrow C_1 \rightarrow O_1 \rightarrow O_2$, as well as $C_4 \rightarrow C_2$, were similarly slowed in either GluN1(C,C)/GluN2A or GluN1/GluN2A(C,C) from those in GluN1/GluN2A (Fig. 3.6A & B). The deactivation transitions $O_2 \rightarrow O_1$ and $C_2 \rightarrow C_3$ were similarly accelerated in GluN1(C,C)/GluN2A and GluN1/GluN2A(C,C) as compared to those in GluN1/GluN2A (Fig. 3.7A & B). Interestingly, the reverse transition, $C_1 \rightarrow C_2$, was affected in a subunit-specific manner, with only GluN1/GluN2A(C,C) accelerating it (Fig. 3.7A & B). Transitions to and from the main desensitization state C_5 were unaffected by the intrasubunit crosslinks (Fig. 3.7A & B).

Free energy plots of the central activation pathway (excluding the desensitization-related states) showed that the GluN1- or GluN2- specific intrasubunit crosslinks generally raised the energy barriers governing the kinetic steps of activation, shifting occupancy away from the open states and towards the longer duration closed states (Fig. 3.6C). Notably though, $C_2 - C_1$ exclusively underwent GluN2A-specific alteration, wherein restricting M3-S2 and S2-M4 separation in GluN2A resulted in decreased occupancy and therefore energetic destabilization of C_1 (Fig. 3.7). In contrast, equivalent gating constraints in GluN1 did not affect C_1 in such a manner.

DTT treatment of GluN1/GluN2A, GluN1(C,C)/GluN2A and GluN1/GluN2A(C,C) restores similar kinetic parameters of activation gating (Fig. 3.8). Now the energetics of gating was overwhelmingly shifted towards channel opening (Fig. 3.8C), especially for the double-cysteine substituted ones as compared to their untreated counterparts (Fig. 3.7C). Although there appears to be some effects of DTT beyond the reduction of disulfide crosslinks, e.g. faster rate of $C_2 \rightarrow C_1$ transition for all three receptor types following DTT treatment (cf. Figs. 3.7A & 3.8A),

presently we do not analyze them further. Nevertheless, these results further emphasize the impairment of pore opening generated by the intrasubunit disulfide crosslinks and its reversibility through DTT-mediated breakage of such crosslinks.

In summary, constraining separation of M3-S2 and S2-M4 in either GluN1 or GluN2A symmetrically slowed the late gating steps ($C_1 – O_1 – O_2$), with entry rates into the long-lived open state being most dramatically reduced. Thus, GluN1 and GluN2 undergo tightly coupled conformational changes leading to pore opening. A single pre-open gating step ($C_2 – C_1$) however appears to be associated exclusively with the GluN2A subunit, suggesting some degree of subunit independent early gating transitions before converging on concerted pore opening movements across all subunits.

DISCUSSION

For NMDA receptors, defining kinetic mechanisms of activation gating has identified key energetic steps including intermediate states between ligand binding and full channel opening (e.g., (Banke and Traynelis, 2003; Auerbach and Zhou, 2005; Schorge et al., 2005; Kussius and Popescu, 2009). These states probably do not represent a single protein conformation but rather a continuum of transiently stable conformations with similar energy profiles. To characterize the dynamics of activation gating in NMDA receptors, we took the novel approach of constraining the M3-S2 linker through intrasubunit crosslinking with S2-M4. The advantage of this approach is that it places a physical constraint at a specific location in the receptor, in these instances at a presumed pivotal juncture between the LBD and the ion channel. Restriciting the relative intrasubunit movements of M3-S2 and S2-M4 greatly affected the energetics of gating, reducing channel open probability by 30- to 75-fold (Table 3.1), while leaving intact the basic kinetic mechanism (e.g., a similar number of closed/open time components) (Figs. 3.4, 3.5 & Table 3.2). Through kinetic analysis, we addressed the contributions of this localized constraint in either GluN1 or GluN2A subunit to the energetics of the gating process in NMDA receptors.

Intrasubunit separation of M3-S2 and S2-M4 during pore opening.

An open-state iGluR structure does not exist. However, based on the closed-state AMPA receptor structure and ligand-bound LBDs and an open K^+ channel, a general model of conformational changes occurring during gating has been proposed (Sobolevsky et al., 2009). One feature of this model is that during pore opening the M3-S2 and S2-M4 linkers within a subunit undergo a rotational and/or linear separation of ~9 Å (Fig. 3.9A). Although there are limitations in comparing the state-dependent positioning of these linkers in AMPA and NMDA

receptor subunits due to significant differences in their sequences and sizes (e.g., Fig. 3.9B), we assume a similar general conformational rearrangements in the NMDA receptor linkers. Hence, by disulfide crosslinking M3-S2 to S2-M4 in an individual NMDA receptor subunit, we covalently constrain their relative separation required for movement of M3 away from the central axis of the pore. Consequently, the most robust effects of the intrasubunit gating constraints was impairment of pore opening by greatly shortening the lifetime of the main long-lived channel open state, leading chiefly to brief or 'flickery' openings (Figs. 3.4-3.6 &, Table 3.2).

Intrasubunit gating actions of M3-S2 and S2-M4 are tightly coupled across all four subunits in an NMDA receptor.

Activation gating in fully-liganded NMDA receptors can generally be divided into early channel-closed/pre-open gating steps ($C_3 \rightarrow C_2 \rightarrow C_1$) and late gating steps mediating pore opening to its most stable state ($C_1 \rightarrow O_1 \rightarrow O_2$) (Banke and Traynelis, 2003; Auerbach and Zhou, 2005; Kussius and Popescu, 2009). Gating constraints in either the glycine-binding GluN1 or glutamate-binding GluN2A subunits symmetrically affected the late gating steps mediating full pore opening ($C_1 - O_1$ and $O_1 - O_2$) to largely the same extent (Fig. 3.7). In addition, although open durations were greatly reduced in NMDA receptors with constrained subunits, these openings had the same conductance level as those found in WT receptors (Table 3.1), rather than displaying prominent subconductance levels. Thus, if pore opening movements of the M3-S2/M3 linker/transmembrane segment is restricted in one subunit (either GluN1 or GluN2A), pore opening movements in the other non-constrained subunits are also blocked. These results demonstrate that the intrasubunit pore opening movements at the level of the linkers are tightly coupled across all four NMDA receptor subunits.

This tight coupling at the level of the linkers must be a manifestation of the concerted gating in NMDA receptors wherein all four ligands—two glycine and two glutamate molecules—have to bind for subsequent channel pore opening to occur (Benveniste and Mayer, 1991a; Clements and Westbrook, 1991; Schorge et al., 2005). Here we demonstrate that the conformational dynamics of specific structural elements, the M3-S2 and S2-M4 linkers and presumably their associated transmembrane segments M3 and M4, act in concert across all four subunits to open the pore in NMDA receptors. The gating transduction mechanism in NMDA receptors is an integrated process stretching from the LBD to the ion channel, with the linkers' gating dynamics firmly incorporated across all kinetically detectable states $C_3 \rightarrow C_2 \rightarrow C_1 \rightarrow O_1 \rightarrow O_2$. Ligand interactions with and initial lobe closure of the LBD occurs prior to the receptor reaching the C_3 conformational state (Kussius and Popescu, 2010).

In contrast to concerted pore opening in NMDA receptors, gating in the related AMPA receptor apparently occurs in a subunit-independent manner manifested as openings to multiple conductance levels (Rosenmund et al., 1998; Smith and Howe, 2000; Poon et al., 2010; Prieto and Wollmuth, 2010). Mechanisms underlying pore opening in AMPA receptors are unknown but may include subunit-independent movements of the M3 segments, the reentrant M2 pore loop, and/or other gating elements more proximal to the LBD such as the pre-M1 helix. Using homologous positions at the linkers of the AMPA receptor, for which a structure already exists (Sobolevsky et al., 2009), the crosslinking approach we used here could be a means to test for the mechanisms of subunit-independent gating in AMPA receptors.

Subunit-independent gating preceding ion channel pore opening.

Immediately following ligand binding, the NMDA receptor undergoes at least two kinetically

distinct channel closed/pre-open gating steps. In the sequential model of NMDA receptor activation, the slower pre-open gating step ($C_3 \rightarrow C_2$) must occur before the faster one ($C_2 \rightarrow C_1$) (Fig. 3.7) (Kussius and Popescu, 2009). Although the gating constraints in either the GluN1 or GluN2A subunit commonly affect overlapping rate constants in these two early gating steps, we do detect a significant subunit-specific components. The reverse rate $C_1 \rightarrow C_2$ was exclusively affected by the GluN2A gating constraints, being ~2-fold accelerated and resulting in C_1 attaining a more unstable energetic state (Fig. 3.7). Although we do not presently explore this further, these results suggest some degree of subunit-independent isomerization events in pre-open gating steps of the NMDA receptor.

Such subunit-independent gating steps in the NMDA receptor have been suggested previously using GluN1- and GluN2- specific partial agonists (Banke and Traynelis, 2003; Erreger et al., 2005b) as well as noting GluN2A- vs GluN2B- specific differences in gating kinetics (Erreger et al., 2005a). Furthermore, a crystal structure of an iGluR has revealed key structural asymmetry between subunits in the extracellular domains, especially at the LBD-TMD linkers, transitioning to 4-fold symmetry at the TMD (Sobolevsky et al., 2009). The subunit-dependent pre-open gating steps, initiated in the LBD subsequent to clam-shell closure, may reflect structural differences in the LBDs where the functional pair is the GluN1/GluN2 heterodimer or the asymmetry between M3-S2s within a dimer pair (Sobolevsky et al., 2009). Hence, the asymmetry between subunits in the pre-open steps may reflect subunit-dependent differences between the S2-M4s or relative movements of M3-S2 to S2-M4 in the different subunits. Future kinetic studies of NMDA receptors with constrained gating elements encompassing other LBD-TMD linkers will be needed to fully resolve the structural mechanisms coupling the energetics of ligand binding to channel pore opening.

Conclusion

Our results with the NMDA receptor are consistent both with previous functional experiments and structural features of iGluRs. In NMDA receptors, allosteric interactions occur between the two subunits in the LBDs (Benveniste and Mayer, 1991a, b; Lester et al., 1993; Regalado et al., 2001), presumably initiating NMDA receptor concerted gating. However, from the LBD to the transmembrane domain there appears to be some degree of subunit-independence ultimately (re)converging on concerted pore opening actions undertaken by all four subunits. This concerted pore opening in NMDA receptors may have functional significance in Ca^{2+} permeation, pore block, and receptor kinetics. Nevertheless, its biological significance as well as its structural basis remain unclear.

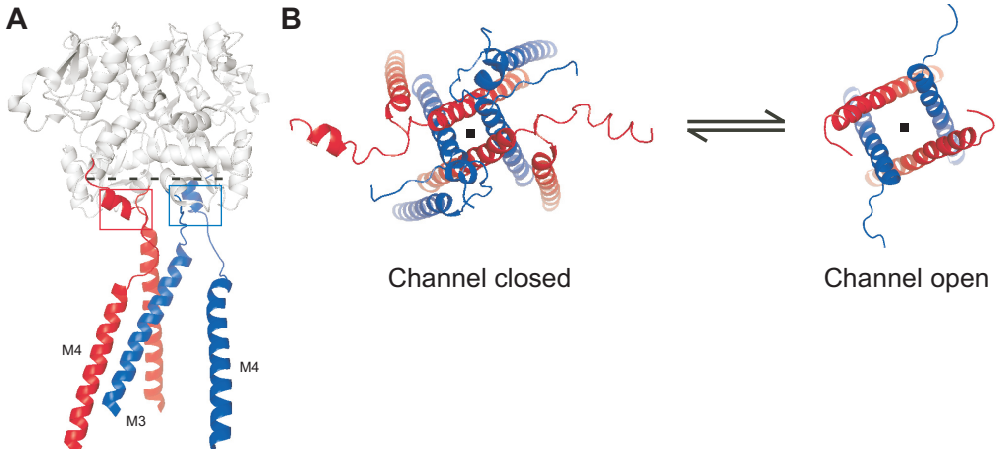

Figure 3.1. The M3 transmembrane segment is the major channel gating element in ionotropic glutamate receptors.

(A) Backbone structure of two glutamate receptor subunits ($GluA2_{cryst}$, subunits B & C, PDB accession code 3KG2), each harboring an extracellular ligand-binding domain (LBD, in gray) comprised of polypeptide segments S1 and S2, transmembrane segments M3 and M4, and their associated linkers M3-S2 and S2-M4. For clarity, the M1 transmembrane segment and the M2 pore loop are not shown. GluN1 is assumed to adopt the A/C conformation (red) and GluN2 the B/D conformation (blue) (Sobolevsky et al., 2009). The dashed line indicates point of view (looking down the ion channel) shown in Fig. 3.1B. Red and blue squares depict regions of intrasubunit crosslinking of the M3-S2 and S2-M4 linkers in GluN1 and GluN2A, respectively. Although there are limitations in comparing NMDA receptors to the AMPA receptor structure and the derived open state structural model, e.g., domain arrangements may be different (Stroebel et al., 2010), we use this information to illustrate general features of gating in iGluRs, specifically for the TMD.

(B) Presumed gating movements of the M3 transmembrane segment leading to pore opening. Left, tetrameric arrangement of M3/M3-S2 and M4/S2-M4 adopting the A/C (~ GluN1, red) and

B/D (~ GluN2A, blue) conformations in an antagonist-bound channel-closed state (Sobolevsky et al., 2009). The M3 transmembrane helices line the channel pore (depicted with a dot), while the external helices surrounding this core are the M4 segments. Right, reorientation of the M3 segments in the channel-open state as predicted from superposition of the $GluA2_{cryst}$ on the closed KcsA and the open Shaker K^+ channels (Sobolevsky et al., 2009). In the present study, we restrict these gating rearrangements of M3 through intrasubunit crosslinking of the M3-S2 and S2-M4 linkers in GluN1 (A, red box) or GluN2A (A, blue box).

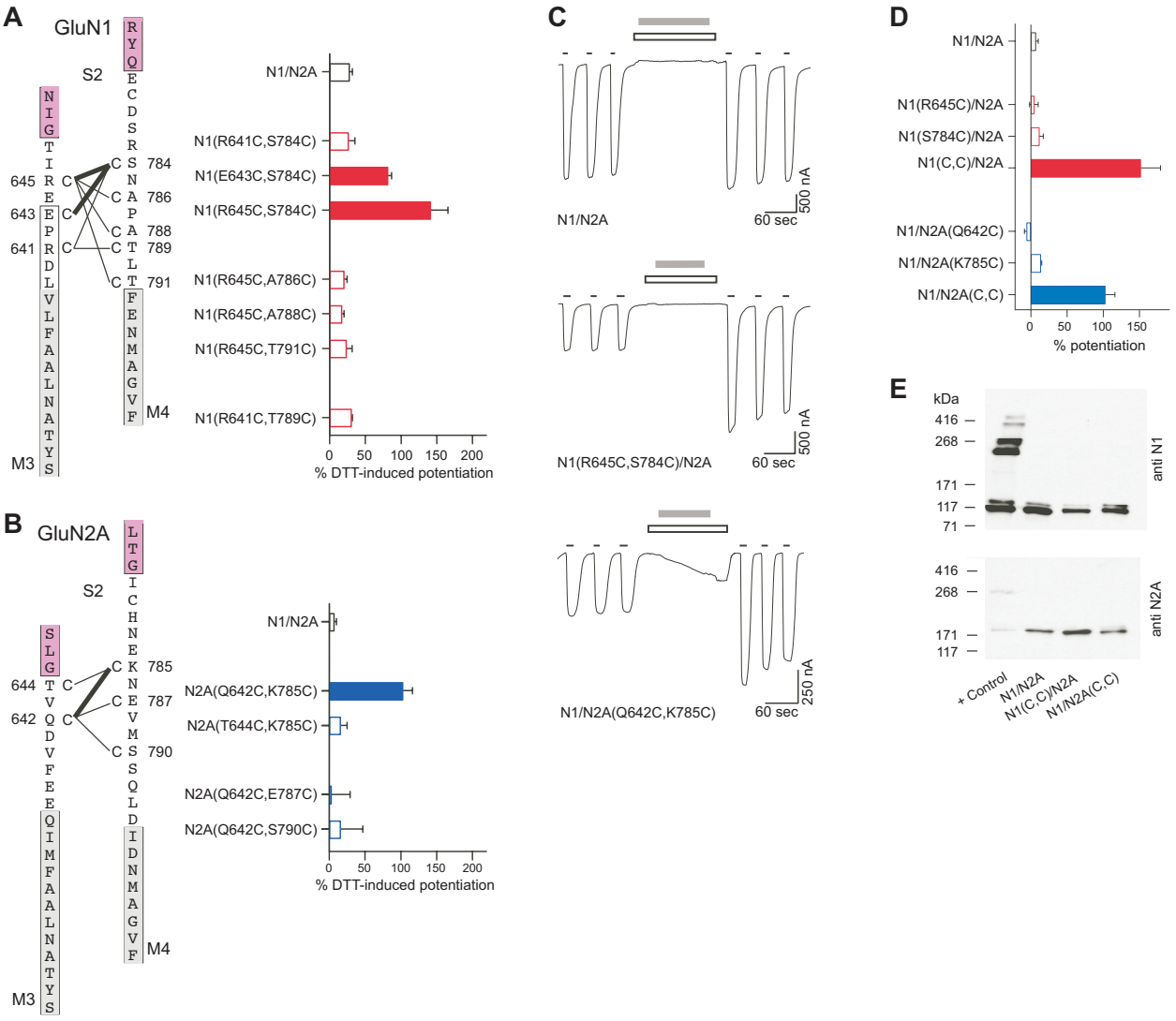

Figure 3.2. DTT-induced potentiation of macroscopic currents in NMDA receptors containing intrasubunit double-cysteine substitutions in GluN1 or GluN2A.

(A & B) NMDA receptors with intrasubunit GluN1- or GluN2A- specific double-cysteine substitutions were assayed for DTT-induced changes in macroscopic current amplitudes using TEVC in *Xenopus* oocytes. Double cysteine-substituted GluN1 (A) or GluN2A (B) subunits were co-expressed with WT GluN2A or GluN1 subunits, respectively. *Left*, schematic representation of regions around M3-S2 and S2-M4 linkers. Positions substituted with cysteine are indicated with a 'C' and numbered next to the endogenous residue. Tested pairs of cysteines

are shown with a connecting line. Darker lines indicate pairs that showed significant DTT-induced current potentiation relative to GluN1/GluN2A and hence can presumably spontaneously crosslink. Numbering is for the mature protein. Proximal parts of S2 and the hydrophobic segments M3 and M4 are colored as magenta and gray, respectively. Boxed regions around the hydrophobic segments represent the α-helical extent of the transmembrane segments in an AMPA receptor structure (Sobolevsky et al., 2009). GluN1 is presumed to adopt the A/C and GluN2A the B/D conformations. *Right*, mean % change (± SEM, n ≥ 4) of current amplitudes following DTT. In the recording protocol for the GluN1 double cysteine-substitutions (A) DTT was applied continuously in the presence and absence of agonists for at least 2 mins (raw recordings not shown). The recording protocol for the GluN2A double cysteine-substitutions (B) was identical to those in Fig. 3.2C. Filled bars indicate values significantly different from those of WT receptors ($P < 0.05$). Our experiments focused on GluN1(R645C,S784C)/GluN2A and GluN1/GluN2A(Q642C,K785C) receptors, which we refer to as GluN1(C,C)/GluN2A and GluN1/GluN2A(C,C).

(C) Representative membrane currents (holding potential, -60 mV) in *Xenopus* oocytes injected with wild-type (WT) GluN1/GluN2A, GluN1(R645C,S784C)/GluN2A or GluN1/GluN2A(Q642C,K785C) receptors. Hereafter GluN1(R645C,S784C) and GluN2A(Q642C,K785C) are referred to as GluN1(C,C) and GluN2A(C,C), respectively. Currents were elicited by co-application of glycine (20 μM) and glutamate (200 μM) (thin black lines). DTT (4 mM, 2 mins, gray bars), applied in the presence of competitive antagonists DCKA (10 μM) and APV (100 μM) (open boxes), strongly potentiated subsequent current amplitudes in the double cysteine-substituted receptors.

(D) Mean % change (± SEM, n ≥ 4) of current amplitudes following DTT. Filled bars indicate values significantly different from those of WT receptors ($P < 0.05$). Tukey or Dunnett tests were used for all multiple comparisons of means, unless otherwise noted.

(E) Western blot analysis of membrane proteins purified from *Xenopus* oocytes under non-reducing conditions. Formation of inter-subunit crosslinking, either homomeric or heteromeric, was assayed with anti-GluN1 (top) or anti-GluN2A (bottom) antibodies. The '+ control' is GluN1(N521C,L777C)/GluN2A(E516C,L780C) receptors that form intersubunit dimers (Furukawa et al., 2005). Expected molecular weights are: monomeric GluN1 (114 kDa) and GluN2A (173 kDa), homodimeric GluN1 (228 kDa) and GluN2A (346 kDa), and heterodimeric GluN1/GluN2A (287 kDA). Other than the monomeric bands, no apparent homomeric or heteromeric dimer bands were detected for GluN1/GluN2A or either of the double cysteine-substituted receptors, though dimers were present for the '+' control (n = 4).

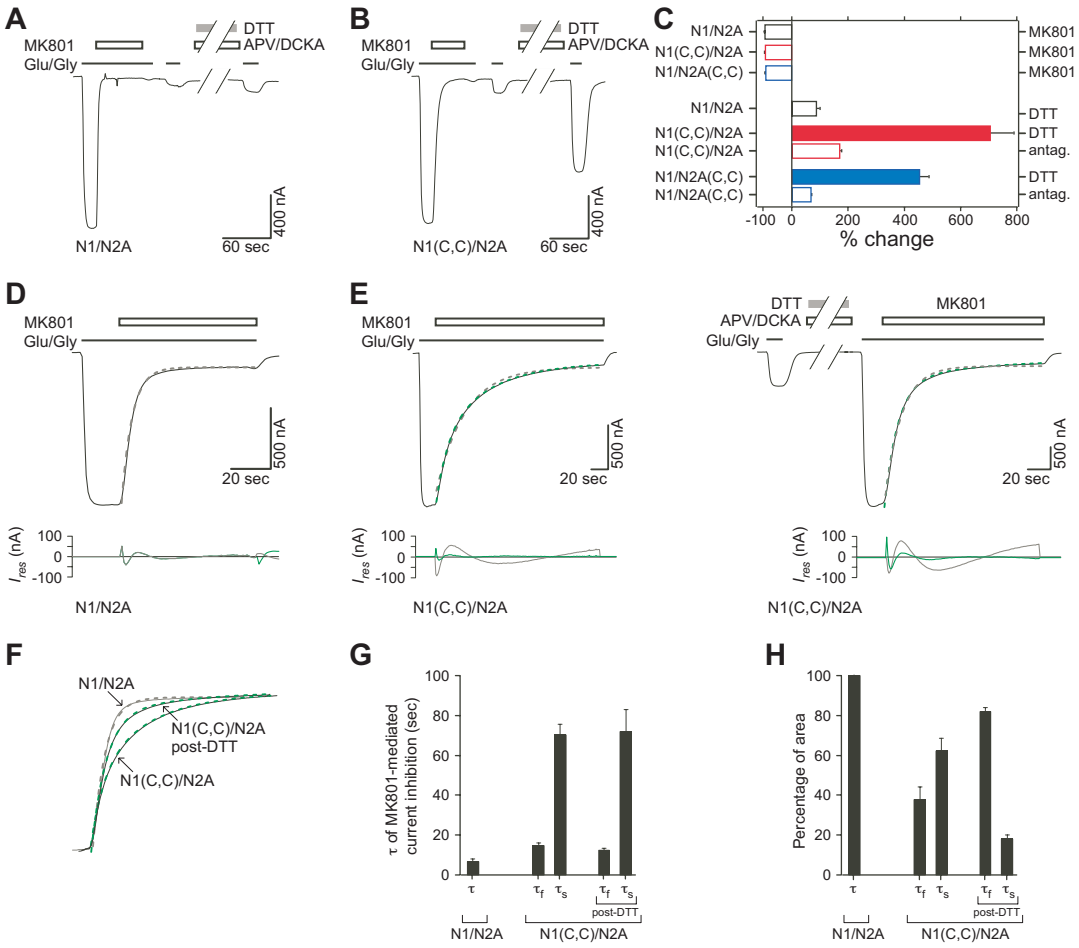

Figure 3.3. A subset of cell-surface NMDA receptors with double-cysteine substituted GluN1 or GluN2A is resistant to pore block by MK801.

To optimize current amplitudes in these experiments, we injected WT GluN1/GluN2A at 1 ng/μL and GluN1(C,C)/GluN2A and GluN1/GluN2A(C,C) at 10 ng/μL into *Xenopus* oocytes. (A & B) Example recordings depicting steady-state MK801 inhibition of NMDA receptor-mediated macroscopic currents. MK801 (unfilled bar, 1-2 μM, 1 min), applied in the presence of agonists (thin lines), inhibited current amplitudes for GluN1/GluN2A (A), GluN1(C,C)/GluN2A (B) and GluN1/GluN2A(C,C) (not shown) receptors. Subsequent application of DTT (filled bar) in the channel closed state (as in Fig. 3.2C) significantly potentiated current amplitudes of the double cysteine-substituted receptor (B) relative to WT GluN1/GluN2A (A).

(C) Mean % change (± SEM, n ≥ 4) in current amplitudes either immediately after MK801 (MK801) or following MK801, but with an intervening treatment by DTT in the presence of antagonists (DTT) or antagonists alone (antag.). For DTT and antag. treatments, % change was calculated relative to the current amplitudes preceding these treatments but following MK801 block. Negative and positive values represent current inhibition and potentiation, respectively. Filled bars indicate values significantly different from those of WT GluN1/GluN2A receptors ($P < 0.05$).

(D & E) MK801 (25 nM) was applied in the presence of agonists until steady-state current inhibition was reached. (E, right) For GluN1(C,C)/GluN2A, MK801 was also applied to DTT-potentiated currents. Single (grey dashed lines) and bi- (green dashed lines) exponential fits to MK801-mediated current inhibition are shown, as well as the residuals (I_{res}) to the two fits. For GluN1/GluN2A, single exponential fits were sufficient to describe time course of MK801-mediated current inhibition, whereas for GluN1(C,C)/GluN2A biexponential fits were required, as determined by qualitative minimization of I_{res}.

(F) Normalized MK801-mediated inhibition of currents with the overlayed best fits (dashed lines).

(G) Averaged time constants of single exponential fits (τ), as well as the fast (τ_f) and slow (τ_s) components of the biexponential fits (± SEM) to MK801-mediated current inhibition.

(H) Averaged percentage of area (± SEM) occupied by each component of the exponential fits.

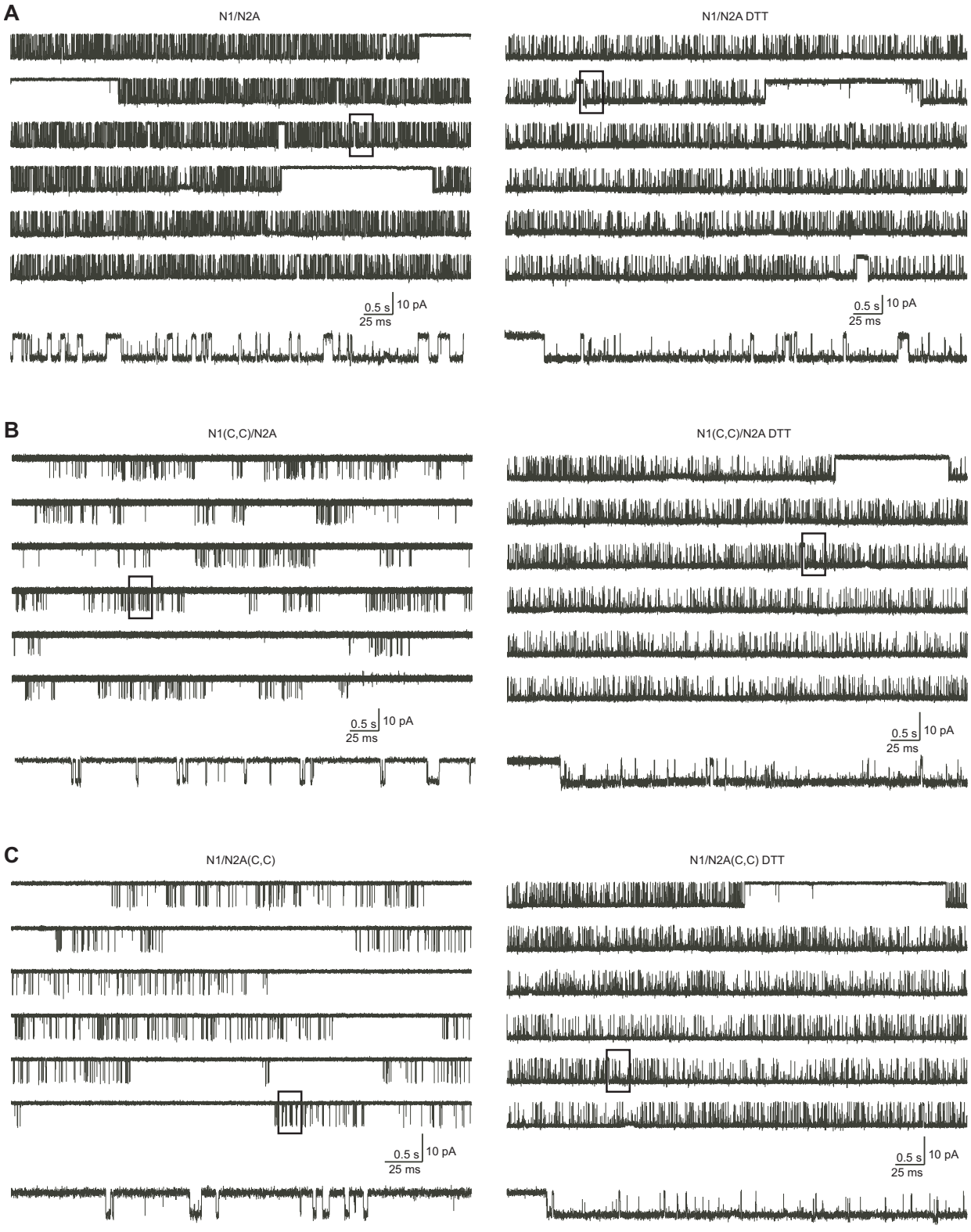
A
N1/N2A
N1/N2A DTT
0.5 s
10 pA
25 ms
B
N1(C,C)/N2A
N1(C,C)/N2A DTT
C
N1/N2A(C,C)
N1/N2A(C,C) DTT

Figure 3.4. NMDA receptors with intrasubunit GluN1 or GluN2A disulfide crosslinks show dramatically reduced single channel activity that can be reversed by DTT.

(A – C) Recordings of on-cell patches containing single GluN1/GluN2A (A), GluN1(C,C)/GluN2A (B) or GluN1/GluN2A(C,C) (C) receptors under steady-state conditions (0.1 mM glycine and 1 mM glutamate) (digitized at 50 kHz, filtered at 1 kHz) from transiently transfected HEK cells. For recordings shown on the right, cells were exposed to DTT (4 mM) in the presence of antagonists DCKA (10 μM) and APV (100 μM) prior to forming the on-cell patches. For each, the bottom trace is an expanded view (filtered at 5 kHz) of the respective boxed regions. The left and right recordings are from different on-cell patches.

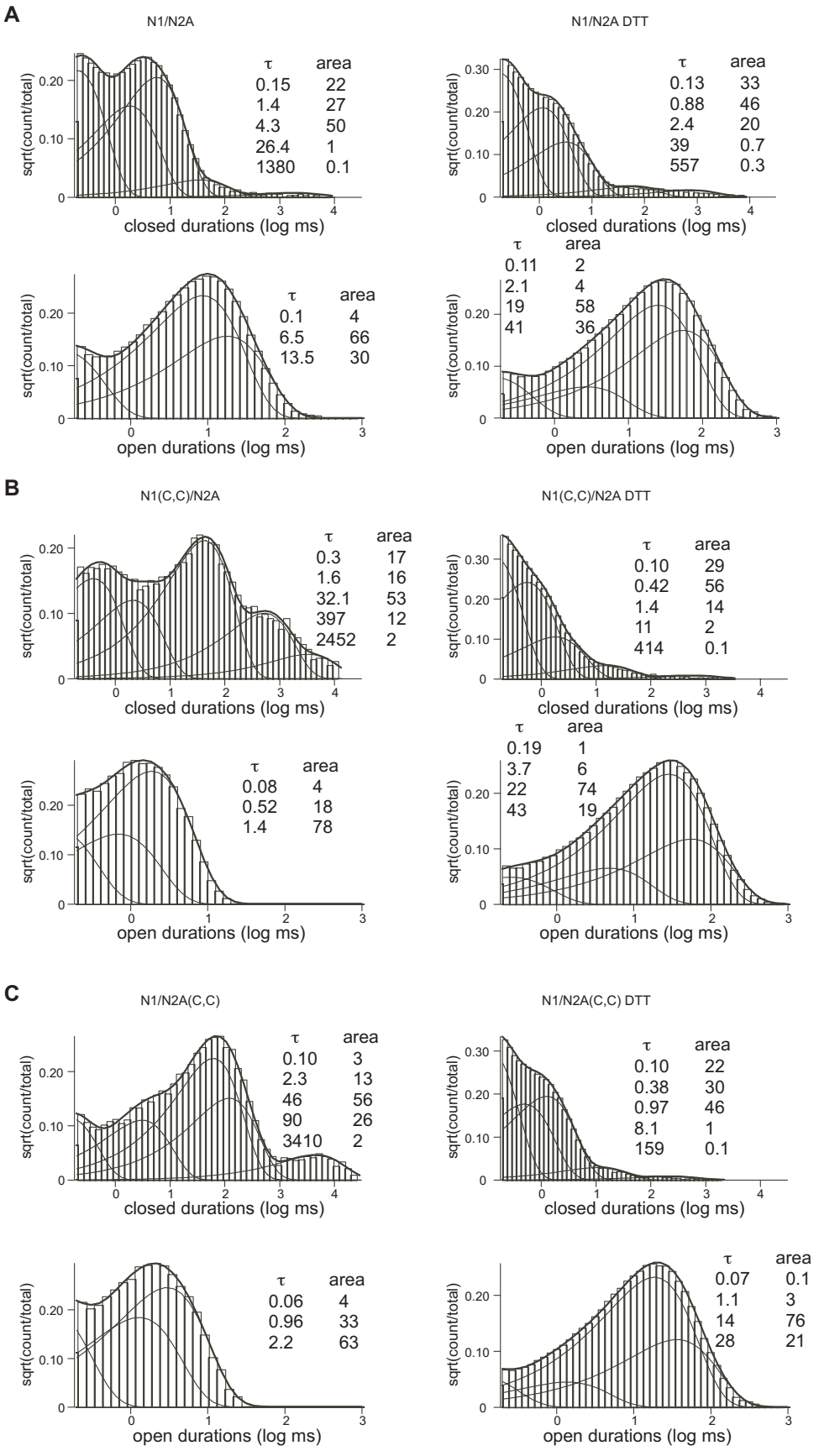
A
N1/N2A
τ area
0.15 22
1.4 27
4.3 50
26.4 1
1380 0.1
closed durations (log ms)
τ area
0.1 4
6.5 66
13.5 30
open durations (log ms)
N1/N2A DTT
τ area
0.13 33
0.88 46
2.4 20
39 0.7
557 0.3
closed durations (log ms)
τ area
0.11 2
2.1 4
19 58
41 36
open durations (log ms)
B
N1(C,C)/N2A
τ area
0.3 17
1.6 16
32.1 53
397 12
2452 2
closed durations (log ms)
τ area
0.08 4
0.52 18
1.4 78
open durations (log ms)
N1(C,C)/N2A DTT
τ area
0.10 29
0.42 56
1.4 14
11 2
414 0.1
closed durations (log ms)
τ area
0.19 1
3.7 6
22 74
43 19
open durations (log ms)
C
N1/N2A(C,C)
τ area
0.10 3
2.3 13
46 56
90 26
3410 2
closed durations (log ms)
τ area
0.06 4
0.96 33
2.2 63
open durations (log ms)
N1/N2A(C,C) DTT
τ area
0.10 22
0.38 30
0.97 46
8.1 1
159 0.1
closed durations (log ms)
τ area
0.07 0.1
1.1 3
14 76
28 21
open durations (log ms)
sqrt(count/total)

Figure 3.5. Exponential fitting of composite histograms identify 5 closed and 2-4 open time components.

(A – C) Shut (top) and open (lower) time duration histograms of the same single channel patches shown in Fig. 3.4. The shut time duration histograms were well-fitted with five exponential components, whereas the open time duration histograms were well-fitted with two to four exponential components. The time constants and relative areas of the exponential components are given in the insets.

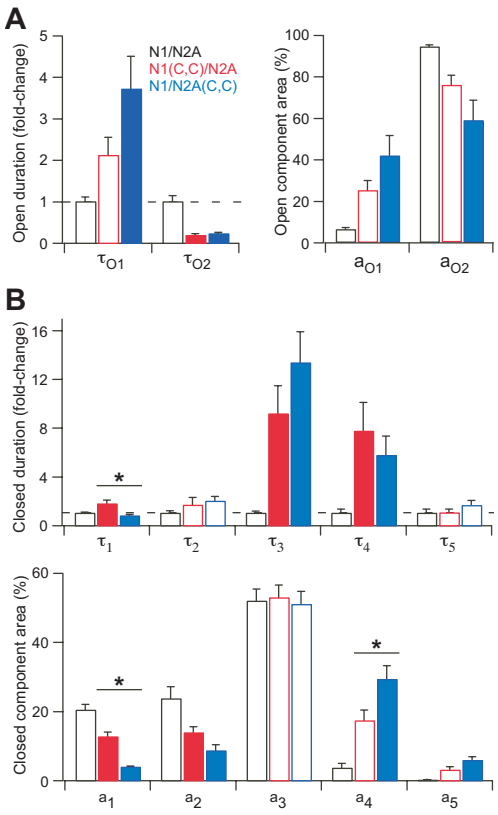

Figure 3.6. NMDA receptors with intrasubunit GluN1 or GluN2A crosslinks display largely symmetrical changes in multiple open and closed time components.

(A) Left, mean fold-change (± SEM) in duration of open-time components as determined by MIL fitting of single channel recordings (see Methods). Although single channel records (in the cell-attached configuration) comprised 2-4 open-time components arising from modal gating behavior of NMDA receptors (Popescu and Auerbach, 2003), they were combined for simplicity into aggregates of two states, one short duration (for N1/N2A 0.12 ± 0.01 ms) and one long duration (for N1/N2A 8.71 ± 0.9 ms) (see Table 3.2). Right, mean relative areas (± SEM) of the open time components.

(B) Top, mean fold-change in duration (± SEM) of closed-time components as determined by MIL fitting of single channel recordings. For WT GluN1/GluN2A, the time constants were (ms): τ_1 0.14 ± 0.01, τ_2 1.03 ± 0.13, τ_3 4.16 ± 0.4, τ_4 26.9 ± 5.6 and τ_5 1789 ± 366 (see Table 3.2).

Bottom, mean relative areas (± SEM) of the closed-time components. Significant differences ($P < 0.05$) relative to WT and between GluN1(C,C)/GluN2A and GluN1/GluN2A(C,C) are indicated with filled bars and asterisks, respectively.

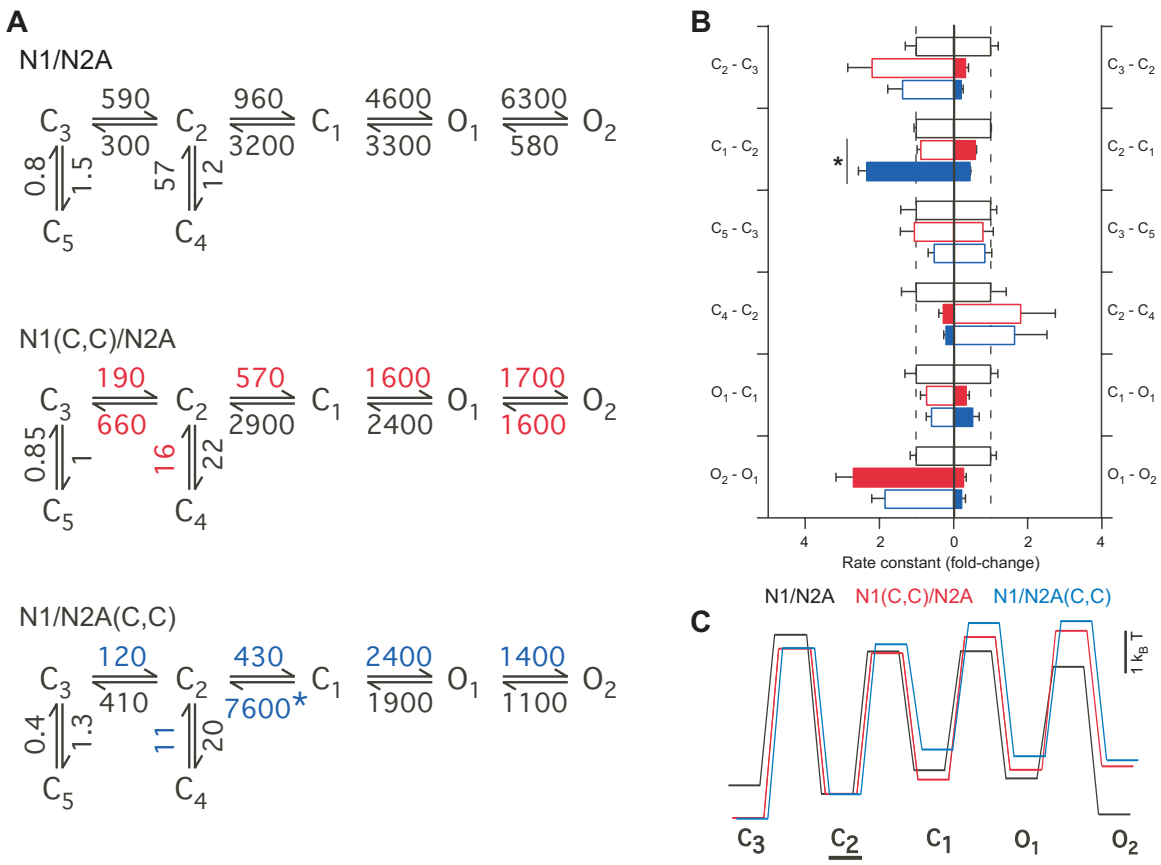

Figure 3.7. Effects of the intrasubunit GluN1 or GluN2A crosslinks on the kinetic mechanism of NMDA receptor activation.

(A) Sequential state model (Kussius and Popescu, 2009) of NMDA receptor activation with the rate constants (s^{-1}) of transitions averaged from fits of individual single channel recordings. Significant differences ($P < 0.05$) relative to WT are indicated with colored rate constants. Significant differences ($P < 0.05$) between GluN1(C,C)/GluN2A and GluN1/GluN2A(C,C) are indicated with asterisks.

(B) Mean fold-change (± SEM) in rate constants relative to GluN1/GluN2A. The left and right axes show the reverse and forward rate constants respectively. Significant differences ($P < 0.05$) relative to WT and between GluN1(C,C)/GluN2A and GluN1/GluN2A(C,C) are indicated with filled bars and asterisks, respectively.

(C) Free-energy landscape plotted with respect to C_2. The off-pathway steps to and from C_4 and C_5 are excluded. The three traces are horizontally offset for clarity.

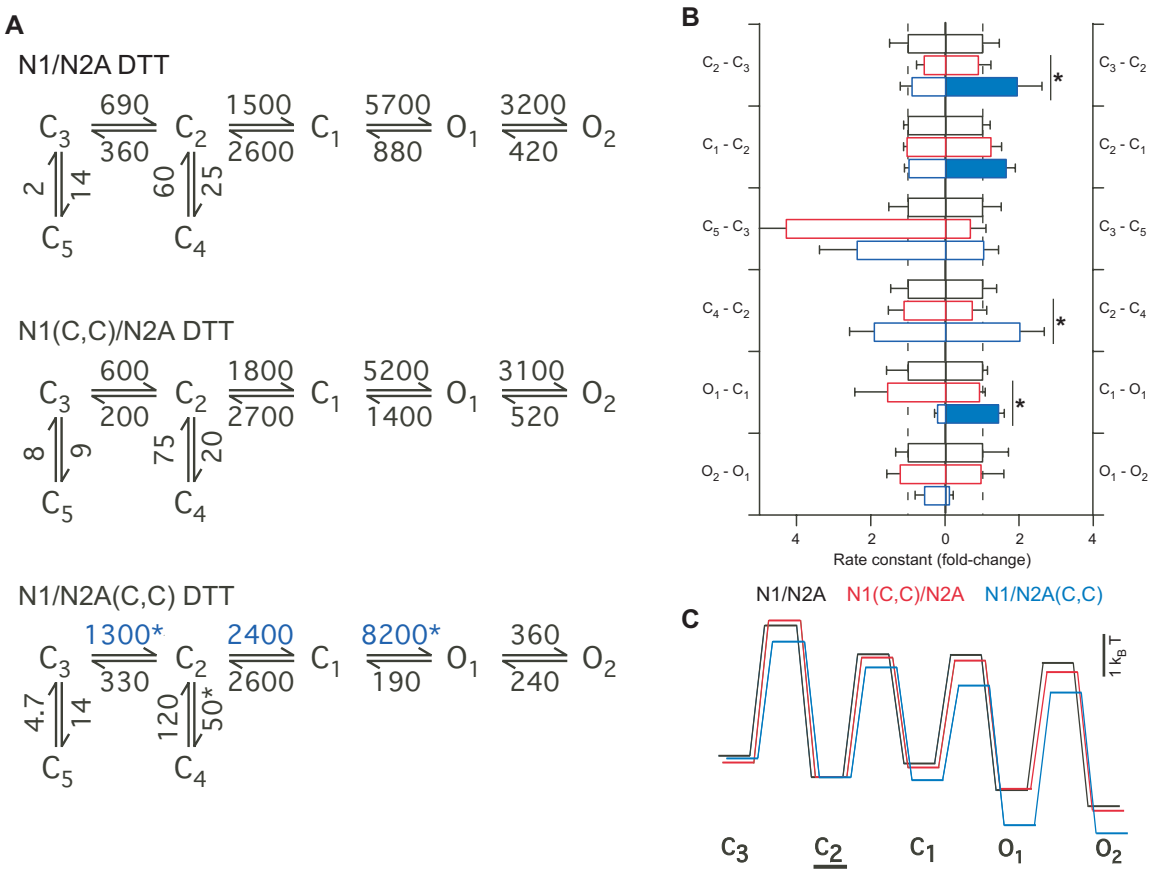

Figure 3.8. When exposed to DTT, NMDA receptors composed of WT or double-cysteine substituted subunits displayed comparable kinetic behavior.

Kinetic analysis, as in Fig. 3.7, for single channel patches exposed to DTT.

(A) Sequential state model (Kussius and Popescu, 2009) of NMDA receptor activation with the rate constants (s^{-1}) of transitions averaged from fits of individual single channel recordings. Significant differences ($P < 0.05$) relative to WT are indicated with colored rate constants. Significant differences ($P < 0.05$) between GluN1(C,C)/GluN2A and GluN1/GluN2A(C,C) are indicated with asterisks.

(B) Mean fold-change (± SEM) in rate constants relative to GluN1/GluN2A. The left and right axes show the reverse and forward rate constants respectively. Significant differences ($P < 0.05$)

relative to WT and between GluN1(C,C)/GluN2A and GluN1/GluN2A(C,C) are indicated with filled bars and asterisks, respectively.

(C) Free-energy landscape plotted with respect to C_2. The off-pathway desensitization-related steps to and from C_4 and C_5 are excluded. The three traces are horizontally offset for clarity.

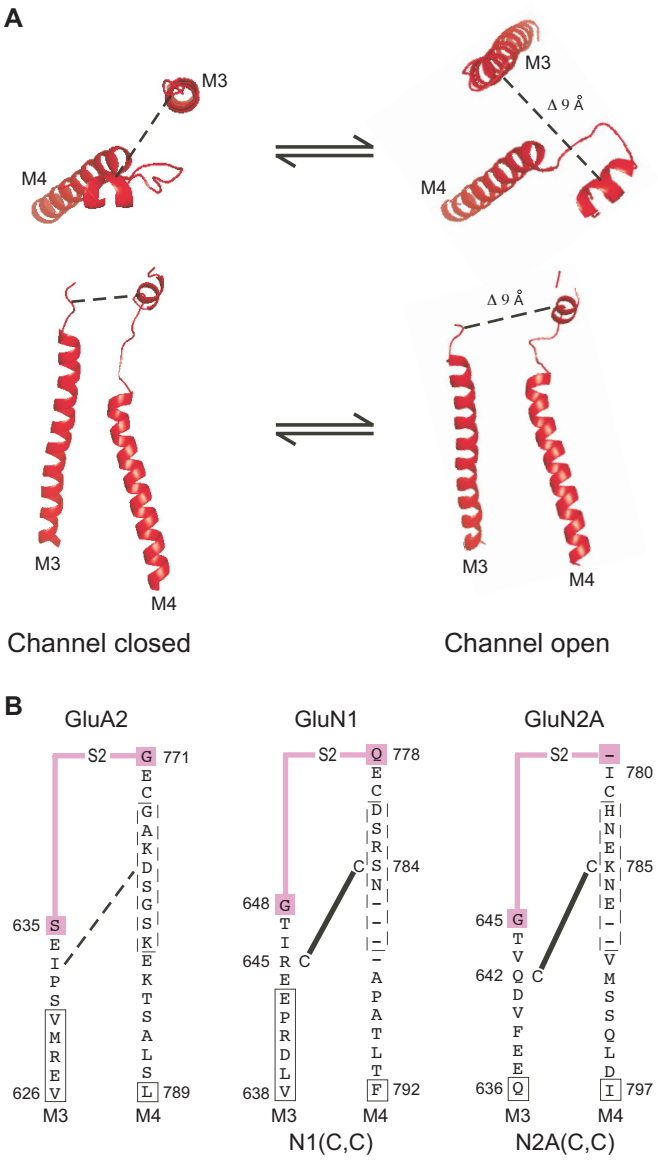

Figure 3.9. A model of the intrasubunit gating dynamics of M3-S2 and S2-M4 in the NMDA receptor.

A. Potential intrasubunit movements of the M3-S2 and S2-M4 linkers during pore opening. The channel closed conformations are from the antagonist-bound GluA2 (subunit C) crystal structure (Sobolevsky et al., 2009). The channel open conformations are based on homology modeling of the channel-closed GluA2 structure with an open Shaker K^+ ion channel and ligand-bound AMPA receptor LBD structure (Sobolevsky et al., 2009). Shown are views from the top-down

(top) and side (bottom). In this model, the centers of the M3-S2 linker (in the A/C subunit) and pre-M4 helix (dashed line) separate by ~ 9 Å in the transition from the closed- to the open-channel states.

B. Sequences of the M3-S2 and S2-M4 linkers in the GluA2, GluN1 and GluN2A subunits. Proximal parts of S2 are colored as magenta. In GluA2, boxed region represent the transmembrane α-helical segments (in the A/C subunit) and the dashed boxed region depicts the pre-M4 helix. GluN1 is presumed to adopt the A/C and GluN2A the B/D conformations. Based on sequence alignment (Sobolevsky et al., 2009), the S2-M4 linkers in the GluN1 and GluN2A subunits have notable gaps, particularly in the presumed pre-M4 helix, complicating a direct comparison of NMDA receptor subunits to the GluA2 structure.

Table 3.1: Constraining relative movements of M3-S2 and S2-M4 in GluN1 or GluN2A disrupts NMDA receptor gating.

	n	I (pA)	eq. P_o	MCT (ms)	MOT (ms)
N1/N2A	7	-9.4 ± 0.6	0.61 ± 0.05	5.1 ± 0.7	8.3 ± 0.8
N1(C,C)/N2A	8	-9.0 ± 0.6	0.021 ± 0.005^	94 ± 20^	1.2 ± 0.1^
N1/N2A(C,C)	9	-8.1 ± 0.4	0.008 ± 0.001^	230 ± 34^*	1.4 ± 0.1^
N1/N2A DTT	5	-8.3 ± 0.2	0.74 ± 0.09	7.5 ± 3.7	23 ± 4.9$
N1(C,C)/N2A DTT	5	-7.7 ± 0.5	0.79 ± 0.08	2.4 ± 0.8	16 ± 5.3
N1(C,C)/N2A DTT	4	-9.2 ± 0.8	0.96 ± 0.01	1.0 ± 0.1	30 ± 5.9

Mean values (± SEM) for single channel current amplitudes (I), equilibrium open probability (eq. P_o), mean closed time (MCT) and mean open time (MOT). Idealization and maximum interval likelihood (MIL) fitting with five closed and two-four open states was done in QuB. A sequential state model for GluN1/GluN2A NMDA receptor gating (Kussius and Popescu, 2009) was used. Eq. P_o is defined as the fractional occupancy of the open states in the MIL fitted single-channel recordings. For statistical analysis, the non-DTT and DTT exposed receptors were considered separately, with the control being the respective values in GluN1/GluN2A. ^$P < 0.05$, relative to GluN1/GluN2A. *$P < 0.05$, GluN1(C,C)/GluN2A relative to GluN1/GluN2A(C,C). $$P < 0.05$, GluN1/GluN2A relative to GluN1/GluN2A DTT.

Table 3.2: Open- and closed- time components for NMDA receptors comprised of WT or double-cysteine substituted subunits.

				DTT		
	N1/N2A	N1(C,C)/N2A	N1/N2A(C,C)	N1/N2A	N1(C,C)/N2A	N1/N2A(C,C)
n	7	8	9	5	5	4
τ_{O1}	0.12 ± 0.01	0.25 ± 0.05	0.45 ± 0.09	3.0 ± 2.7	1.0 ± 0.7	4.7 ± 2.2
a_{O1}	6 ± 1.1	25 ± 4.7	42 ± 9.6	10 ± 5.7	7.2 ± 1.2	17 ± 8.2
τ_{O2}	8.7 ± 0.9	1.6 ± 0.2	1.9 ± 0.13	26 ± 7	17 ± 5.6	34 ± 6.9
a_{O2}	94 ± 1.1	75 ± 4.7	59 ± 9.6	90 ± 5.7	93 ± 1.2	83 ± 8.2
τ_1	0.14 ± 0.01	0.25 ± 0.04	0.11 ± 0.01	0.12 ± 0.01	0.13 ± 0.01	0.10 ± 0.004
a_1	20 ± 1.5	13 ± 1.3	3.7 ± 0.3	31 ± 2.8	26 ± 3.5	31 ± 3.1
τ_2	1.0 ± 0.1	1.7 ± 0.6	2.1 ± 0.3	0.77 ± 0.16	0.8 ± 0.1	0.42 ± 0.02
a_2	24 ± 3.4	14 ± 1.6	8.7 ± 1.4	38 ± 6.9	44 ± 5.6	37 ± 3.3
τ_3	4.2 ± 0.4	38 ± 8.6	56 ± 9.0	3.8 ± 1.5	2.5 ± 0.4	1.1 ± 0.1
a_3	52 ± 3.4	53 ± 3.6	48 ± 4.4	29 ± 8.6	29 ± 8.5	30 ± 6.6
τ_4	27 ± 5.6	210 ± 45	150 ± 27	35 ± 15	20 ± 4.9	9.1 ± 0.7
a_4	3.6 ± 1.3	17 ± 3	33 ± 4.9	2.5 ± 1.0	1.2 ± 0.3	7.0 ± 5.1
τ_5	1800 ± 370	1800 ± 310	2900 ± 360	1100 ± 450	1200 ± 680	250 ± 52
a_5	0.13 ± 0.03	3 ± 0.9	5.7 ± 0.9	0.5 ± 0.2	0.13 ± 0.03	0.13 ± 0.02

Mean values (± SEM) for the exponential time constants (τ) and their relative areas (a) of the open and closed interval distributions. Idealization and maximum interval likelihood (MIL) fitting with the sequential NMDA receptor gating model comprising five closed and two open channel states was done in QuB (see Methods). These data are shown as ratios relative to WT receptors in Fig. 3.6.

CHAPTER 5: CONCLUDING REMARKS

With the advent of the first crystal structure of an almost full-length (no CTD) AMPA receptor in 2009, a new era of structure-function research on iGluRs has dawned. Although crystal structures of isolated LBDs in a multitude of conformational states have already revealed their global conformational dynamics, how these conformational rearrangements are coupled to the ion channel remain largely conjectural. The AMPA receptor structure has for the first time revealed the general arrangement of the specific elements that make up the gating machinery, including the LBD-TMD linkers and segments within the TMD, as well as the location of the ion channel gate. Yet this single static snapshot of an iGluR in an antagonist-bound state, although absolutely ground-breaking in many regards, falls short is assessing the necessarily dynamic nature of these proteins.

It is only the marriage of structural data with functional studies, which in the ion channel field often involves electrophysiology, that meaningful information of how the protein works in nature can be ascertained. This idea has been the overarching theme of the research studies presented in this dissertation. In fact, both studies (chapters 2 & 3) were conceived prior to the release of the AMPA receptor structure and even with it, direct structural correlations to my studies on NMDA receptors are to be made cautiously. Still general gating principles involving the proximal elements close to the ion channel appear to be conserved in the AMPA and NMDA receptors. For example, structural comparisons of the closed-state AMPA receptor, closed- and open- state isolated LBDs and closed- and open- state K^+ channels have lead to the hypothesis that an intrasubunit separation of M3-S2/M3 and S2-M4/M4 is required for pore opening to occur (Sobolevsky et al., 2009). In accordance with this conjecture, I have found that by constraining the relative movements of M3-S2 and S2-M4 within specific subunits, pore opening

in the NMDA receptor is dramatically impaired. Thus, although definitive proof as to whether both M3-S2 and S2-M4 undergo gating movements or one moves while the other stays stationary is still lacking; combining the structural and functional data in this way add up to greater than the sum of each individual parts in terms of new knowledge learned.

Keeping this in mind, I, along with the help of an undergraduate student, have now ventured into the prototypical structure-function experiments following up on the functional data presented in chapter 2, but addressed through a better known structural framework. Specifically, from my findings that specific sites within the S1-M1 and S2-M4 linkers of the NMDA receptor can modulate gating, I had proposed the structural hypothesis that these sites are located at transient contact interfaces important to the energetic of gating (see Chapter 2). However, at that time I could not identify the exact contacting partners to further test my hypothesis. Now though, using the AMPA receptor structure as a framework for the general arrangements of these linkers, we have undertaken systemic scans of potentially closely apposed linker positions in the NMDA receptor and have indeed made positive hits. Because of the intriguing possibility that the pre-M1 helices control opening of the channel gate as seen in the AMPA receptor, we have started with this region of the linkers in NMDA receptors. By using the disulfide crosslinking strategy described in chapter 3, we can now constrain the movements of the presumed pre-M1 helix in either the GluN1 or the GluN2A subunits through either intra- or inter- subunit crosslinks. Employing whole-cell and single-channel functional experiments, we are now examining the functional consequences of such constraints and eagerly await the conclusions drawn from them. In fact, analyzed results have already shown us that these constraints severely impair pore opening and therefore provide direct evidence, backed up by structural mechanisms, that other linkers independent of M3-S2 heavily influence channel gating.

Presently I am also working on a separate project assessing the redox effects of an endogenous intrasubunit GluN1 disulfide bond on the kinetic mechanism of NMDA receptor activation. I am doing this work in conjunction with a junior graduate student. From the results discussed in chapter 3 we observed that DTT was having a gating effect that was beyond its reduction of the introduced disulfide bonds. Specifically, it was accelerating the $C_2 \rightarrow C_1$ gating steps, an effect that occurred in WT as well as the double-cysteine substituted receptors (see Chapter 3). The most likely cause of this effect is reduction of the functionally-important endogenous disulfide bond in the GluN1 LBD (Sullivan et al., 1994; Leszkiewicz and Aizenman, 2002) that likely controls the degree of agonist-induced LBD clamshell closure (Furukawa and Gouaux, 2003). Thus, our hypothesis that global movements at the GluN1 LBD specifically affect a single pre-open gating step is indeed a hot pursuit.

The conformational diversity that include resting, active, desensitized and any unnamed states that an iGluR adopts makes it unlikely a comprehensive set of snapshot crystal structures encompassing all the states will be available. Furthermore, the rapid fluctuations between multiple states in otherwise constant conditions (Plested and Mayer, 2009) questions the relevance of the stable conformations necessary for crystal formation to actual iGluR behavior in its native environment. Therefore it is essential that other experimental modalities be used in complement with crystallography and traditional electrophysiology to fully understand structure-function. Two emerging techniques worth mentioning are molecular dynamics (MD) simulations and concurrent patch clamp recordings with fluorescence resonance energy transfer (FRET). Calculations performed using MD of the free energy landscape have already begun to provide information about the highly flexible nature of the LBDs, as well as the binding of water and allosteric ions to LBD and their resultant effect on the protein electric fields (Lau and Roux,

2007; Vijayan et al., 2009; Vijayan et al., 2010). Additionally, simultaneous electrophysiology recordings which distinguish between the closed and open ion channel conformations and FRET measurements which report on the conformational changes of the protein have begun to be used to assign specific structural rearrangements to underlying channel opening and closing (Campos et al., 2008; Villalba-Galea et al., 2008; Sandoz et al., 2011). It is only a matter of time that the tremendous power of this technique will be harnessed at the level of single protein entities by coupling single-channel recordings to single molecule FRET measurements. Thus, the precise conformational changes underlying the intermediate gating transitions in NMDA receptors, which have eluded researchers so far, can remain hidden only for so long.

REFERENCES

Abele, R., K. Keinanen, and D.R. Madden. 2000. Agonist-induced isomerization in a glutamate receptor ligand-binding domain. A kinetic and mutagenetic analysis. *J Biol Chem*. 275:21355-21363.

Albers, G.W., L.B. Goldstein, D. Hall, and L.M. Lesko. 2001. Aptiganel hydrochloride in acute ischemic stroke: a randomized controlled trial. *JAMA*. 286:2673-2682.

Armstrong, N., and E. Gouaux. 2000. Mechanisms for activation and antagonism of an AMPA-sensitive glutamate receptor: crystal structures of the GluR2 ligand binding core. *Neuron*. 28:165-181.

Armstrong, N., Y. Sun, G.Q. Chen, and E. Gouaux. 1998. Structure of a glutamate-receptor ligand-binding core in complex with kainate. *Nature*. 395:913-917.

Auerbach, A., and Y. Zhou. 2005. Gating reaction mechanisms for NMDA receptor channels. *J Neurosci*. 25:7914-7923.

Balannik, V., F.S. Menniti, A.V. Paternain, J. Lerma, and Y. Stern-Bach. 2005. Molecular mechanism of AMPA receptor noncompetitive antagonism. *Neuron*. 48:279-288.

Banke, T.G., and S.F. Traynelis. 2003. Activation of NR1/NR2B NMDA receptors. *Nat Neurosci*. 6:144-152.

Barria, A., and R. Malinow. 2002. Subunit-specific NMDA receptor trafficking to synapses. *Neuron*. 35:345-353.

Barth, A.L., and R.C. Malenka. 2001. NMDAR EPSC kinetics do not regulate the critical period for LTP at thalamocortical synapses. *Nat Neurosci*. 4:235-236.

Beck, C., L.P. Wollmuth, P.H. Seeburg, B. Sakmann, and T. Kuner. 1999. NMDAR channel segments forming the extracellular vestibule inferred from the accessibility of substituted cysteines. *Neuron*. 22:559-570.

Benveniste, M., and M.L. Mayer. 1991a. Kinetic analysis of antagonist action at N-methyl-D-aspartic acid receptors. Two binding sites each for glutamate and glycine. *Biophys J*. 59:560-573.

Benveniste, M., and M.L. Mayer. 1991b. Structure-activity analysis of binding kinetics for NMDA receptor competitive antagonists: the influence of conformational restriction. *Br J Pharmacol*. 104:207-221.

Birmingham, K. 2002. Future of neuroprotective drugs in doubt. *Nat Med*. 8:5.

Blanke, M.L., and A.M. VanDongen. 2008. The NR1 M3 domain mediates allosteric coupling in the N-methyl-D-aspartate receptor. *Mol Pharmacol*. 74:454-465.

Blanpied, T.A., R.J. Clarke, and J.W. Johnson. 2005. Amantadine inhibits NMDA receptors by accelerating channel closure during channel block. *J Neurosci*. 25:3312-3322.

Brotchie, J.M. 2000. The neural mechanisms underlying levodopa-induced dyskinesia in Parkinson's disease. *Ann Neurol*. 47:S105-112; discussion S112-104.

Campos, F.V., B. Chanda, P.S. Beirao, and F. Bezanilla. 2008. Alpha-scorpion toxin impairs a conformational change that leads to fast inactivation of muscle sodium channels. *J Gen Physiol*. 132:251-263.

Carlton, S.M., and R.E. Coggeshall. 1999. Inflammation-induced changes in peripheral glutamate receptor populations. *Brain Res*. 820:63-70.

Chang, H.R., and C.C. Kuo. 2008. The activation gate and gating mechanism of the NMDA receptor. *J Neurosci*. 28:1546-1556.

Chen, G.Q., C. Cui, M.L. Mayer, and E. Gouaux. 1999a. Functional characterization of a potassium-selective prokaryotic glutamate receptor. *Nature*. 402:817-821.

Chen, G.Q., Y. Sun, R. Jin, and E. Gouaux. 1998. Probing the ligand binding domain of the GluR2 receptor by proteolysis and deletion mutagenesis defines domain boundaries and yields a crystallizable construct. *Protein Sci*. 7:2623-2630.

Chen, H.S., and S.A. Lipton. 2005. Pharmacological implications of two distinct mechanisms of interaction of memantine with N-methyl-D-aspartate-gated channels. *J Pharmacol Exp Ther*. 314:961-971.

Chen, N., T. Luo, and L.A. Raymond. 1999b. Subtype-dependence of NMDA receptor channel open probability. *J Neurosci*. 19:6844-6854.

Choi, D.W. 1987. Ionic dependence of glutamate neurotoxicity. *J Neurosci*. 7:369-379.

Choi, Y., H.V. Chen, and S.A. Lipton. 2001. Three pairs of cysteine residues mediate both redox and zn2+ modulation of the nmda receptor. *J Neurosci*. 21:392-400.

Chumakov, I., M. Blumenfeld, O. Guerassimenko, L. Cavarec, M. Palicio, H. Abderrahim, L. Bougueleret, C. Barry, H. Tanaka, P. La Rosa, A. Puech, N. Tahri, A. Cohen-Akenine, S. Delabrosse, S. Lissarrague, F.P. Picard, K. Maurice, L. Essioux, P. Millasseau, P. Grel, V. Debailleul, A.M. Simon, D. Caterina, I. Dufaure, K. Malekzadeh, M. Belova, J.J. Luan, M. Bouillot, J.L. Sambucy, G. Primas, M. Saumier, N. Boubkiri, S. Martin-Saumier, M. Nasroune, H. Peixoto, A. Delaye, V. Pinchot, M. Bastucci, S. Guillou, M. Chevillon, R. Sainz-Fuertes, S. Meguenni, J. Aurich-Costa, D. Cherif, A. Gimalac, C. Van Duijn, D. Gauvreau, G. Ouellette, I. Fortier, J. Raelson, T. Sherbatich, N. Riazanskaia, E. Rogaev, P. Raeymaekers, J. Aerssens, F. Konings, W. Luyten, F. Macciardi, P.C. Sham, R.E. Straub, D.R. Weinberger, N. Cohen, and D. Cohen. 2002. Genetic and physiological data implicating the new human gene G72 and the gene for D-amino acid oxidase in schizophrenia. *Proc Natl Acad Sci U S A*. 99:13675-13680.

Clements, J.D., and G.L. Westbrook. 1991. Activation kinetics reveal the number of glutamate and glycine binding sites on the N-methyl-D-aspartate receptor. *Neuron*. 7:605-613.

Cline, D.J., S.E. Redding, S.G. Brohawn, J.N. Psathas, J.P. Schneider, and C. Thorpe. 2004. New water-soluble phosphines as reductants of peptide and protein disulfide bonds: reactivity and membrane permeability. *Biochemistry*. 43:15195-15203.

Colquhoun, D., and A.G. Hawkes. 1990. Stochastic properties of ion channel openings and bursts in a membrane patch that contains two channels: evidence concerning the number of channels present when a record containing only single openings is observed. *Proc R Soc Lond B Biol Sci*. 240:453-477.

Coyle, J.T. 2006. Glutamate and schizophrenia: beyond the dopamine hypothesis. *Cell Mol Neurobiol*. 26:365-384.

Cull-Candy, S.G., and D.N. Leszkiewicz. 2004. Role of distinct NMDA receptor subtypes at central synapses. *Sci STKE*. 2004:re16.

Davies, S.N., and D. Lodge. 1987. Evidence for involvement of N-methylaspartate receptors in 'wind-up' of class 2 neurones in the dorsal horn of the rat. *Brain Res*. 424:402-406.

Davis, S.M., G.W. Albers, H.C. Diener, K.R. Lees, and J. Norris. 1997. Termination of Acute Stroke Studies Involving Selfotel Treatment. ASSIST Steering Committed. *Lancet*. 349:32.

Dickenson, A.H., and A.F. Sullivan. 1987. Evidence for a role of the NMDA receptor in the frequency dependent potentiation of deep rat dorsal horn nociceptive neurones following C fibre stimulation. *Neuropharmacology*. 26:1235-1238.

Dilmore, J.G., and J.W. Johnson. 1998. Open channel block and alteration of N-methyl-D-aspartic acid receptor gating by an analog of phencyclidine. *Biophys J*. 75:1801-1816.

Dravid, S.M., K. Erreger, H. Yuan, K. Nicholson, P. Le, P. Lyuboslavsky, A. Almonte, E. Murray, C. Mosely, J. Barber, A. French, R. Balster, T.F. Murray, and S.F. Traynelis. 2007. Subunit-specific mechanisms and proton sensitivity of NMDA receptor channel block. *J Physiol*. 581:107-128.

Dravid, S.M., A. Prakash, and S.F. Traynelis. 2008. Activation of recombinant NR1/NR2C NMDA receptors. *J Physiol*. 586:4425-4439.

Edmonds, B., A.J. Gibb, and D. Colquhoun. 1995. Mechanisms of activation of glutamate receptors and the time course of excitatory synaptic currents. *Annu Rev Physiol*. 57:495-519.

Erisir, A., and J.L. Harris. 2003. Decline of the critical period of visual plasticity is concurrent with the reduction of NR2B subunit of the synaptic NMDA receptor in layer 4. *J Neurosci*. 23:5208-5218.

Erreger, K., P.E. Chen, D.J. Wyllie, and S.F. Traynelis. 2004. Glutamate receptor gating. *Crit Rev Neurobiol*. 16:187-224.

Erreger, K., S.M. Dravid, T.G. Banke, D.J. Wyllie, and S.F. Traynelis. 2005a. Subunit-specific gating controls rat NR1/NR2A and NR1/NR2B NMDA channel kinetics and synaptic signalling profiles. *J Physiol*. 563:345-358.

Erreger, K., M.T. Geballe, S.M. Dravid, J.P. Snyder, D.J. Wyllie, and S.F. Traynelis. 2005b. Mechanism of partial agonism at NMDA receptors for a conformationally restricted glutamate analog. *J Neurosci*. 25:7858-7866.

Fisahn, A., A. Contractor, R.D. Traub, E.H. Buhl, S.F. Heinemann, and C.J. McBain. 2004. Distinct roles for the kainate receptor subunits GluR5 and GluR6 in kainate-induced hippocampal gamma oscillations. *J Neurosci*. 24:9658-9668.

Furukawa, H., and E. Gouaux. 2003. Mechanisms of activation, inhibition and specificity: crystal structures of the NMDA receptor NR1 ligand-binding core. *EMBO J*. 22:2873-2885.

Furukawa, H., S.K. Singh, R. Mancusso, and E. Gouaux. 2005. Subunit arrangement and function in NMDA receptors. *Nature*. 438:185-192.

Geiger, J.R., J. Lubke, A. Roth, M. Frotscher, and P. Jonas. 1997. Submillisecond AMPA receptor-mediated signaling at a principal neuron-interneuron synapse. *Neuron*. 18:1009-1023.

Gibb, A.J., and D. Colquhoun. 1992. Activation of N-methyl-D-aspartate receptors by L-glutamate in cells dissociated from adult rat hippocampus. *J Physiol*. 456:143-179.

Gielen, M., B. Siegler Retchless, L. Mony, J.W. Johnson, and P. Paoletti. 2009. Mechanism of differential control of NMDA receptor activity by NR2 subunits. *Nature*. 459:703-707.

Gill, A., A. Birdsey-Benson, B.L. Jones, L.P. Henderson, and D.R. Madden. 2008. Correlating AMPA receptor activation and cleft closure across subunits: crystal structures of the GluR4 ligand-binding domain in complex with full and partial agonists. *Biochemistry*. 47:13831-13841.

Hansen, K.B., H. Furukawa, and S.F. Traynelis. 2010. Control of assembly and function of glutamate receptors by the amino-terminal domain. *Mol Pharmacol*. 78:535-549.

Hansen, K.B., and S.F. Traynelis. 2010. Structural and Mechanistic Determinants of a Novel Site for Noncompetitive Inhibition of GluN2D-Containing NMDA Receptors. *J Neurosci*. 31:3650-3661.

Hansen, K.B., H. Yuan, and S.F. Traynelis. 2007. Structural aspects of AMPA receptor activation, desensitization and deactivation. *Curr Opin Neurobiol*. 17:281-288.

Hilf, R.J., and R. Dutzler. 2008. X-ray structure of a prokaryotic pentameric ligand-gated ion channel. *Nature*. 452:375-379.
Huettner, J.E., and B.P. Bean. 1988. Block of N-methyl-D-aspartate-activated current by the anticonvulsant MK-801: selective binding to open channels. *Proc Natl Acad Sci U S A*. 85:1307-1311.
Isaac, J.T., M. Ashby, and C.J. McBain. 2007. The role of the GluR2 subunit in AMPA receptor function and synaptic plasticity. *Neuron*. 54:859-871.
Jahr, C.E. 1992. High probability opening of NMDA receptor channels by L-glutamate. *Science*. 255:470-472.
Jayaraman, V., R. Keesey, and D.R. Madden. 2000. Ligand--protein interactions in the glutamate receptor. *Biochemistry*. 39:8693-8697.
Jiang, Y., A. Lee, J. Chen, M. Cadene, B.T. Chait, and R. MacKinnon. 2002. Crystal structure and mechanism of a calcium-gated potassium channel. *Nature*. 417:515-522.
Jin, R., S.K. Singh, S. Gu, H. Furukawa, A.I. Sobolevsky, J. Zhou, Y. Jin, and E. Gouaux. 2009. Crystal structure and association behaviour of the GluR2 amino-terminal domain. *EMBO J*. 28:1812-1823.
Jonas, P., J. Bischofberger, D. Fricker, and R. Miles. 2004. Interneuron Diversity series: Fast in, fast out--temporal and spatial signal processing in hippocampal interneurons. *Trends Neurosci*. 27:30-40.
Jones, K.S., H.M. VanDongen, and A.M. VanDongen. 2002. The NMDA receptor M3 segment is a conserved transduction element coupling ligand binding to channel opening. *J Neurosci*. 22:2044-2053.
Kalia, L.V., S.K. Kalia, and M.W. Salter. 2008. NMDA receptors in clinical neurology: excitatory times ahead. *Lancet Neurol*. 7:742-755.
Karakas, E., N. Simorowski, and H. Furukawa. 2009. Structure of the zinc-bound amino-terminal domain of the NMDA receptor NR2B subunit. *EMBO J*. 28:3910-3920.
Kashiwagi, K., T. Masuko, C.D. Nguyen, T. Kuno, I. Tanaka, K. Igarashi, and K. Williams. 2002. Channel blockers acting at N-methyl-D-aspartate receptors: differential effects of mutations in the vestibule and ion channel pore. *Mol Pharmacol*. 61:533-545.
Kawate, T., J.C. Michel, W.T. Birdsong, and E. Gouaux. 2009. Crystal structure of the ATP-gated P2X(4) ion channel in the closed state. *Nature*. 460:592-598.
Kemp, J.A., and R.M. McKernan. 2002. NMDA receptor pathways as drug targets. *Nat Neurosci*. 5 Suppl:1039-1042.
Kerchner, G.A., and R.A. Nicoll. 2008. Silent synapses and the emergence of a postsynaptic mechanism for LTP. *Nat Rev Neurosci*. 9:813-825.
Kessels, H.W., and R. Malinow. 2009. Synaptic AMPA receptor plasticity and behavior. *Neuron*. 61:340-350.
Kohda, K., Y. Wang, and M. Yuzaki. 2000. Mutation of a glutamate receptor motif reveals its role in gating and delta2 receptor channel properties. *Nat Neurosci*. 3:315-322.
Kotermanski, S.E., J.T. Wood, and J.W. Johnson. 2009. Memantine binding to a superficial site on NMDA receptors contributes to partial trapping. *J Physiol*. 587:4589-4604.
Krupp, J.J., B. Vissel, S.F. Heinemann, and G.L. Westbrook. 1996. Calcium-dependent inactivation of recombinant N-methyl-D-aspartate receptors is NR2 subunit specific. *Mol Pharmacol*. 50:1680-1688.
Krupp, J.J., B. Vissel, S.F. Heinemann, and G.L. Westbrook. 1998. N-terminal domains in the NR2 subunit control desensitization of NMDA receptors. *Neuron*. 20:317-327.

Krystal, J.H., D.C. D'Souza, D. Mathalon, E. Perry, A. Belger, and R. Hoffman. 2003. NMDA receptor antagonist effects, cortical glutamatergic function, and schizophrenia: toward a paradigm shift in medication development. *Psychopharmacology (Berl)*. 169:215-233.

Krystal, J.H., L.P. Karper, J.P. Seibyl, G.K. Freeman, R. Delaney, J.D. Bremner, G.R. Heninger, M.B. Bowers, Jr., and D.S. Charney. 1994. Subanesthetic effects of the noncompetitive NMDA antagonist, ketamine, in humans. Psychotomimetic, perceptual, cognitive, and neuroendocrine responses. *Arch Gen Psychiatry*. 51:199-214.

Kumar, J., P. Schuck, R. Jin, and M.L. Mayer. 2009. The N-terminal domain of GluR6-subtype glutamate receptor ion channels. *Nat Struct Mol Biol*. 16:631-638.

Kuner, T., P.H. Seeburg, and H.R. Guy. 2003. A common architecture for K+ channels and ionotropic glutamate receptors? *Trends Neurosci*. 26:27-32.

Kussius, C.L., and G.K. Popescu. 2009. Kinetic basis of partial agonism at NMDA receptors. *Nat Neurosci*. 12:1114-1120.

Kussius, C.L., and G.K. Popescu. 2010. NMDA receptors with locked glutamate-binding clefts open with high efficacy. *J Neurosci*. 30:12474-12479.

Kuusinen, A., R. Abele, D.R. Madden, and K. Keinanen. 1999. Oligomerization and ligand-binding properties of the ectodomain of the alpha-amino-3-hydroxy-5-methyl-4-isoxazole propionic acid receptor subunit GluRD. *J Biol Chem*. 274:28937-28943.

Lau, A.Y., and B. Roux. 2007. The free energy landscapes governing conformational changes in a glutamate receptor ligand-binding domain. *Structure*. 15:1203-1214.

Lees, K.R., K. Asplund, A. Carolei, S.M. Davis, H.C. Diener, M. Kaste, J.M. Orgogozo, and J. Whitehead. 2000. Glycine antagonist (gavestinel) in neuroprotection (GAIN International) in patients with acute stroke: a randomised controlled trial. GAIN International Investigators. *Lancet*. 355:1949-1954.

Lerma, J. 2006. Kainate receptor physiology. *Curr Opin Pharmacol*. 6:89-97.

Lester, R.A., G. Tong, and C.E. Jahr. 1993. Interactions between the glycine and glutamate binding sites of the NMDA receptor. *J Neurosci*. 13:1088-1096.

Leszkiewicz, D., and E. Aizenman. 2002. A role for the redox site in the modulation of the NMDA receptor by light. *J Physiol*. 545:435-440.

Lipton, S.A. 2005. The molecular basis of memantine action in Alzheimer's disease and other neurologic disorders: low-affinity, uncompetitive antagonism. *Curr Alzheimer Res*. 2:155-165.

Lipton, S.A. 2006. Paradigm shift in neuroprotection by NMDA receptor blockade: memantine and beyond. *Nat Rev Drug Discov*. 5:160-170.

Lipton, S.A. 2007. Pathologically-activated therapeutics for neuroprotection: mechanism of NMDA receptor block by memantine and S-nitrosylation. *Curr Drug Targets*. 8:621-632.

Lisman, J. 2010. Working memory: the importance of theta and gamma oscillations. *Curr Biol*. 20:R490-492.

Lu, H.C., E. Gonzalez, and M.C. Crair. 2001. Barrel cortex critical period plasticity is independent of changes in NMDA receptor subunit composition. *Neuron*. 32:619-634.

Lu, T., B. Nguyen, X. Zhang, and J. Yang. 1999. Architecture of a K+ channel inner pore revealed by stoichiometric covalent modification. *Neuron*. 22:571-580.

Luby, E.D., B.D. Cohen, G. Rosenbaum, J.S. Gottlieb, and R. Kelley. 1959. Study of a new schizophrenomimetic drug; sernyl. *AMA Arch Neurol Psychiatry*. 81:363-369.

Malenka, R.C., and R. Malinow. 2010. Alzheimer's disease: Recollection of lost memories. *Nature*. 469:44-45.

Mayer, M.L. 2005a. Crystal structures of the GluR5 and GluR6 ligand binding cores: molecular mechanisms underlying kainate receptor selectivity. *Neuron*. 45:539-552.
Mayer, M.L. 2005b. Glutamate receptor ion channels. *Curr Opin Neurobiol*. 15:282-288.
Mayer, M.L. 2006. Glutamate receptors at atomic resolution. *Nature*. 440:456-462.
Mayer, M.L. 2011. Structure and mechanism of glutamate receptor ion channel assembly, activation and modulation. *Curr Opin Neurobiol*.
Mohrmann, R., G. Kohr, H. Hatt, R. Sprengel, and K. Gottmann. 2002. Deletion of the C-terminal domain of the NR2B subunit alters channel properties and synaptic targeting of N-methyl-D-aspartate receptors in nascent neocortical synapses. *J Neurosci Res*. 68:265-275.
Mony, L., J.N. Kew, M.J. Gunthorpe, and P. Paoletti. 2009. Allosteric modulators of NR2B-containing NMDA receptors: molecular mechanisms and therapeutic potential. *Br J Pharmacol*. 157:1301-1317.
Monyer, H., R. Sprengel, R. Schoepfer, A. Herb, M. Higuchi, H. Lomeli, N. Burnashev, B. Sakmann, and P.H. Seeburg. 1992. Heteromeric NMDA receptors: molecular and functional distinction of subtypes. *Science*. 256:1217-1221.
Morris, G.F., R. Bullock, S.B. Marshall, A. Marmarou, A. Maas, and L.F. Marshall. 1999. Failure of the competitive N-methyl-D-aspartate antagonist Selfotel (CGS 19755) in the treatment of severe head injury: results of two phase III clinical trials. The Selfotel Investigators. *J Neurosurg*. 91:737-743.
Mosbacher, J., R. Schoepfer, H. Monyer, N. Burnashev, P.H. Seeburg, and J.P. Ruppersberg. 1994. A molecular determinant for submillisecond desensitization in glutamate receptors. *Science*. 266:1059-1062.
Mullasseril, P., K.B. Hansen, K.M. Vance, K.K. Ogden, H. Yuan, N.L. Kurtkaya, R. Santangelo, A.G. Orr, P. Le, K.M. Vellano, D.C. Liotta, and S.F. Traynelis. A subunit-selective potentiator of NR2C- and NR2D-containing NMDA receptors. *Nat Commun*. 1:90.
O'Hara, P.J., P.O. Sheppard, H. Thogersen, D. Venezia, B.A. Haldeman, V. McGrane, K.M. Houamed, C. Thomsen, T.L. Gilbert, and E.R. Mulvihill. 1993. The ligand-binding domain in metabotropic glutamate receptors is related to bacterial periplasmic binding proteins. *Neuron*. 11:41-52.
Oswald, R.E., A. Ahmed, M.K. Fenwick, and A.P. Loh. 2007. Structure of glutamate receptors. *Curr Drug Targets*. 8:573-582.
Paas, Y. 1998. The macro- and microarchitectures of the ligand-binding domain of glutamate receptors. *Trends Neurosci*. 21:117-125.
Panchenko, V.A., C.R. Glasser, and M.L. Mayer. 2001. Structural similarities between glutamate receptor channels and K(+) channels examined by scanning mutagenesis. *J Gen Physiol*. 117:345-360.
Paoletti, P., and J. Neyton. 2007. NMDA receptor subunits: function and pharmacology. *Curr Opin Pharmacol*. 7:39-47.
Perez-Otano, I., C.T. Schulteis, A. Contractor, S.A. Lipton, J.S. Trimmer, N.J. Sucher, and S.F. Heinemann. 2001. Assembly with the NR1 subunit is required for surface expression of NR3A-containing NMDA receptors. *J Neurosci*. 21:1228-1237.
Petrenko, A.B., T. Yamakura, H. Baba, and K. Shimoji. 2003. The role of N-methyl-D-aspartate (NMDA) receptors in pain: a review. *Anesth Analg*. 97:1108-1116.
Petryshen, T.L., F.A. Middleton, A. Kirby, K.A. Aldinger, S. Purcell, A.R. Tahl, C.P. Morley, L. McGann, K.L. Gentile, G.N. Rockwell, H.M. Medeiros, C. Carvalho, A. Macedo, A. Dourado, J. Valente, C.P. Ferreira, N.J. Patterson, M.H. Azevedo, M.J. Daly, C.N. Pato,

M.T. Pato, and P. Sklar. 2005. Support for involvement of neuregulin 1 in schizophrenia pathophysiology. *Mol Psychiatry*. 10:366-374, 328.
Pinheiro, P., and C. Mulle. 2006. Kainate receptors. *Cell Tissue Res*. 326:457-482.
Plested, A.J., and M.L. Mayer. 2009. AMPA receptor ligand binding domain mobility revealed by functional cross linking. *J Neurosci*. 29:11912-11923.
Poon, K., L.M. Nowak, and R.E. Oswald. 2010. Characterizing single-channel behavior of GluA3 receptors. *Biophys J*. 99:1437-1446.
Popescu, G., and A. Auerbach. 2003. Modal gating of NMDA receptors and the shape of their synaptic response. *Nat Neurosci*. 6:476-483.
Prieto, M.L., and L.P. Wollmuth. 2010. Gating modes in AMPA receptors. *J Neurosci*. 30:4449-4459.
Puddifoot, C.A., P.E. Chen, R. Schoepfer, and D.J. Wyllie. 2009. Pharmacological characterization of recombinant NR1/NR2A NMDA receptors with truncated and deleted carboxy termini expressed in Xenopus laevis oocytes. *Br J Pharmacol*. 156:509-518.
Qian, A., and J.W. Johnson. 2002. Channel gating of NMDA receptors. *Physiol Behav*. 77:577-582.
Qin, F. 2004. Restoration of single-channel currents using the segmental k-means method based on hidden Markov modeling. *Biophys J*. 86:1488-1501.
Quinlan, E.M., B.D. Philpot, R.L. Huganir, and M.F. Bear. 1999. Rapid, experience-dependent expression of synaptic NMDA receptors in visual cortex in vivo. *Nat Neurosci*. 2:352-357.
Regalado, M.P., A. Villarroel, and J. Lerma. 2001. Intersubunit cooperativity in the NMDA receptor. *Neuron*. 32:1085-1096.
Rezak, M. 2007. Current pharmacotherapeutic treatment options in Parkinson's disease. *Dis Mon*. 53:214-222.
Roberts, A.C., J. Diez-Garcia, R.M. Rodriguiz, I.P. Lopez, R. Lujan, R. Martinez-Turrillas, E. Pico, M.A. Henson, D.R. Bernardo, T.M. Jarrett, D.J. Clendeninn, L. Lopez-Mascaraque, G. Feng, D.C. Lo, J.F. Wesseling, W.C. Wetsel, B.D. Philpot, and I. Perez-Otano. 2009. Downregulation of NR3A-containing NMDARs is required for synapse maturation and memory consolidation. *Neuron*. 63:342-356.
Rosenmund, C., A. Feltz, and G.L. Westbrook. 1995. Synaptic NMDA receptor channels have a low open probability. *J Neurosci*. 15:2788-2795.
Rosenmund, C., Y. Stern-Bach, and C.F. Stevens. 1998. The tetrameric structure of a glutamate receptor channel. *Science*. 280:1596-1599.
Rothstein, J.D., and H. Brem. 2001. Excitotoxic destruction facilitates brain tumor growth. *Nat Med*. 7:994-995.
Sachidhanandam, S., C. Blanchet, Y. Jeantet, Y.H. Cho, and C. Mulle. 2009. Kainate receptors act as conditional amplifiers of spike transmission at hippocampal mossy fiber synapses. *J Neurosci*. 29:5000-5008.
Sandoz, G., S.C. Bell, and E.Y. Isacoff. 2011. Optical probing of a dynamic membrane interaction that regulates the TREK1 channel. *Proc Natl Acad Sci U S A*. 108:2605-2610.
Schmid, S.M., C. Korber, S. Herrmann, M. Werner, and M. Hollmann. 2007. A domain linking the AMPA receptor agonist binding site to the ion pore controls gating and causes lurcher properties when mutated. *J Neurosci*. 27:12230-12241.
Schorge, S., S. Elenes, and D. Colquhoun. 2005. Maximum likelihood fitting of single channel NMDA activity with a mechanism composed of independent dimers of subunits. *J Physiol*. 569:395-418.

Semyanov, A., and D.M. Kullmann. 2001. Kainate receptor-dependent axonal depolarization and action potential initiation in interneurons. *Nat Neurosci*. 4:718-723.

Smith, T.C., and J.R. Howe. 2000. Concentration-dependent substate behavior of native AMPA receptors. *Nat Neurosci*. 3:992-997.

Sobolevsky, A.I., C. Beck, and L.P. Wollmuth. 2002. Molecular rearrangements of the extracellular vestibule in NMDAR channels during gating. *Neuron*. 33:75-85.

Sobolevsky, A.I., M.L. Prodromou, M.V. Yelshansky, and L.P. Wollmuth. 2007. Subunit-specific contribution of pore-forming domains to NMDA receptor channel structure and gating. *J Gen Physiol*. 129:509-525.

Sobolevsky, A.I., M.P. Rosconi, and E. Gouaux. 2009. X-ray structure, symmetry and mechanism of an AMPA-subtype glutamate receptor. *Nature*. 462:745-756.

Stern, P., P. Behe, R. Schoepfer, and D. Colquhoun. 1992. Single-channel conductances of NMDA receptors expressed from cloned cDNAs: comparison with native receptors. *Proc Biol Sci*. 250:271-277.

Stroebel, D., S. Carvalho, and P. Paoletti. 2010. Functional evidence for a twisted conformation of the NMDA receptor GluN2A subunit N-terminal domain. *Neuropharmacology*. 60:151-158.

Sudhof, T.C., and R.C. Malenka. 2008. Understanding synapses: past, present, and future. *Neuron*. 60:469-476.

Sullivan, J.M., S.F. Traynelis, H.S. Chen, W. Escobar, S.F. Heinemann, and S.A. Lipton. 1994. Identification of two cysteine residues that are required for redox modulation of the NMDA subtype of glutamate receptor. *Neuron*. 13:929-936.

Sun, Y., R. Olson, M. Horning, N. Armstrong, M. Mayer, and E. Gouaux. 2002. Mechanism of glutamate receptor desensitization. *Nature*. 417:245-253.

Takano, T., J.H. Lin, G. Arcuino, Q. Gao, J. Yang, and M. Nedergaard. 2001. Glutamate release promotes growth of malignant gliomas. *Nat Med*. 7:1010-1015.

Talukder, I., P. Borker, and L.P. Wollmuth. 2010. Specific sites within the ligand-binding domain and ion channel linkers modulate NMDA receptor gating. *J Neurosci*. 30:11792-11804.

Tang, Y.P., E. Shimizu, G.R. Dube, C. Rampon, G.A. Kerchner, M. Zhuo, G. Liu, and J.Z. Tsien. 1999. Genetic enhancement of learning and memory in mice. *Nature*. 401:63-69.

Traynelis, S.F., and S.G. Cull-Candy. 1990. Proton inhibition of N-methyl-D-aspartate receptors in cerebellar neurons. *Nature*. 345:347-350.

Traynelis, S.F., L.P. Wollmuth, C.J. McBain, F.S. Menniti, K.M. Vance, K.K. Ogden, K.B. Hansen, H. Yuan, S.J. Myers, and R. Dingledine. 2010. Glutamate receptor ion channels: structure, regulation, and function. *Pharmacol Rev*. 62:405-496.

Tymianski, M., M.P. Charlton, P.L. Carlen, and C.H. Tator. 1993. Source specificity of early calcium neurotoxicity in cultured embryonic spinal neurons. *J Neurosci*. 13:2085-2104.

van Zundert, B., A. Yoshii, and M. Constantine-Paton. 2004. Receptor compartmentalization and trafficking at glutamate synapses: a developmental proposal. *Trends Neurosci*. 27:428-437.

Vicini, S., J.F. Wang, J.H. Li, W.J. Zhu, Y.H. Wang, J.H. Luo, B.B. Wolfe, and D.R. Grayson. 1998. Functional and pharmacological differences between recombinant N-methyl-D-aspartate receptors. *J Neurophysiol*. 79:555-566.

Vijayan, R., A.J. Plested, M.L. Mayer, and P.C. Biggin. 2009. Selectivity and cooperativity of modulatory ions in a neurotransmitter receptor. *Biophys J*. 96:1751-1760.

Vijayan, R., M.A. Sahai, T. Czajkowski, and P.C. Biggin. 2010. A comparative analysis of the role of water in the binding pockets of ionotropic glutamate receptors. *Phys Chem Chem Phys*. 12:14057-14066.

Villalba-Galea, C.A., W. Sandtner, D.M. Starace, and F. Bezanilla. 2008. S4-based voltage sensors have three major conformations. *Proc Natl Acad Sci U S A*. 105:17600-17607.

Villarroel, A., M.P. Regalado, and J. Lerma. 1998. Glycine-independent NMDA receptor desensitization: localization of structural determinants. *Neuron*. 20:329-339.

Wall, M.J., A. Robert, J.R. Howe, and M.M. Usowicz. 2002. The speeding of EPSC kinetics during maturation of a central synapse. *Eur J Neurosci*. 15:785-797.

Watanabe, J., C. Beck, T. Kuner, L.S. Premkumar, and L.P. Wollmuth. 2002. DRPEER: a motif in the extracellular vestibule conferring high Ca2+ flux rates in NMDA receptor channels. *J Neurosci*. 22:10209-10216.

Waxman, E.A., and D.R. Lynch. 2005. N-methyl-D-aspartate receptor subtypes: multiple roles in excitotoxicity and neurological disease. *Neuroscientist*. 11:37-49.

Williams, N.M., A. Preece, G. Spurlock, N. Norton, H.J. Williams, R.G. McCreadie, P. Buckland, V. Sharkey, K.V. Chowdari, S. Zammit, V. Nimgaonkar, G. Kirov, M.J. Owen, and M.C. O'Donovan. 2004. Support for RGS4 as a susceptibility gene for schizophrenia. *Biol Psychiatry*. 55:192-195.

Wo, Z.G., and R.E. Oswald. 1995. Unraveling the modular design of glutamate-gated ion channels. *Trends Neurosci*. 18:161-168.

Woo, T.U., R.E. Whitehead, D.S. Melchitzky, and D.A. Lewis. 1998. A subclass of prefrontal gamma-aminobutyric acid axon terminals are selectively altered in schizophrenia. *Proc Natl Acad Sci U S A*. 95:5341-5346.

Wood, M.W., H.M. VanDongen, and A.M. VanDongen. 1995. Structural conservation of ion conduction pathways in K channels and glutamate receptors. *Proc Natl Acad Sci U S A*. 92:4882-4886.

Wroblewska, B., J.T. Wroblewski, S. Pshenichkin, A. Surin, S.E. Sullivan, and J.H. Neale. 1997. N-acetylaspartylglutamate selectively activates mGluR3 receptors in transfected cells. *J Neurochem*. 69:174-181.

Wyllie, D.J., P. Behe, M. Nassar, R. Schoepfer, and D. Colquhoun. 1996. Single-channel currents from recombinant NMDA NR1a/NR2D receptors expressed in Xenopus oocytes. *Proc Biol Sci*. 263:1079-1086.

Yao, Y., C.B. Harrison, P.L. Freddolino, K. Schulten, and M.L. Mayer. 2008. Molecular mechanism of ligand recognition by NR3 subtype glutamate receptors. *EMBO J*. 27:2158-2170.

Yelshansky, M.V., A.I. Sobolevsky, C. Jatzke, and L.P. Wollmuth. 2004. Block of AMPA receptor desensitization by a point mutation outside the ligand-binding domain. *J Neurosci*. 24:4728-4736.

Yuan, H., K. Erreger, S.M. Dravid, and S.F. Traynelis. 2005. Conserved structural and functional control of N-methyl-D-aspartate receptor gating by transmembrane domain M3. *J Biol Chem*. 280:29708-29716.

Yuan, H., K.B. Hansen, K.M. Vance, K.K. Ogden, and S.F. Traynelis. 2009. Control of NMDA receptor function by the NR2 subunit amino-terminal domain. *J Neurosci*. 29:12045-12058.

Zucker, R.S., and W.G. Regehr. 2002. Short-term synaptic plasticity. *Annu Rev Physiol*. 64:355-405.